THESIS

DYNAMIC STRUCTURAL ANALYSIS OF RAMMING IN BIGHORN SHEEP

Submitted by

Aaron Michael Drake

Department of Mechanical Engineering

In partial fulfillment of the requirements

For the Degree of Master of Science

Colorado State University

Fort Collins, Colorado

Fall 2015

Master's Committee:

Advisor: Tammy L. Haut Donahue
Co-Advisor: Seth W. Donahue

Mitchell Stansloski
Paul Heyliger

ABSTRACT

DYNAMIC STRUCTURAL ANALYSIS OF RAMMING IN BIGHORN SHEEP

Concussions are the most common traumatic brain injury and are caused by impulsive loads applied to the skull, resulting in relative motion of the brain within the brain cavity. Despite wearing helmets, athletes involved in full contact sports, such as football, are highly susceptible to concussive injuries. Short term symptoms of concussions include nausea, headache and confusion and there is evidence of more serious, long term effects from repeated concussions. Furthermore, the physical mechanisms of concussions are not well understood, making them difficult to diagnose and treat clinically.

Male bighorn sheep sustain massive impact loads to the head during ramming, which is done as a means of determining hierarchy and gaining mating privileges. These large animals thrust themselves, horns first, at one another and collide violently, repeating this ritual for up to several hours until the subdominant male succumbs. After a collision, the animals are stunned momentarily but otherwise appear to suffer no ill effects, based on behavioral observations. This simple fact provided the motivation to examine the dynamic structural behavior of bighorn sheep horns and skulls. For reference, the average translational brain cavity accelerations observed during finite element model impact were found to be 111g (1091 m/s^2) and impacts thought to be damaging to human brains occur at around 100g.

A dynamic finite element impact model was produced using the geometry, obtained from a CT scan, of a mature male bighorn sheep's skull and horns. Quantitative and qualitative results of the simulation were examined to determine mechanisms of energy dissipation and stress distribution during an idealized impact event. Video analysis of particularly forceful ramming sequences of wild bighorn sheep was carried out to estimate the dynamics involved with ramming. In order to investigate the relative contributions of the horn curl as well as the internal foamy bone architecture, three separate finite element models were produced. One model had one half of the horn length removed, another had the internal foam-like bone removed and these models were compared to the fully intact model to determine the structural contributions of these features during impact. Removing one half of the horn curl had the effect of increasing the peak brain cavity translational acceleration by 49%. Eliminating the internal foamy bone architecture resulted in a dramatic 442% increase in brain cavity rotational accelerations. The dynamic (vibrational) response of bighorn sheep horns and skulls was investigated using two, related methods: finite element modal analysis and experimental modal analysis. The finite element modal analysis revealed five dominant natural frequencies with values ranging from 118 to 309 Hz. Experimental modal analysis revealed several natural frequencies between 100 and 300 Hz, however, differentiating specific modes was difficult. For both vibrational analyses the dominant vibrational mode shape was side-to-side oscillations of the horn tip. This study hopes to promote and guide further research on the mechanisms of brain trauma prevention in bighorn sheep, with an emphasis on the structural and material characteristics of the horn and skull, to increase our understanding of, and ways to prevent traumatic brain injuries in humans.

ACKNOWLEDGEMENTS

I would first like to acknowledge both my advisor, Dr. Tammy Haut Donahue, and my co-advisor, Dr. Seth Donahue, for providing me with such an interesting and meaningful project. They have provided guidance and assistance, while confidently allowing me to investigate this complex problem largely by my own means.

I would also like to acknowledge Dr. Mitchell Stansloski for his invaluable guidance in regards to all of the vibrations related work for the project. He first suggested examining vibration in the horn and gave instruction and direction on how to carry out experiments. I also would like to thank Dr. Paul Heyliger for serving on my committee. Next, I would like to acknowledge Benjamin Wheatley for his assistance with finite element modeling techniques used in this study. In addition, I would like to acknowledge all of my lab-mates including Kristine Fischenich, Hannah Pauly, Brett Steineman, Kate Remley and Alex Tomsick for proving feedback throughout the duration of this research.

TABLE OF CONTENTS

LIST OF TABLES

LIST OF FIGURES

Chapter 1 - Introduction

1.1 Motivation: Concussions in Humans

Concussions are the most common type of mild traumatic brain injury (mTBI), with an estimated 300,000 sport-related concussions resulting in loss of consciousness in the United States each year [1]. In addition, studies suggest that only between 8% [2] and 19.2% [3] of TBIs result in loss of consciousness, which leads to the more generous approximate of between 1.6 and 3.8 million sports-related concussions occurring each year in the United States [4]. The 4th International Conference on Concussion in Sport formally defines concussion as follows: "Concussion is a brain injury and is defined as a complex pathophysiological process affecting the brain, induced by biomechanical forces [5]." Concussion may be caused by either a direct blow to the head, face, neck or elsewhere on the body with an "impulsive" force being transmitted to the head [6]. Concussions can result in the rapid onset of neurological impairment [7] with symptoms including headache, temporary loss of consciousness, confusion, nausea, vomiting, fatigue and emotional lability [8].

High speed, full contact sports result in the highest incidence of sport-related concussions. The NCAA reported that football had the highest occurrence of concussion for males and soccer for females, with football accounting for an astonishing 37% of all concussions in collegiate athletes from 2004-2009. Studies have shown that athletes who have sustained concussions are at higher risk for future brain trauma [1], [9]. Guskiewics et al. found that collegiate football players with 3 or more previous concussions were 3 times more likely to sustain subsequent concussions [1]. Additionally, concussion sufferers are susceptible to a life threatening condition known as second-impact syndrome. Second-impact syndrome occurs when an athlete sustains an initial

brain injury, such as a concussion, and then sustains a second brain injury before symptoms of the initial blow have cleared [9]. The second blow can be relatively minor yet still yield catastrophic results.

Several studies suggest that repeated concussions can result in long term neurological effects; however these relationships have not been universally accepted [10]. Persisting ill effects of multiple concussion patients were studied in retired professional football players and included mild cognitive impairment, memory loss, depression, and early onset of Alzheimers disease [1], [11].

In the 1990s, concussions became a primary issue for discussion among the media, sports sponsors, sports medicine professionals, and athletes [12]. Despite the large boom in concussion research and awareness in recent decades, there is still no consensus amongst researcher on what input variable is the most telling of concussive impacts. The most commonly accepted input parameters seen to cause concussions are rotational and translational accelerations, which are both typically present in real impacts. Translational accelerations create intracranial pressure gradients, while rotational acceleration rotates the skull relative to the brain, causing shear strains in connective tissues [13]. Furthermore, there is no good clinical evidence suggesting that currently available helmets and mouth guards have a definite role in reducing concussion incidence [6]. Also, common neuroimaging modalities (CT, MRI) rarely show any detectable structural damage for concussive injuries [14], further increasing the difficulty of diagnosing and treating concussions.

1.2 Bighorn Sheep and Ramming

Biomimetics, a term coined in the 1950's, is defined by the Merriam-Webster dictionary as, "The study of the formation, structure, or function of biologically produced substances and materials and biological mechanisms and processes especially for the purpose of synthesizing similar products by artificial mechanisms which mimic natural ones." Biological structures are highly adapted via evolution to perform specific, and sometimes astonishing, functions in nature provided only the building materials supplied through a species' nutritional content. This fact has led many researchers to observe, analyze, and mimic biological structures with state-of-the-art engineering and manufacturing techniques to solve complex human problems. Some scientists have adopted this approach to address the critical issue of brain trauma in humans, namely by looking to bighorn sheep.

Rocky mountain bighorn sheep (Ovis canadensis) are a member of the bovidae family and inhabit the mountains of the western United States and Canada (Figure 1). Bighorn sheep are extremely agile, utilizing hard, split hooves to traverse rugged terrain with ease. Rams can grow to be between 5 and 6 feet long, 3-3½ feet tall, and can weigh between 140 and 300 lbs (63-136 kg). The horns of a bighorn sheep can grow to be over 30 inches long with a base circumference of over 15 inches. Bighorn sheep's horns are used as a means of intraspecific combat and as a symbol of status, with larger horns indicating that a ram has been well nourished throughout its lifetime [15]. These facts make the horns of a male bighorn sheep a primary component to the animal's reproductive success, a driving evolutionary force in the animal kingdom.

Figure 1: Rocky Mountain Bighorn Sheep (Ovis Canadensis). Attribution: Michael P. Flaherty http://www.bighorn.org/biology.html

Male bighorn sheep (Ovis canadensis) are known to violently butt heads, primarily during mating season, as a means of determining hierarchy and gaining mating privileges. During such bouts, rams will rear up on their hind legs, and charge one another for 3-5 steps while lowering their heads, then thrust themselves at one another, colliding horn-to-horn with a resounding clash [16]. Video analysis carried out on bighorn ramming sequences revealed maximum impact velocities of 6 m/s and maximum decelerations of 34 m/s². By assuming an animal body mass of 100 kg, these violent clashes have been estimated to produce forces up to 3400 N [17], which is 60 times higher than necessary to cause fracture of a human skull [18]. Despite being stunned momentarily the rams appear to show no ill effects from the impact, and will continue to ritualistically perform the collision, for up to several hours, until a victor has been determined [15].

It can be assumed that the skull and horns of bighorn sheep have been specifically adapted through evolution to perform the function of ramming and that there are structural attributes associated with sustaining such loads and preventing injury. In fact, the ability of rams to

withstand such violent, head-to-head collisions has led researchers to investigate the anatomy, structure, and material properties of bighorn sheep skulls and horns. The impetus of such research is generally to gain insight on the shock wave mitigation, load bearing capabilities, and failure prevention mechanisms of bighorn sheep horns and skulls in order to eventually mimic the structure in synthetic engineering applications. The impressive functionality of bighorn sheep skulls and horns in nature makes them a suitable candidate for imploring state-of-the-art engineering and analysis techniques currently associated with biomimetics.

1.3 Bighorn Sheep Skulls and Horns

Structural biological materials have gained interest from materials scientists and engineers in recent decades as a source of inspiration for developing lightweight, tough, and impact resilient structures and synthetic materials. In structural biological materials there exists a balance between function, available building constituents, and energy consumption. Therefore, only constituents derived from a species diet are available to produce these structures so they must be light weight enough to carry around without wasting excess energy, and they often must sustain several complex load states in order to fulfill their function. For these reasons, many biological structures have evolved to be lightweight, porous materials with high specific material properties, and display significant anisotropy. Anisotropy in biological structures is often a consequence of oriented regions of stiff constituents embedded in a matrix of more compliant material. Generally, higher material properties are observed in the primary loading directions of such biological structures. Several biological materials have sparked the interest of researchers and some areas of focus include bones, teeth, mollusk shells and hooves. Horns and skulls of

bighorn sheep have been studied by few researchers, and to a lesser extent than other biological materials.

The skull of the bighorn sheep has a few notable features. First, there are two distinct, thick cortical (compact) bone layers present in the skull (Figure 2). The innermost layer (makes up brain cavity) is separated from the outermost layer by boney struts, the septa, and open cell cavities. The presence of two distinct cortical shells has led to ram skulls being called "double layered." This is similar to human skulls which also have two layers of compact bone, but a much thinner region of spongy bone separating them (Figure 3). In bighorn sheep, the brain cavity itself is cradled within the outer skull layer with boney struts, and is largely surrounded by open space (Figure 2). The enlarged, frontal sinuses of sheep and goats are primarily air filled and have been thought to aid in shock mitigation [19]. Skull sutures (regions between skull bones) have been shown to accommodate large strains as shown by *in vitro* impact studies of goat skulls. This lead to the conclusion that sutures act as hinges or springs to aid in load bearing during ramming [18]. Material properties of bighorn sheep skull bones have not been published.

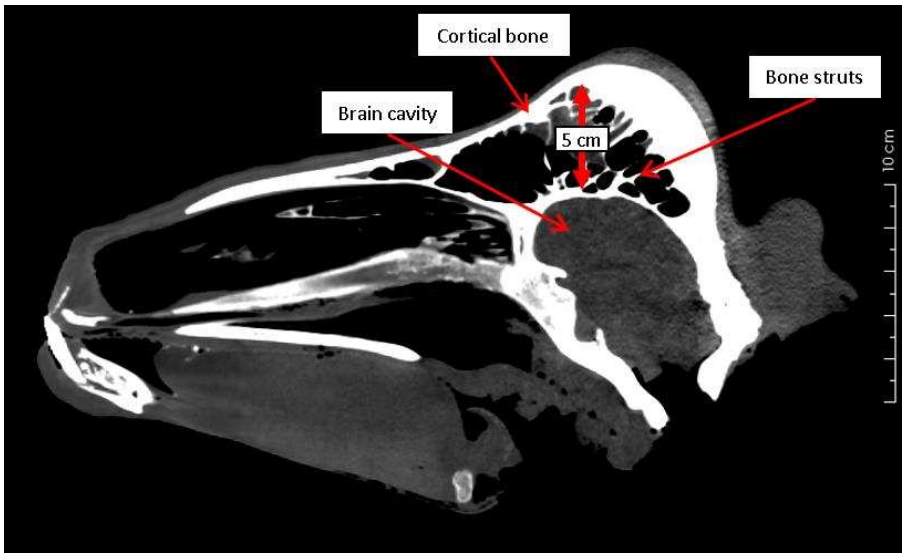

Figure 2: Bighorn Sheep Skull CT Slice. This image is from the sagittal plane; note the large open space above the brain cavity.

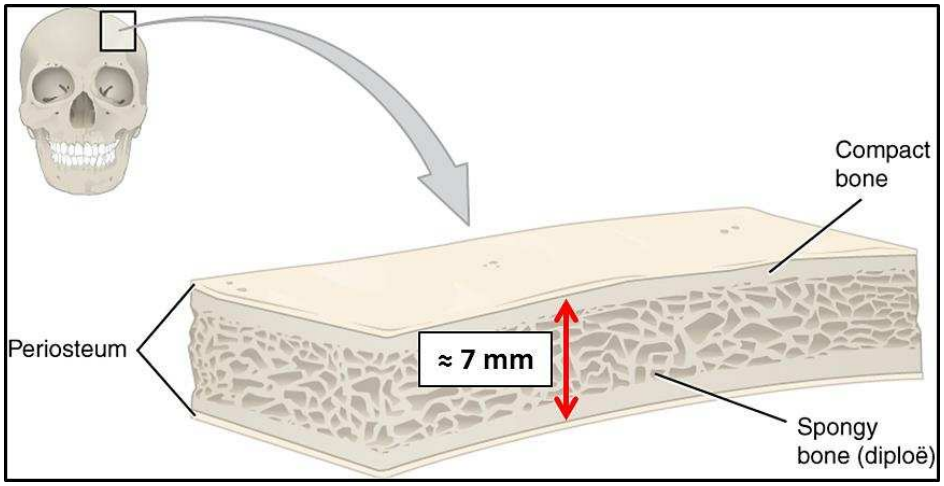

Figure 3: Human Skull. Note: the gap between cortical (compact) bone layers is much larger in the ram skull than in the human skull (5 cm for rams vs 7 mm for humans). Skull bone attribution: By OpenStax College [CC BY 3.0 (http://creativecommons.org/licenses/by/3.0)], via Wikimedia Commons

Horns are made up of an outer sheath that encases a boney core (horncore). The base of goat horncores are subjected to considerable bending strain (700 με anterior, -2000 με posterior) during impact loading [18], which is the case for bighorn sheep horncores as well. The horncore of a bighorn sheep is about one third of the total horn length, and can be approximated as a curved cone. The horncores of bighorn sheep consists of a relatively thick cortical shell filled with large boney struts and plates. These struts and plates form a 3D network of both open and closed cells, which form a bubble wrap like structure (Figure 4). These struts and plates differ

from typical spongey (A.K.A., trabecular) bone in that they are much larger (mm rather than μm), and they form a different structure. Typical trabecular bone consists of small, rod-like struts whereas the foamy bone present in ram horncores consists of larger, plate-like struts (Figure 4). No work has been done to characterize the structure and mechanical properties of bighorn sheep horncore bone.

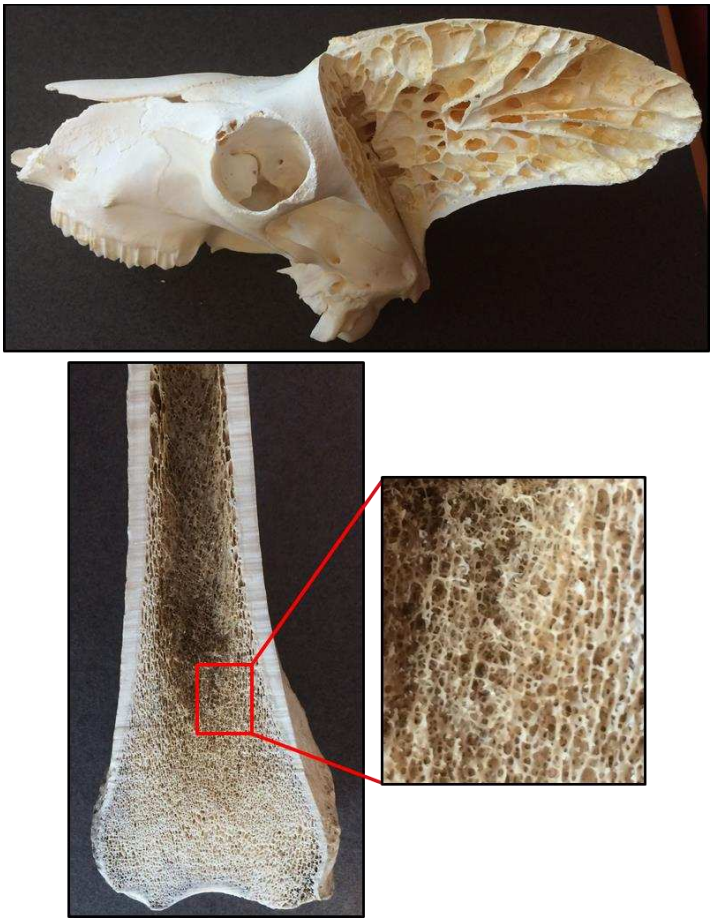

Figure 4: Horncore Internal Architecture. The top image is a bighorn sheep horncore cut away revealing the internal architecture. Note the large plate-like structure of the internal foamy bone. The bottom image is a cross section of the distal femur of a black bear. The blown up image reveals the small rod-like trabecular struts.

Horns exist on animals from the bovidae family, which includes cattle, sheep, goats, antelope, oryx and waterbuck, and are generally tough, resilient and highly impact resistant [20]. Horn is an avascular (does not contain blood vessels) tissue and therefore has no regenerative capabilities. Unlike antlers, horns are permanent structures that continue to grow throughout the

entire life of an animal. This makes it particularly important that horns do not fail mechanically, as this would reduce or eliminate an animal's chances of reproductive success. Horns grow from their base, where the skin is a germinative epithelium that generates new cells to grow the horn [20]. Therefore, the oldest part of the horn is that which is the furthest from the base of the horn.

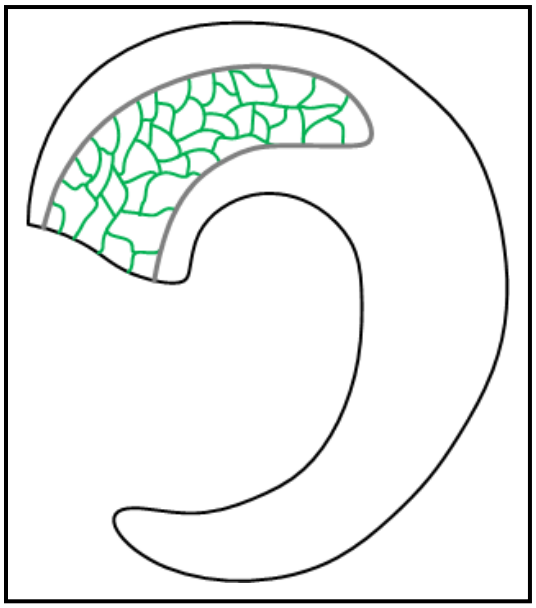

Figure 5: Horn & Horncore Diagram. This image depicts the horn outer sheath (outlined in black) as well as the horncore which consists of a cortical bone shell (grey) and internal foam-like bone struts (green).

The outer sheath encasing the horncore is commonly what is referred to as the horn itself, and henceforth the term *horn* will refer to the outer sheath. The horn of a bighorn sheep is primarily composed of keratin, which is characterized as a biopolymer and exits in several structures seen in nature such as horse hooves, fingernails, bird beaks, and reptile claws. Keratin exists in two basic forms: α-helices and β-sheets, the former is most commonly present in mammalian structures, such as horns [21], while β-sheets are typically seen in bird and reptile claws and beaks. Keratins are composed of two α-helices bundled into a superhelix, or coiled-coil [20]. These coiled-coils (also known as dimers) assemble via crosslinking into staggered rows oriented tail-to-head to form protofibrils, 1 nm in diameter. Four oriented protofibrils form what is known as an intermediate filament (IF), 17 nm in diameter [20]. These short, crystalline IFs are

embedded in an amorphous protein-based, keratin matrix, which has been modeled as an elastomer. Thus, keratin is essentially a polymer/polymer composite. Also, it should be noted that the alignment of keratin molecules within the matrix have a large effect on tensile properties [22]. It has been well documented that the mechanical properties of keratinized structures are highly dependent on moisture content [23], [24]. At a high relative humidity the matrix swells, becomes weak and exhibits viscoelasticity. At lower humidity the matrix becomes much stiffer, and the properties approach those of IFs [25]. In the fully hydrated state, oryx horn matrix has a modulus of 0.9 GPa where the modulus of the fibers (IFs) was measured to be 6.1 GPa [26]. It was also revealed that oryx horn sheath keratin displays linear viscoelasticity when tested in dry or fresh conditions [27].

Optical and scanning electron microscopy (SEM) elucidated the microstructure of bighorn sheep horn keratin and common material testing techniques characterized material properties. In bighorn sheep horns, the composite of IFs and protein-based matrix form into lamellar sheets with hollow, elliptical tubules dispersed between layers. Tubules extend along the length of the horn in the growth direction [23]. Other tough biological structures such as hoof, bone and antler also display this dispersed tubule microstructure. Keratin sheets, or lamellae, are oriented in the growth direction of the horn, stacking radially, with IFs dispersed randomly within the matrix [24]. The directionally oriented microstructure of horn keratin causes it to display transverse isotropy, meaning similar material properties are observed in the radial and transverse directions while significantly different properties are observed in the longitudinal direction. Elastic modulus of bighorn sheep horn keratin has been determined to be 0.63-2.2 GPa [23] or 0.9-4.1 GPa [24] and varies depending on hydration level, load state, and sample orientation with

hydration level being the greatest factor. Several failure mechanisms contribute to the observed toughness of horn keratin and include delamination, ligament bridging, and IF fracture [23].

Circumferential undulations exist on the exterior of bighorn sheep horns and result from growth spurts associated with seasonal changes in nutrition content. For example, large distances between undulations are due to significant horn growth, which is indicative of a bountiful foraging season. Due to the climate in which the animals inhabit, each seasonal growth undulation is representative of one year, which is why counting undulations is a valid method for quantifying a ram's age.

The overall shape of a bighorn sheep horn can be generalized as a tapered helix or tapered spiral that protrudes laterally from the skull. Similar spiral shapes appear in other biological materials such as seashells, and the geometry itself has been studied in the literature [28]. Ecologists and hunters alike use a metric known as "horn curl" to quantify the size and maturity of a bighorn sheep's horns. Horn curl is essentially the fraction of a full circle created by a sheep's horn when viewed from a side profile (Figure 6).

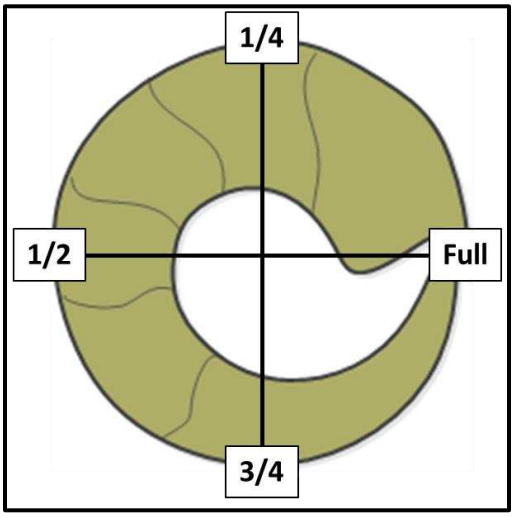

Figure 6: Horn Curl Diagram. The image depicts a full curl ram horn with seasonal growth rings.

The impressive function and interesting geometry of bighorn sheep horns has provoked interest in researchers that has manifested itself in two forms: experimental testing and theoretical modeling. Difficulties associated with testing the structure *in vivo* (in a living animal) and replicating load states experimentally make the problem particularly well suited for theoretical modeling techniques.

1.4 Modeling Efforts

Scientists and engineers often develop models based on principles of physics and mathematics in order to approximate physical phenomena and gain insight that would be difficult or impossible, to obtain experimentally. Modeling techniques have been implored in all realms of engineering and, when used wisely, can approximate existing events or predict theoretical outcomes. It is not possible to account for all of the complexities of a real physical system; therefore assumptions must be made when developing a model to eliminate factors with negligible contributions. Having a sound understanding of the phenomenon being modeled and knowing what factors will affect output variables is of key importance when developing a model. Also, it is important to understand the limitations and weaknesses of a model when presenting results. It is often difficult to analyze biological structures *in vivo* for obvious reasons, which makes the use of representative models a valuable alternative.

Finite element analysis is a powerful modeling technique that is commonly utilized by mechanical, civil and electrical engineers with countless applications, with the study of biological structures being no exception. The finite element method is a mathematical tool for approximating solutions to partial differential equations, given some boundary state. Using this

approach, a continuous, potentially complex domain is broken up into discrete, simply shaped subdomains, known as finite elements. Next, numerical, variational methods are used to solve the problem by minimizing an associated error function. In structural mechanics this process is typically performed using the following steps: mesh the geometry (discretize the domain), apply boundary conditions, assign material properties, and apply loads. Common outputs in structural mechanics include stresses, strains, displacements and strain energies. This technique has been adopted by many researchers to study the behavior of biological structures during loading situations typically seen in nature. Also, finite element models allow the flexibility to easily modify the geometry or the material's constitutive model to study how these affect output parameters.

Previous finite element modeling efforts have been aimed at studying impact in biological structures, including sheep and goat skulls and horns. One finite element study found that the tapered spiral geometry of bighorn sheep horns is effective at mitigating an impulse load as compared to less complex geometries. Simplified geometries were studied and included a cylindrical bar, a tapered cylinder, a cylindrical spiral and a tapered spiral. It was found that the taper had the largest effect on reducing impulse due to greater uniaxial deformations allowed by the decreasing cross-sectional area [28]. Another study that analyzed the real geometry of bighorn sheep horns via finite element analysis found that the structural constituents of the horn and frontal sinuses are important elements in sustaining quasi-static loads [29]. Various models were created incorporating different aspects of the skull geometry. This study implemented a quasi-static pressure load and did not account for the effects of momentum. A similar quasi-static finite element analysis was carried out on goat skulls in an attempt determine the role of the

frontal sinus during loading [19]. This study found mixed support for the role of frontal sinuses in protecting the skull from impact loads.

There has yet to be a dynamic finite element impact study of sheep or goat skulls, so impact studies of other biological structures were examined. Finite element models have been created to study impact in the skull of woodpeckers during pecking [30], [31]. Wang et al. carried out several studies on the topic, including a dynamic impact finite element model produced from micro-CT images. In this model, the beak impacted a rigid wall with an initial velocity, and resulting stress distributions were observed during the impact. It was found that a particular bone that wraps around the woodpecker's skull is a key geometric feature for sustaining loads during pecking.

1.5 Problem Statement

To the author's knowledge there exists no dynamic impact model of the skull and horn geometry of a bighorn sheep simulating loading during ramming. Such a model could help researchers understand mechanisms at play during these forceful bouts with regards to energy dissipation, stress distribution and acceleration mitigation. Also, there have been no dynamic experimental analyses performed on bighorn sheep horns geared towards characterizing the dynamic response of these structures. Knowledge on these topics could influence the development and manufacture of impact resistant structures and materials that are subjected to repeated impact loads.

Currently, finite element models of sheep and goat skulls incorporate quasi-static loading conditions that neglect the potential response to inertial factors. Therefore, a dynamic impact finite element model has been generated, utilizing the real geometry of a male bighorn sheep's

horns and skull developed from CT scan images. Previously determined mechanical properties and initial velocities were applied to the model to simulate an idealized impact.

In order to examine the contributions of the horn and horncore bone struts during impact loading, three different models were produced. One model included all geometric features present in a real ram skull. In the second model, a portion of the overall horn length was removed. In the third model, the internal horncore bone struts were manually removed.

A modal frequency analysis was performed on the mesh of the full model to determine theoretical natural frequency values and mode shapes associated with the structure. Experimental modal analysis was carried out on real skulls and horns of two bighorn sheep, in conjunction with modeling efforts. The results from this experimentation were utilized to validate the finite element model.

1.6 Specific Aims

Specific Aim 1:

Determine the role of the horn (keratin) and the horncore (bone) in terms of energy absorption and local stress distribution by utilizing a dynamic finite element model. Keratin is a tough and resilient biomaterial and the tapered spiral geometry has been shown to provide superior impulse reduction when compared to simpler geometries [28]. Therefore **it was hypothesized** that the horns would account for the largest percentage of elastic energy dissipated in a model subject to impact loading (1a). Goat horncores accommodate a large relative portion of skull strains during impact loading [32]. Therefore **it was hypothesized** that the horncore of bighorn sheep would

also experience large bending stresses and strains in comparison to horn keratin (1b). **Approach 1:** CT scan images of a bighorn sheep's skull and horns were segmented to generate a 3-dimensional geometry and finite element volume mesh. Material properties and boundary conditions were estimated from previously published reports and an impact load on the horns simulated using finite element analysis software. The magnitude and percentage of total energy was calculated for element sets comprising skull and horn materials (1a). The maximum principal stresses and strains were calculated and compared between bone and keratin material element sets (1b).

Specific Aim 2:

Quantify translational and rotational accelerations of a bighorn sheep's skull subject to impact loads seen in nature by utilizing finite element models. Concussions are the most common traumatic brain injury and are caused by impact loads to the head or body. While there is no consensus among the research community about what physical quantity is responsible for causing concussions, the input variables that are most commonly associated with concussions are translational and rotational accelerations of the skull. Impacts that cause skull translational and rotational accelerations approaching 100g (980 m/s^2) and 6000 rad/s^2, respectively, are more likely to result in concussion in humans [33]. **It was hypothesized** that loading and vibration of the horns (2a) and the presence of the horncore trabecular bone infrastructure (2b) aids in reducing translational and/or rotational accelerations within the brain cavity when the skull is subjected to impact loading. **Approach 2:** Using the finite element model from Aim 1, nodal values of translational and rotational accelerations were recorded at multiple locations within the brain cavity. To examine the effect of horn loading and vibrations on intracranial accelerations, simulations were conducted with the whole horn intact and with one half of the overall horn

length removed (2a). A model was created without the horncore trabecular bone to determine the effect of this foam-like bone material on brain cavity acceleration mitigation (2b).

Specific Aim 3:

Determine the natural frequencies and primary deformation modes of bighorn sheep horns and estimate the fraction of critical damping. During preliminary finite element impact modeling it was found that lateral-medial horn tip oscillations were induced by impact, leading to the assumption that this dynamic response was an important mechanism of brain injury prevention in bighorn sheep. **It was hypothesized** that the lateral-medial horn tip oscillations induced from impact occur at a frequency near one of the structure's natural frequencies and that mode shapes of the lowest natural frequencies will mimic the observed lateral-medial oscillation pattern (3a). **It was also hypothesized** that natural frequencies of a real bighorn sheep skull and horns are in the same range as approximated by a finite element frequency analysis (3b). **Approach 3:** A modal frequency analysis was performed on the skull and horn mesh to determine frequencies and mode shapes of the lowest natural frequencies (3a). Experimental modal analysis via impact hammer testing was performed to determine natural frequencies, mode shapes, and approximate damping of real bighorn sheep horns during free vibration (3b).

Chapter 2 - Impact

2.1 Introduction: Impact

The purpose of this section was to investigate the response of the bighorn sheep's horns and skull geometry to impact loading both qualitatively and quantitatively. The primary investigatory method was developing a finite element impact model incorporating the geometry of a real bighorn sheep's horns and skull. The goal of the model was to simulate a very direct and idealized impact situation. Due to the complexity of the phenomenon being simulated, and due to the lack of a comprehensive constitutive model of the materials being analyzed, it would be impractical to confidently report exact output values. Thus, patterns and relative values of output parameters were of primary interest in this study. Video analysis of bighorn sheep ramming was performed in conjunction with development of the finite element model in order to produce rough estimates of the dynamics associated with bighorn sheep ramming. This work reiterates previous research efforts but with more modern techniques. Specific points on the animal were tracked through several video frames using video analysis software to approximate values of velocities, accelerations and contact times associated with impact. Based on this impact study, various structural characteristics of the bighorn sheep's horns and skull are hypothesized to help prevent brain trauma.

2.2 Methods: Finite Element Impact Model Development

Computed tomography (CT) scan images of a mature male bighorn sheep were provided courtesy of Dr. Karen Fox (DVM) of the Colorado Division of Parks and Wildlife. Dr. Fox

utilized these images in a previous, unrelated study. The animal in this scan had tumors present in the sinus and horncores and these tumors can effect bone remodeling. Dr. Karen Fox has studied these tumors extensively and upon inspecting the scan stated that there appeared to be no effect on bone remodeling caused by the tumor in this particular animal.

A CT scan produces cross-sectional images (virtual 'slices') by combining several X-rays taken from various angles. Cross-sectional images produced from CT scans are made up of voxels (3D analog of a pixel) with a range of greyscale, or brightness, values which will be henceforth referred to as the voxel intensity. Voxel intensity is related to the radiodensity (and therefore mass density) of the material being scanned, with higher intensity values correlating to more dense materials (Figure 7). The CT scan for this study was performed using a Philips GEMINI TF Big Bore PET/CT located at CSU's Veterinary Medical Center. The scan was carried out with a slice spacing of 1 mm in the axial plane and 0.88 mm in the coronal and sagittal planes (see Figure 8 for anatomical directions). The scan yielded Digital Imaging and Communication in Medicine files, which are commonly referred to as DICOM images (Figure 7). Processing of the DICOM images was performed using 3D Slicer medical image analysis and visualization software. 3D Slicer is a free, open source software package that was developed as part of the National Alliance for Medical Image Computing (NA-MIC) and is funded by the National Institute of Health (NIH).

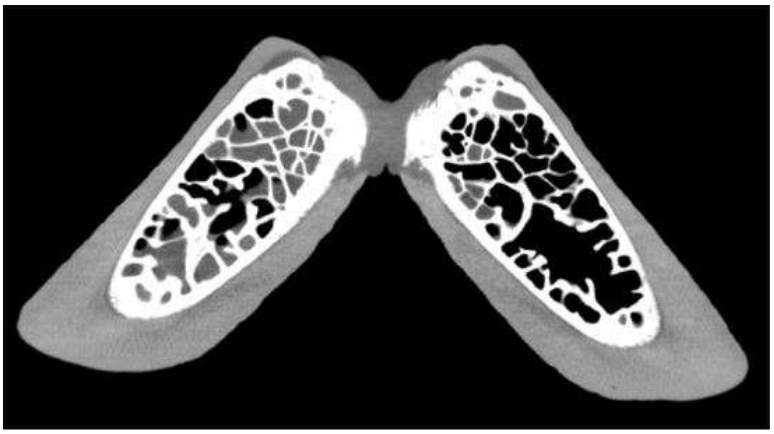

Figure 7: Example DICOM Slice. Two different materials are depicted in this image which is evidenced by the different voxel intensities. The brighter white material is bone (more dense) and the grey material is horn (less dense).

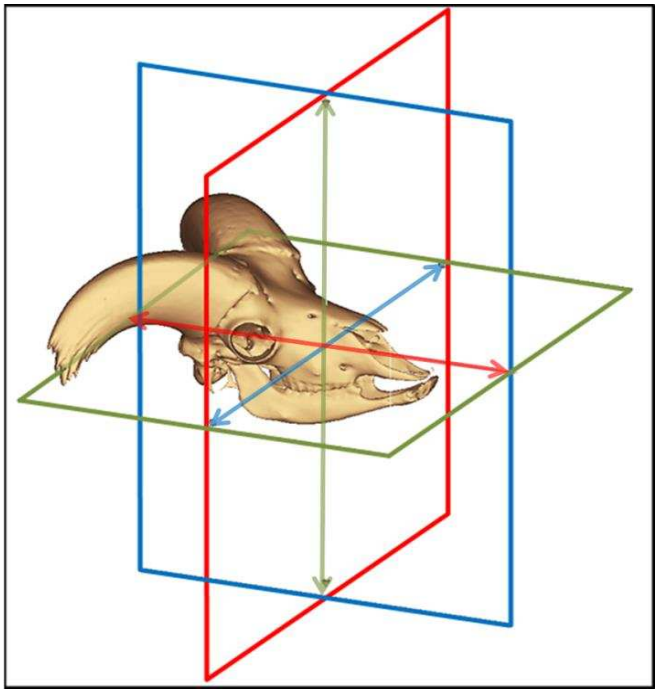

Figure 8: Anatomic Planes. a) Blue: sagittal (medial-lateral) b) Green: axial (transverse) c) Red: coronal

A stack of 737 DICOM images was imported into 3D Slicer, and the volume of interest was cropped to remove unwanted portions of the scan. Next, various manual and semi-automated image segmentation techniques were used to precisely define the structure of the horn and skull, as well as to differentiate bone from horn keratin. Bone has a much higher mass density than horn keratin, and therefore bone voxels appear much brighter (higher intensity value) in CT images. Taking advantage of this fact, bone and horn keratin were defined as two different

materials within the 3D Slicer environment using threshold segmentation. Threshold segmentation is a semi-automated image segmentation tool that defines all voxels within a certain intensity range as being one material. A manual image segmentation tool that mimics a painting interface was applied to correct erroneously labeled sections resulting from automated segmentation techniques and to remove tumor material from the images. The result of the segmentation is a set of DICOM images or 'slices' with two clearly defined materials: bone and horn keratin (Figure 9b). Regions of the DICOM images that have been defined as a specific material will be referred to as labels.

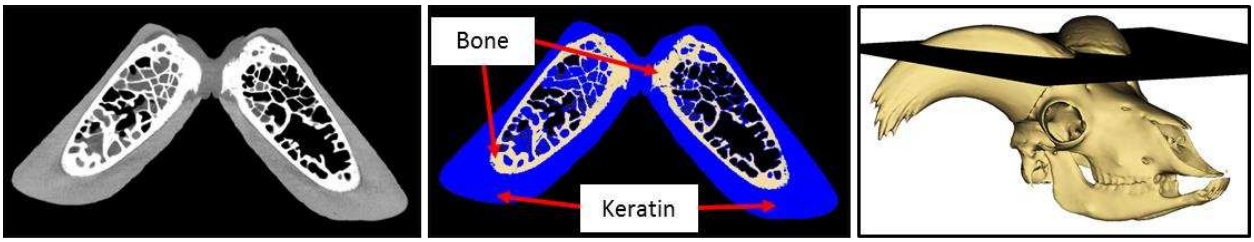

Figure 9: DICOM Segmentation. a) Example DICOM image b) Segmented image Note the erroneously marked keratin regions within the bone region. These were tumor material and were removed manually. c) 3D model depicting location of the example DICOM (horn not included)

Once the materials were segmented, 3-dimensional models of the two materials were created from the image stack. In order to produce a geometry that could be readily converted into a volume mesh, it was necessary to perform smoothing on the segmented labels, particularly in the case of the complex skull geometry. The segmented bone labels were subjected to 40 iterations of Laplace smoothing in the generation of the 3D skull model (Figure 9c). Only 25 iterations of Laplace smoothing were used in the development of the horn 3D model due its lack of small geometric intricacies, as compared to the skull. A small volumetric change was observed as a result of the smoothing of the skull when compared to an unsmoothed model. This volume change was calculated to be a 2.8% increase, and was considered to be negligible. The 3D models created were in the form of continuous triangular surface meshes with 'empty' volumes.

This type of 3D surface geometry is then stored in the stereolithography (STL) file format which is commonly utilized in rapid prototyping applications, such as 3D printing. This file format can be readily exported to most commercially available CAD, finite element analysis, and meshing software platforms.

Prior to exporting the surface models of the skull, a transformation was applied to the geometry. The skull and horn geometry were not perfectly oriented in the Cartesian coordinate system as a result of a slight misalignment during the CT scan. To account for this misalignment, a rotational transformation matrix (Appendix A) was applied to all portions of the model to reorient the sagittal plane, causing it to perfectly bisect the skull. Applying this transformation was a crucial step as it provided the correct orientation for a plane of symmetry to be created. This symmetry plane allowed for a drastic reduction in the complexity of the model and will be discussed in detail later. Once the rotational transformation was applied to the overall model, two separate 3D surface mesh files (separate files for horn and skull) were exported from 3D Slicer.

ICEM CFD mesh generation software (a product of ANSYS, Inc.) was chosen to compute volume meshes for its ability to efficiently mesh large, complex models from dirty CAD or faceted (STL) geometries. Volume meshing of the horn and skull was done independently, and the meshes were later reassembled in the finite element analysis software. Discussion of meshing techniques will focus on volume meshing of the skull geometry, as it was more complex and required more steps. After importing the skull surface mesh, a symmetry plane was defined as the sagittal plane directly bisecting the skull. This was done by creating a rectangular surface that intersected the skull geometry (Figure 10a). The intersections of the rectangular surface with the skull geometry were defined as curves to precisely define regions cut by the symmetry plane. The symmetry plane part was defined as an internal wall so that the meshing algorithm would

respect the plane, rather than creating elements that penetrated it. The "Build Diagnostic Topology" function was used to define sharp features within the model by creating a series of curves and points from surface edges. Creating these points and curves, in conjunction with applying proximity and curvature based mesh refinement, allowed for a mesh to be produced that included small and intricate bone strut features within the skull and horncores. The Robust (Octree) tetrahedral meshing algorithm was used to produce a volume mesh of the entire skull, which was separated into two distinct regions separated by the symmetry plane. The left half of the skull was deleted and the remaining nodes and elements of right half of the skull were then renumbered. Only one half of the skull geometry was used in the impact simulation to take advantage of sagittal plane symmetry and greatly reduce computational cost. Global volume mesh smoothing was performed while allowing mesh refinement. Bandwidth optimization was performed to minimize the size of the global system matrix. The final mesh of one half of the skull geometry contained 1,027,874 tetrahedral elements and 253,807 nodes. Similar techniques were used to generate the mesh of the right horn geometry, which contained 261,788 tetrahedral elements and 62,586 nodes. Finally, element information and associated node coordinates were exported to text documents.

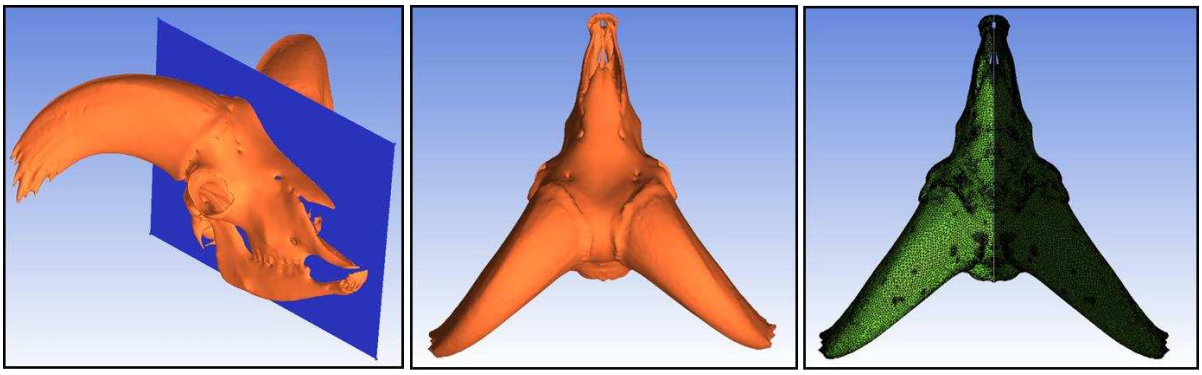

Figure 10: Symmetry Plane & Meshing. a) Symmetry plane bisecting skull geometry. b) Full skull geometry top view (STL faceted format) c) Half skull tetrahedral mesh mirrored about symmetry plane (note how closely the mirrored mesh mimics the full skull geometry)

Node and element information for each mesh (horn and half skull) was compiled into text documents and formatted as ABAQUS input files. Abaqus is a commercial finite element analysis software package distributed by Dassault Systemes, and was used for all impact and vibration simulations in this study. Horn and half skull input files were imported into Abaqus CAE, the software's graphical user interface. Next, the horn and half skull meshes were assigned material properties of horn keratin and bone, respectively, based on values presented in previous literature. The material properties of bighorn sheep skull bone have yet to be characterized and published to the scientific community, so values for human bone were used, as has been done in previous models [29] (Table 1). A 3D deformable plate was next created and meshed within the Abaqus CAE environment to serve as an impact surface. This plate was meshed with 8 node brick elements given material properties of horn keratin, and will henceforth be referred to as the 'impact plate.' At this point, three independent part instances (horn, half skull, impact plate) were present in the model environment with no particular orientation relative to one another.

Table 1: Material Properties**.** Values stated in both SI and SI (mm). SI (mm) units were used in the model because the imported horn and skull meshes had length dimensions in millimeters and Abaqus requires a consistent unit convention.

	SI			**SI (mm)**		
	Units	Keratin	Bone	**Units**	**Keratin**	**Bone**
Density	*kg/m^3*	1300	1725	***tonne/mm^3***	**1.300E-09**	**1.725E-09**
Modulus	*Pa*	2.0E+09	1.5E+10	***MPa***	**2000**	**15000**
Poisson's Ratio	*Unitless*	0.3	0.28	***Unitless***	**0.3**	**0.28**

The next step was to assemble the part instances spatially and add engineering features in order to simulate an idealized impact. The horn mesh was first attached to the half skull mesh at the horncore using an instance merging approach. To accomplish this, the horn was first carefully rotated and translated to fit onto the horncore. In fact, the same transformation matrix that was used to rotate the skull geometry in the 3D Slicer software was incorporated to align the horn and

horncore perfectly in the Abaqus CAE environment. Once aligned, the merge instance operation was performed, which slightly modified the position of nodes on the inner surface of the horn and on the outer surface of the horncore to be coincident with one another. This effectively combined the two part instances, while allowing them to have independent material properties. Next, the combined horn and half skull instance was aligned facing the impact plate with the leading edge of the horn approximately two centimeters from the impact plate. To do so, the symmetry plane of the half skull was defined as being parallel to the edge of the impact plate. The horn and skull were rotated an angle of 43° from horizontal about the axis normal to the sagittal plane, which has been defined as being the angle of impact for ram skulls [17]. In order to account for the momentum and force produced by the rest of the animal (e.g. neck, torso, legs) a point mass of 43.53 kg was created. This mass value was determined by assuming an animal total mass of 100 kg, then dividing this by two due to the symmetry of the model, and then subtracting the mass of the horn and half skull instance. The point mass was positioned on the symmetry plane of the model in a location that approximates the center of mass of the animal. The position of the point mass was determined using ImageJ image processing software by calculating the centroid of a side profile image of a bighorn sheep's torso. The point mass was connected to a reference point located at the base of the skull (where the neck would attach) by a one dimensional spring and dashpot element, which will henceforth be referred to as the 'spine spring.' The stiffness and damping coefficients for sheep spine [34] were used as baseline values for this element, however, using these values resulted in a 'pinball effect' upon running the simulation. This means that the skull bounced back and forth between the impact plate and point mass, which was an undesirable response. The spine spring stiffness and damping coefficient were increased several times until this phenomenon was no longer observed.

Several nontrivial boundary conditions were applied to the model to replicate the complex physical phenomenon of bighorn sheep ramming. The back face of the impact plate was defined as having an 'encastre' boundary condition, which restricts the nodes from any rotation or translation, in any direction (Figure 11a). In order to exploit the symmetry in the model, an axis-symmetric boundary condition was imposed. This condition allows no displacement in the medial direction (X-direction) and no rotation about the Y-axis and Z-axis (Figure 11b). This X-axis symmetric boundary condition was applied to all nodes lying on the symmetry plane that was defined in the ICEM CFD meshing software. To comprehend the validity of these restrictions it is helpful to recall that any of these movements would cause the skull material to overlap the skull's hypothetical mirror image. The point mass was restricted from all translations and rotations except translation in the Z-direction, which was unhindered (Figure 11c). This was done to produce an idealized impact where all of the momentum of the animal's mass was translated into the skull and impact plate via the spine spring/dashpot element. The neck attachment reference point was connected to several nodes at the base of the skull by a continuum distribution kinematic coupling constraint. This constraint allowed all boundary conditions and loads applied to the reference point to also be transmitted to the neck connection nodes (Figure 11d). Boundary conditions were applied to the neck connection reference point restricting rotation about the X-axis and displacements in the Z-direction. These boundary conditions are in place to simulate reaction torques and forces produced by the neck musculature during impact. In order to produce the momentum of impact, an initial velocity field of 4.7 m/s in the Z-direction was assigned to all nodes of the horn and skull instance, as well as the point mass. This velocity value was determined by Kitchener et al. to be the average impact velocity of

bighorn sheep during ramming [17]. Boundary conditions and the general spatial assembly of the model can be seen in Figure 11.

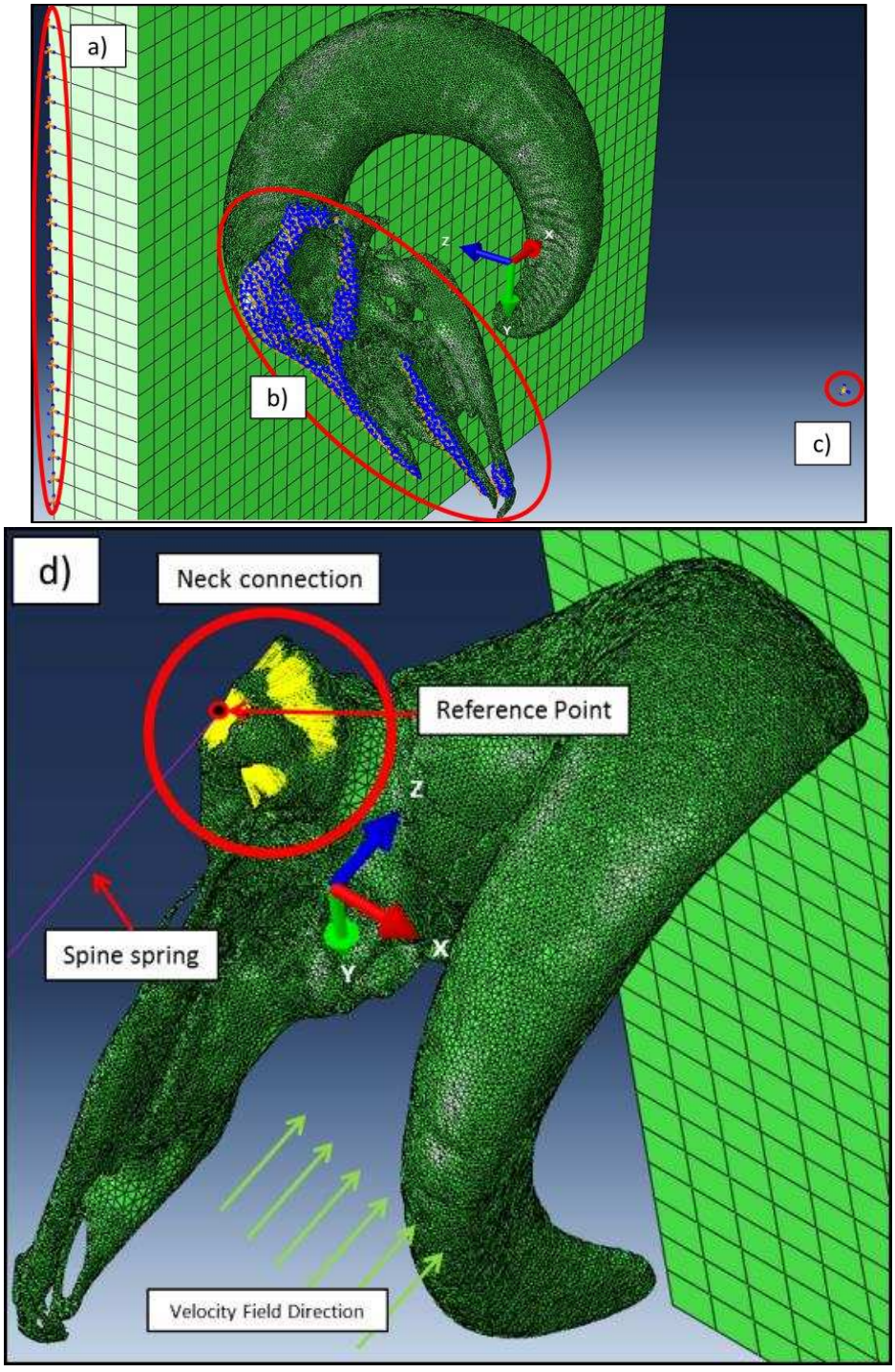

Figure 11: Boundary Conditions. a) Impact plate encastre. b) Symmetry plane BCs (x-axis symmetric) c) Point mass BCs (y=x=0) d) Neck Connection BCs (y=x_rotation=0) Note: yellow lines attach reference point to neck connection nodes.

Accelerations within the brain cavity were of particular interest in this study, as they are thought to be relevant input variables causing brain trauma. Five node sets containing 40 nodes each were created at five different regions within the brain cavity to monitor translational accelerations (Figure 12a). Nodes of continuum elements have no rotational degrees of freedom; therefore a different technique had to be used to monitor rotational acceleration within the brain cavity. All nodes of the interior surface of the brain cavity were coupled to a reference point via a kinematic coupling constraint (similar to the neck connection) and rotational acceleration of this 'brain cavity reference point' was monitored (Figure 12b).

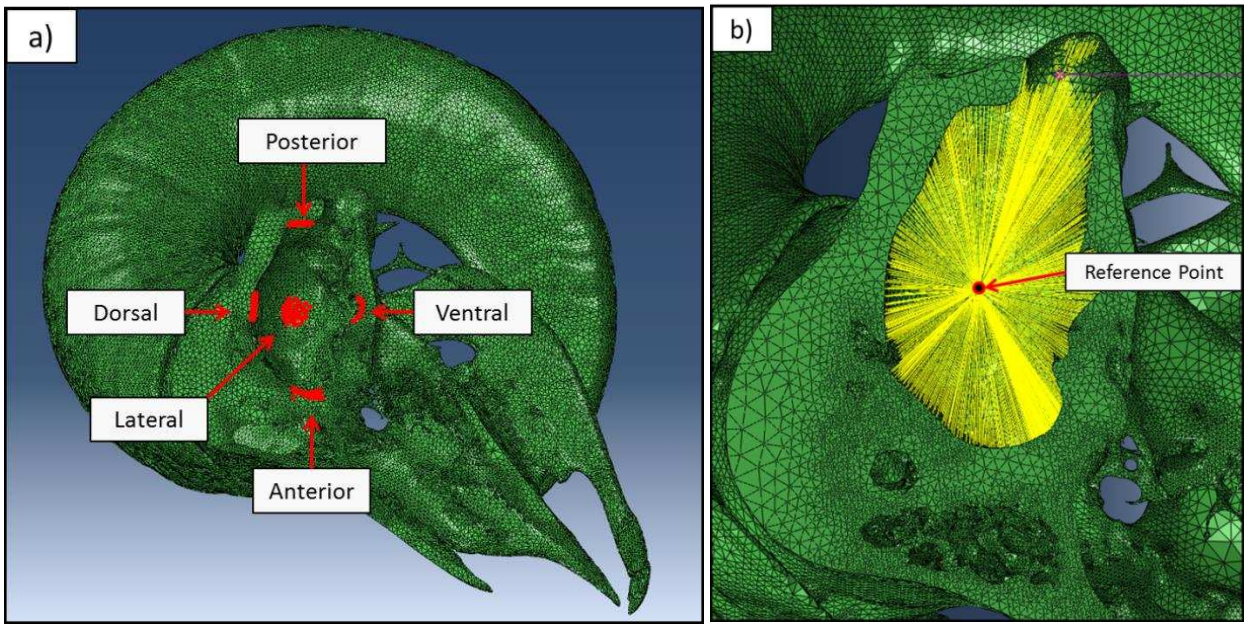

Figure 12: Brain Cavity Acceleration Measurement Locations. a) Translational acceleration node set locations b) Rotational acceleration kinematic coupling constraint and reference point

The simulation was carried out with the explicit solver of Abaqus (Abaqus/Explicit), which is particularly well suited for transient dynamic events and effectively handles severely nonlinear behavior such as contact. The implicit procedure (Abaqus/Standard) must iterate to determine the solution to a nonlinear problem, whereas the explicit solver advances the kinematic state from the previous time increment. The explicit solver is commonly used for impact and contact

problems and is typically less computationally expensive for such simulations. A step time of 0.03 seconds was implemented and was found to capture the skull and horn approaching the impact plate, contacting the plate, and rebounding from impact. The simulation was run on a virtual machine and was decomposed to be run on 12 processors. Even with this many processors the simulation took a long time to run (~4 days), and a technique called mass scaling was used to impose some control over the run time. Using the explicit solver, the step time of the model is discretized into stable time increments, which are often controlled by the smallest elements in the model. Therefore a few, very small elements, can increase the computational time substantially. Mass scaling was used to scale up the mass of the smallest, critical elements to significantly increase the stable time increment (reducing the simulation time) while having a negligible effect on the overall dynamic behavior. Using this method, the simulation time was reduced to about two days. Field outputs were requested for the whole model and included nodal values of stresses, strains, displacements, velocities, accelerations and forces. Field outputs were requested for 100 evenly spaced time intervals throughout the simulation. A specific field output was requested for the brain cavity reference point in order to capture rotational acceleration within this region. Three different history outputs were requested; one for all horn (keratin) elements, one for all skull (bone) elements, and one for the entire model. The history outputs returned elemental total energy values such as kinetic energy, strain energy and work associated with mass scaling.

2.3 Results: Impact Model

Stress Patterns

Given a number of unknown exact quantities, such as material properties, patterns of stress in the horn and bone are presented instead of reporting exact values. This section aims to describe visually and textually the stress patterns observed in the impact model, in both the horn and bone materials. Stress patterns described in the horn will be for a sequence of time points, as the horn displayed a dynamic response to the loading. There was minimal dynamic response observed for the skull portion of the model, so the patterns described will be for the time point where maximum stresses were observed. The entire impact took place over 24 frames, with 0.3 milliseconds (0.0003 s) between each frame for a total impact time of approximately 7.2 milliseconds. Images contain the time at which they were taken. Note that initial contact began at 0.0051 seconds. Stresses are reported as signed maximum principal stresses and the highest stresses were observed during the first half of the impact.

Upon initial impact, the maximum principal stresses in the horn are very localized at the impact site (Figure 13); however these stresses are spread over a much broader area on the inside horn surface, where it interfaces with the horncore (Figure 13 cutout).

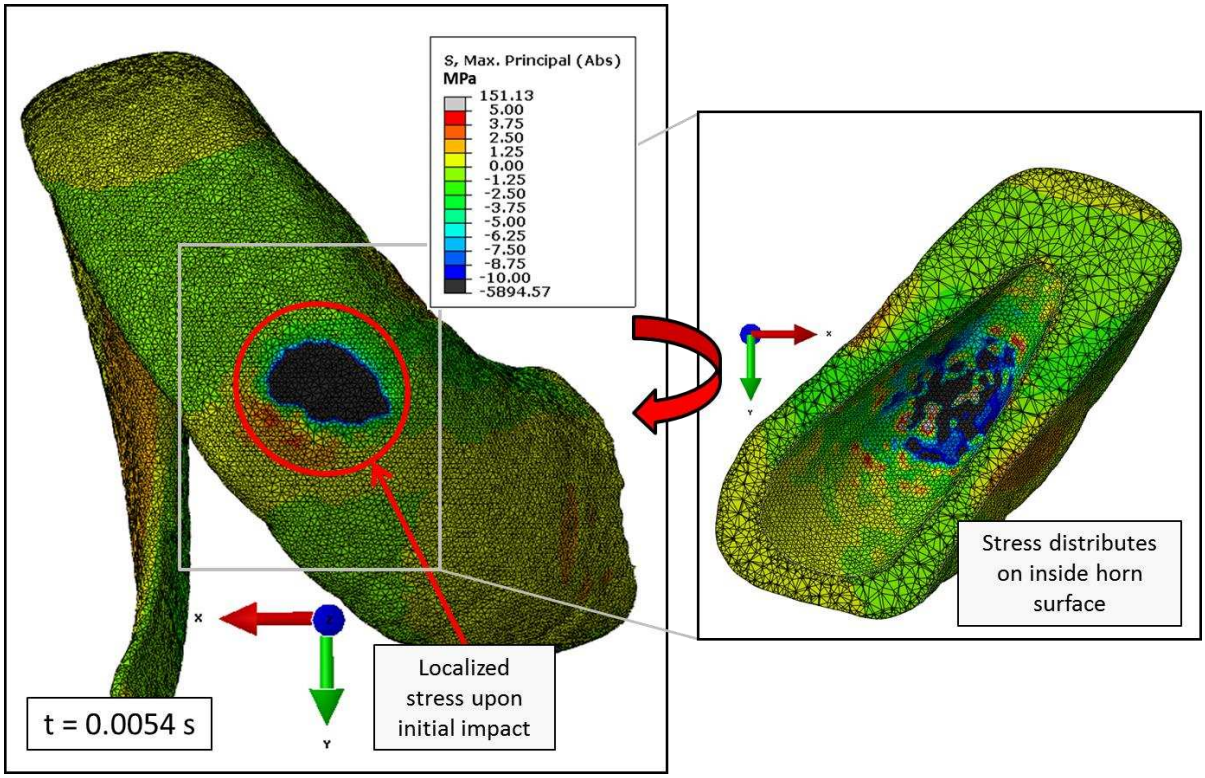

Figure 13: Localized Horn Stress. The stress is initially localized at the horn impact site. The cutout shows a cross section of the inside horn surface at the impact site. Note how the stress distributes over a greater surface area on the inner surface of the horn (Contact stress area of 1948 mm² spreads to 3208 mm² on inner horn surface).

Approximately 0.9 milliseconds later in the impact, the momentum of the lagging back half of the horn loads the inner diameter of the horn in compression and the outer diameter of the curl in tension (Figure 14). There is less surface area on the inner diameter of the horn curl than on the outer diameter; therefore the compressive stresses on the inner diameter of the curl have larger magnitudes than the tensile stresses on the outer curl. This momentum loading phenomenon will be discussed further later. The base of the horn has high compressive stresses on the back side (opposite of impact, -Z), near where it meets the skull, and relatively lower tensile stresses on the front, again due to the differences in surface area. This phenomenon is analogous to loading of a curved beam. Eventually, the momentum loading stresses progress to the horn tip, however the stresses now produce a torque on the horn near the tip, which causes horn tip lateral-medial displacement (Figure 15).

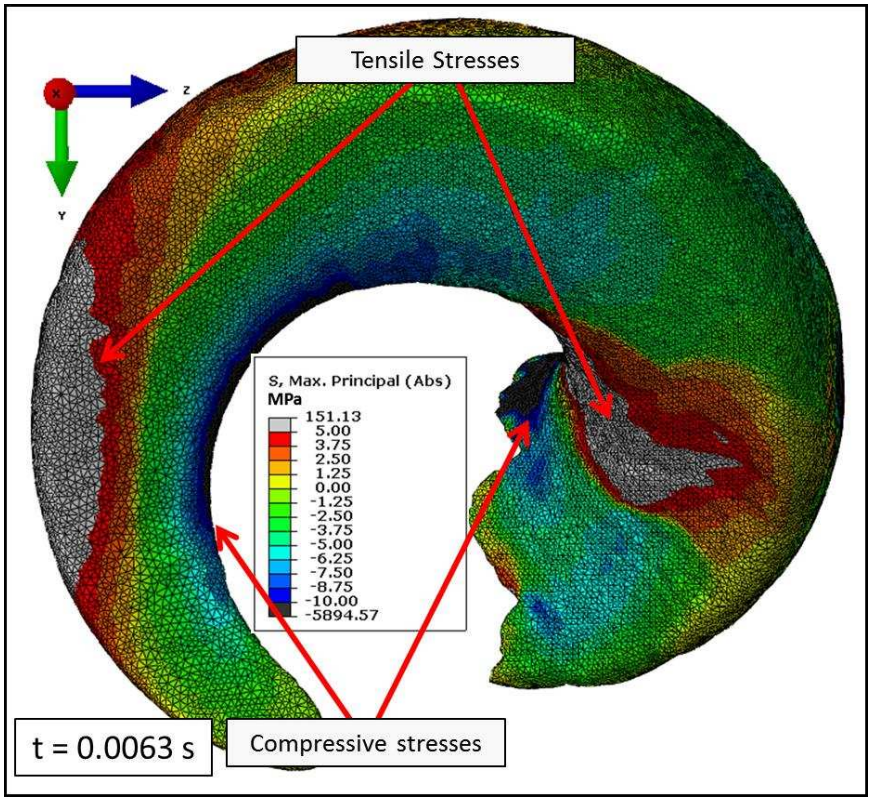

Figure 14: Horn Momentum Loading. Compressive stresses exist at the inner diameter of the horn curl due to momentum loading of the horn and at the base due to bending. Tensile stresses exist at the outer diameter of the horn curl.

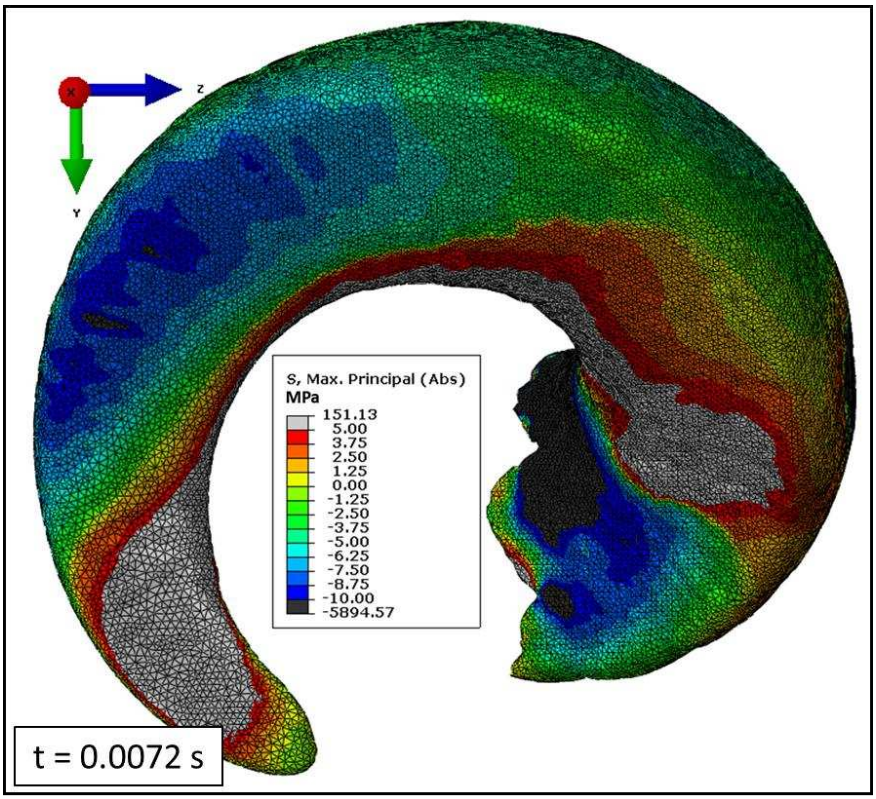

Figure 15: Horn Tip Stresses. The stresses have evolved to the tension compression couple on the same side of the horn, which induces horn tip lateral-medial displacement.

The horncore is essentially loaded as a curved cantilever. The stress is distributed over the horncore with little evidence of localized stress at the impact site. Again, stresses on back (opposite of impact, -Z) surface of the horncore are relatively larger than the front (+Z) due to decreased surface area due to the curved nature of the horncore. The horncore/skull stresses are compressive in the back (Figure 16) and tensile in the front (Figure 17). The highest stresses in the horncore arise at the base, where it attaches to the skull. The tensile stresses at the front horncore base arise where a thick bone plate exists between the two horn cores in the Y-Z plane (Figure 17). Stresses observed in the skull and horncore are much larger than seen in the horn.

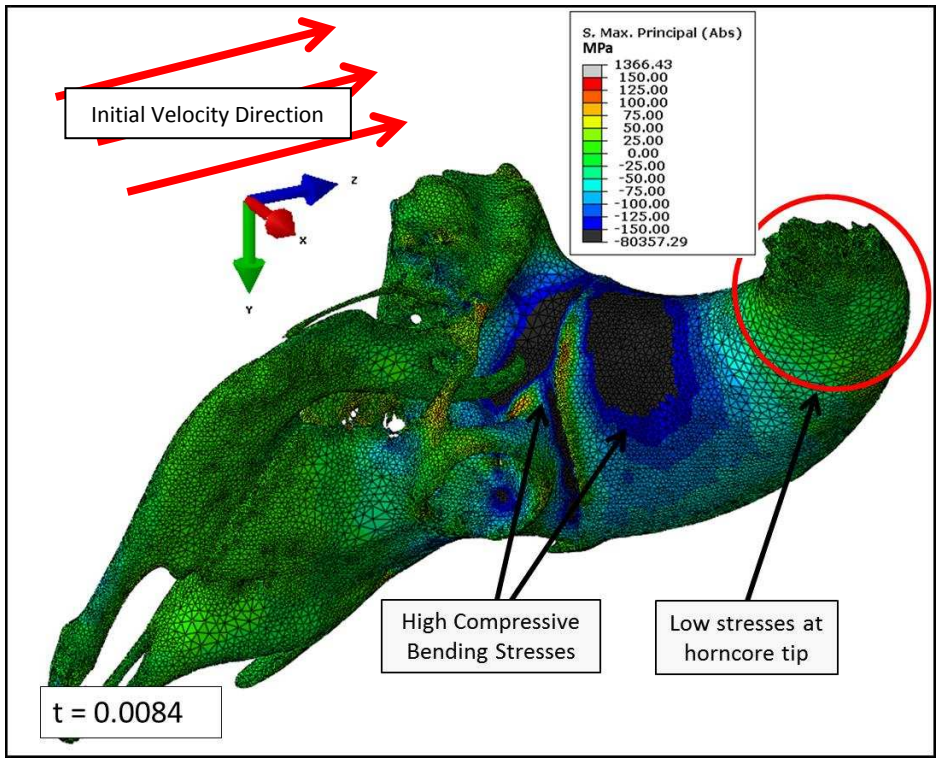

Figure 16: Skull Compressive Stresses. As to be expected, there are compressive stresses on the back (-Z) side of the horncore; the highest of which are located at the base of the horncore where it attaches to the skull.

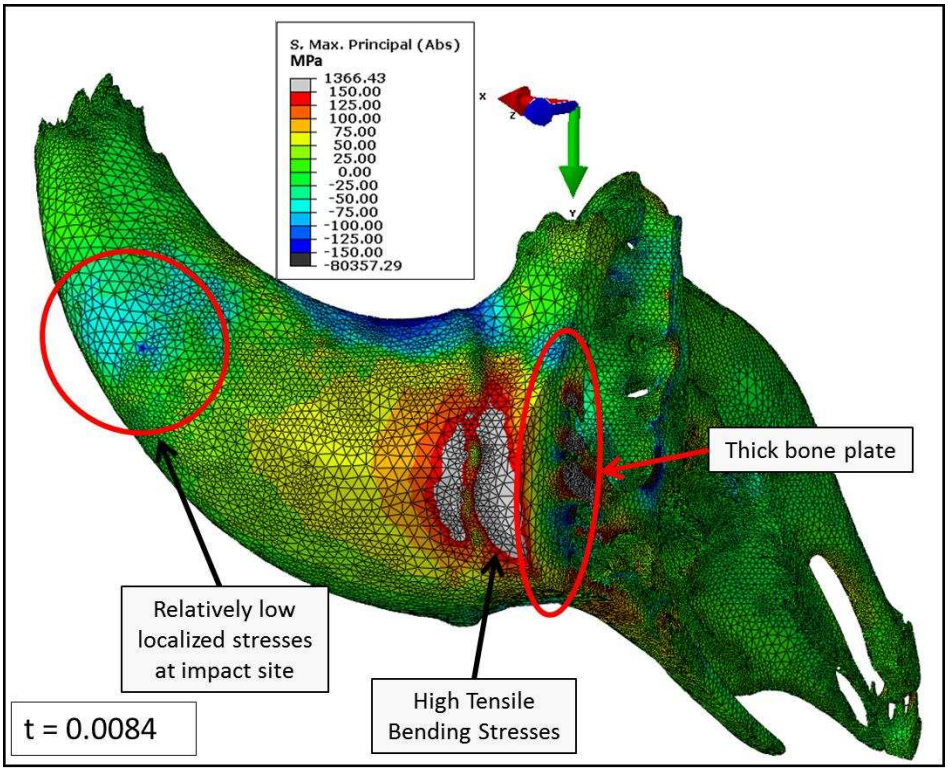

Figure 17: Skull Tensile Stresses. Tensile stresses are present at the front (+Z) portion of the horncore. The largest stress area is located where the horncore meets the skull. Interestingly, this region contains a thick bone plate between the bases of the two horncores.

Horn Dynamic Response

During and after impact, an interesting dynamic response is observed in the horn. Prior to impact, the entire horn moves at the same, constant velocity (Figure 18a) in the +Z direction. During impact, the front portion of the horn decelerates rapidly, however it takes time for the lagging back half of the horn to recognize the momentum change, so it keeps moving forward. This causes the horn to load in a manner similar to a torsion spring (Figure 18b). The unique horn geometry causes this loading to be dissipated as horn tip lateral-medial (side-to-side) oscillations (Figure 18c&d).

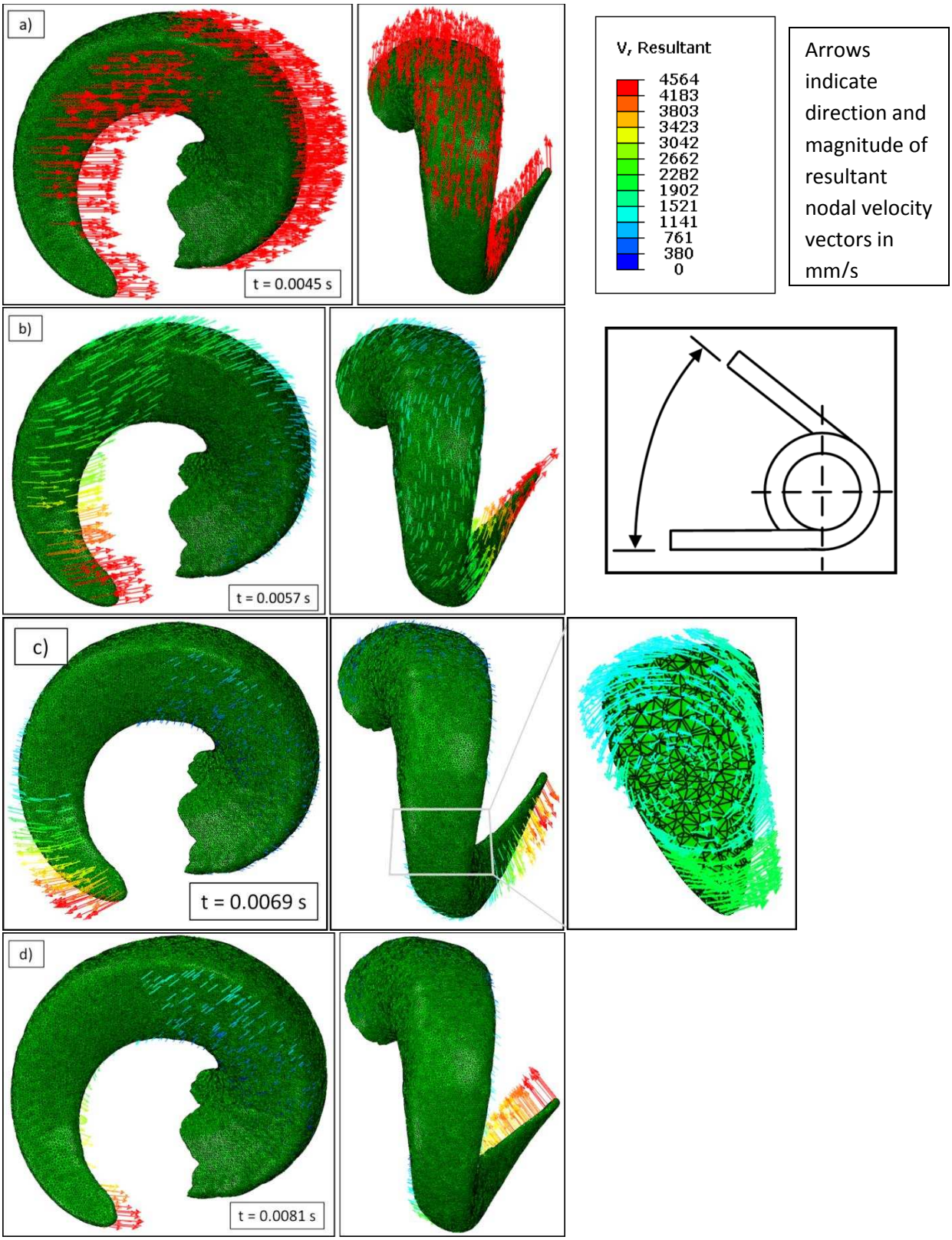

Figure 18: Horn Loading and Tip Oscillation. a) Constant velocity prior to impact b) Horn momentum loading (similar to loading a torsion spring) c) Momentum loading induces lateral horn tip movement (cutout shows a cross section of the horn where torque is produced) d) Side to side horn tip oscillation

This horn loading and unloading phenomenon provided motivation to further investigate the horn's dynamic response resulting from impact. Next, the lateral-medial displacement of the horn tip was observed. This was done by selecting approximately 40 nodes from the tip of the horn and averaging the X-displacement response (Figure 19). A frequency analysis was performed on the horn tip oscillation data to decompose the response into its primary frequencies (Figure 20)

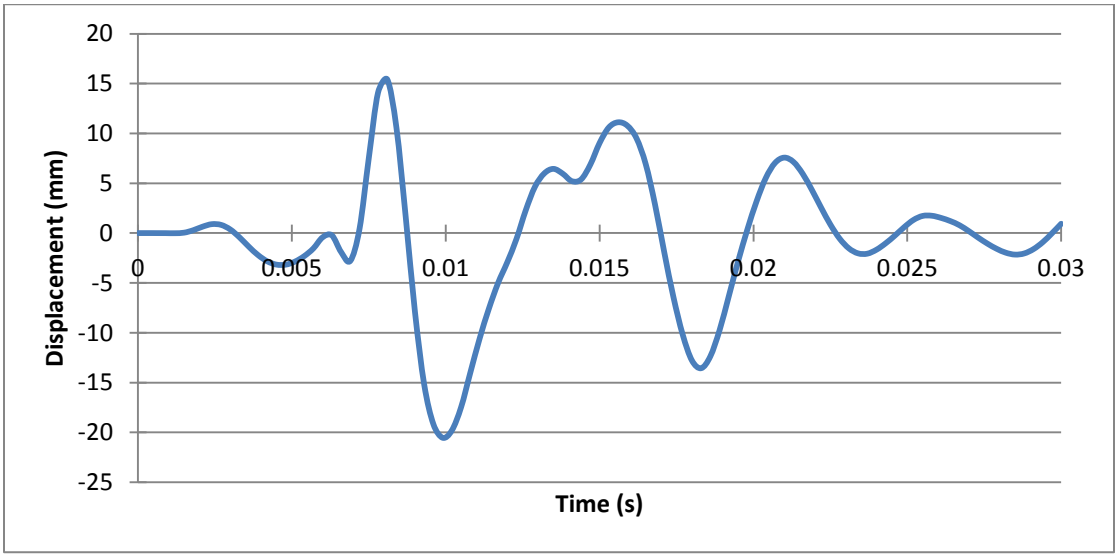

Figure 19: Horn Tip X-Displacement

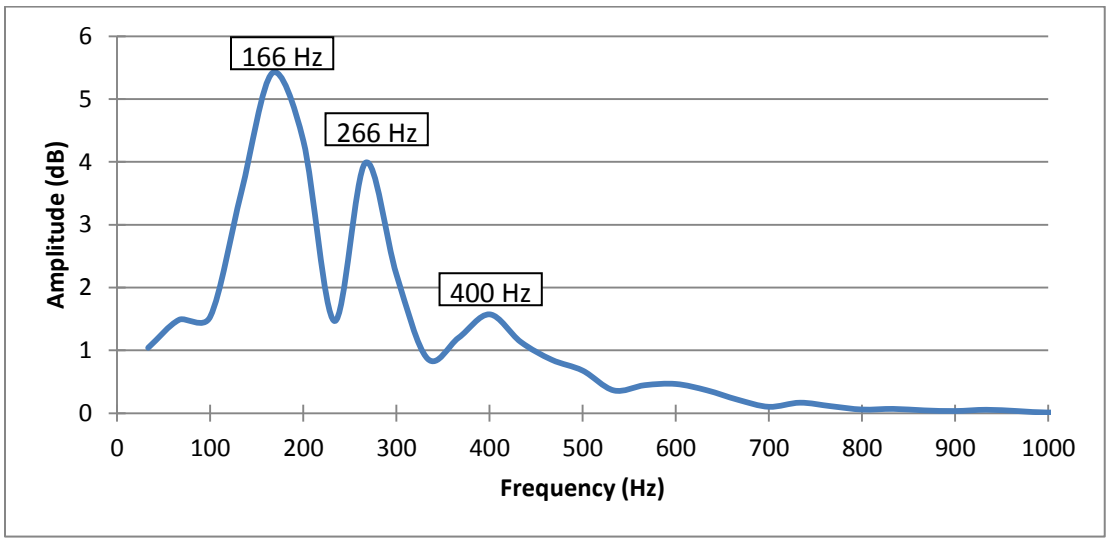

Figure 20: Spectral Measurement of Horn Tip X-Displacement (peaks depict primary frequencies of oscillation)

It should be noted that the horn tip oscillation velocity (X-direction) during impact was in fact higher than the horn tip velocity in the impact direction (Z-direction). During impact the horn tip velocity in the direction of impact peaked at around 12 m/s, whereas the lateral oscillation induced from impact had a peak velocity around 27 m/s.

Energy Analysis

Strain and kinetic energy values for the horn and skull materials, as well as for the whole model, were examined throughout the duration of the simulation. The "Whole Model" includes energy associated with the spine spring/dashpot element, point mass, impact plate as well as the skull and horn, however; energies associated with the horn and skull were of primary interest. The skull mentioned in this section includes all bone material in the model, including the horncore. It was observed that the skull sustained much higher strain energies than the horn (3 times higher) during impact (Figure 21), which is largely due to the higher modulus value of this material. This also implies that the horn distributed the load to the horncore and skull.

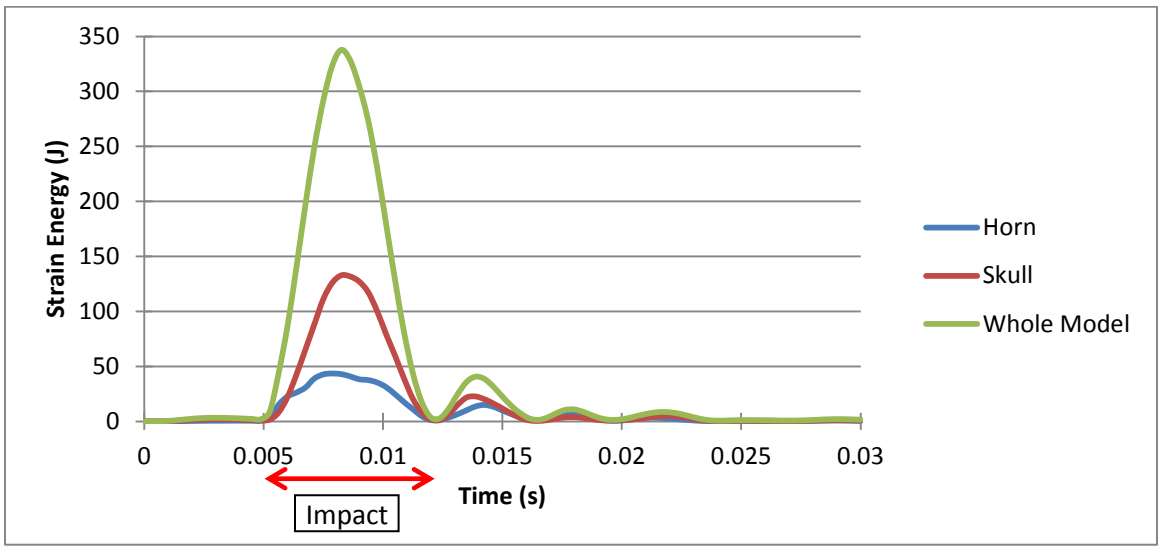

Figure 21: Strain Energies. The skull sustained much higher strain energy than the horn. The remaining whole model strain energy is stored in the impact plate and spine spring.

The majority of the remaining energy of impact in the "Whole Model" data set exists in the spine spring and dashpot elements. This portion of the energy represents the energy absorbed by the animal's body during impact. The peak strain energy of the spring equaled 130 J and the total viscous energy dissipated by the spine dashpot equaled 40 J, for combined peak energy of 170 J which accounts for 31% of the total energy of the model during impact.

The horn had much higher kinetic energy than the skull throughout the duration of the simulation (Figure 22). For the most part, this is not surprising because the horn had a much larger mass. The one interesting observation involving kinetic energy is that there was a notable kinetic energy hump during impact, when the overall velocity would be expected to be very low. This occurred due to the horn side-to-side oscillation that was induced by the initial impact, as evidenced by overlaying horn tip x-velocity magnitude and horn kinetic energy plots (Figure 23). Note that there is almost no kinetic energy in the skull during impact.

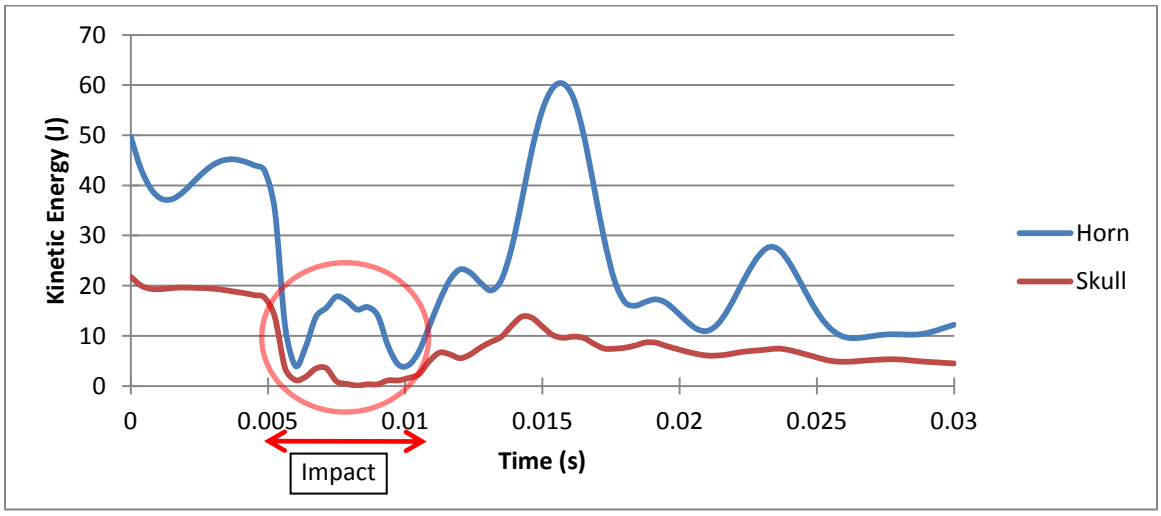

Figure 22: Horn and Skull Kinetic Energies. The horn has much higher kinetic energy, even during impact. Note the kinetic energy hump during impact. The large horn kinetic energy hump after impact results from the combination of the horn recoil velocity (-Z direction) and side to side horn oscillations (X direction).

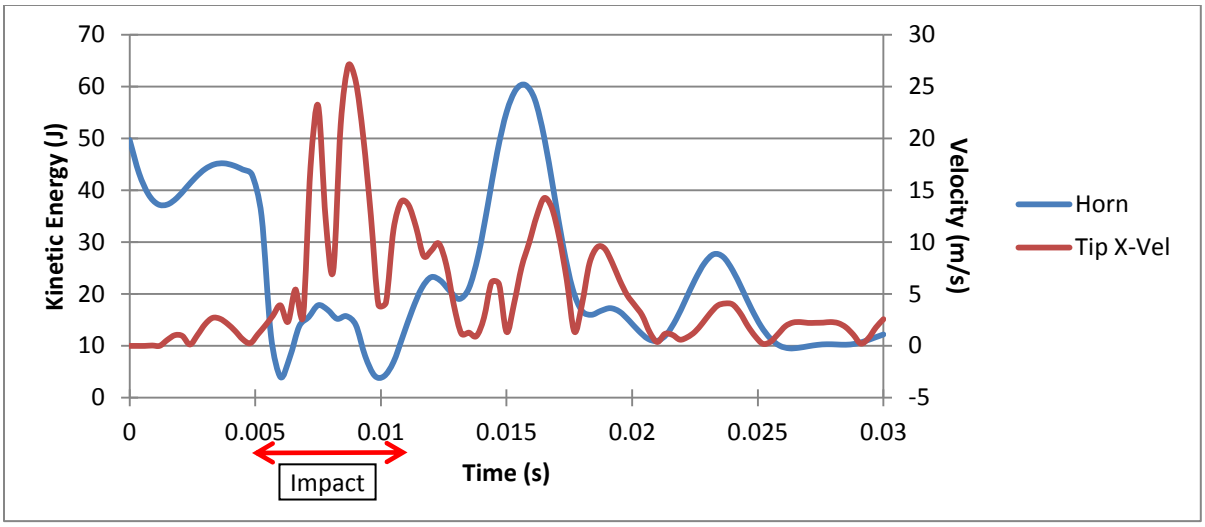

Figure 23: Horn Kinetic Energy and Horn Tip X-Velocity. This plot shows the horn tip x-direction velocity magnitude overlaid on the previous horn kinetic energy plot. This is evidence that the kinetic energy of the horn is in fact partially due to horn side to side horn tip oscillations.

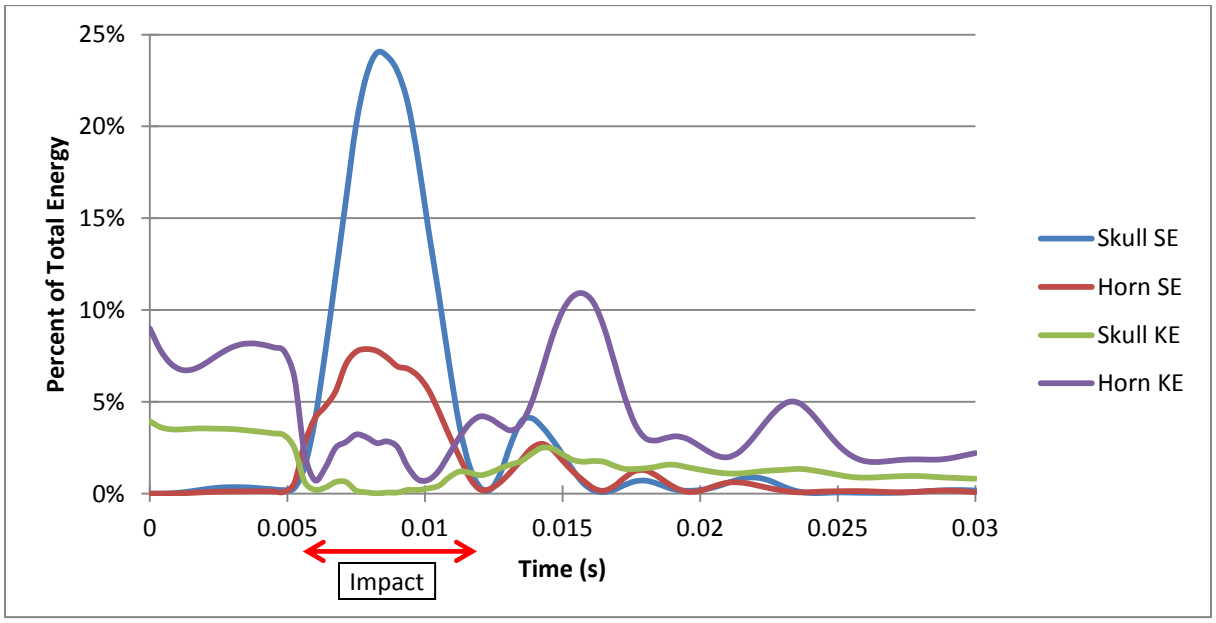

Figure 24: Percentage of Total Energy. Horn and skull kinetic and potential energies as a percentage of the total energy of the model.

Figure 24 portrays the relative energy contributions of different components of the model. The total energy of the entire model remained relatively constant (552.8 J±0.1%) throughout the simulation, which means the model was near energetic equilibrium. Before and after impact, the kinetic energy of the point mass made up the vast majority of the total energy, due to its large mass.

2.4 Methods: Ramming Video Analysis

Two videos that depicted ramming of male bighorn sheep were chosen for video analysis. These videos were chosen because they portrayed relatively forceful impacts, and because they were captured at an angle nearly perpendicular to the camera. Videos were downloaded from youtube.com and links to the videos can be found in Appendix A. The first video was captured at 24 frames per second (fps) and individual frames had dimensions of 1920x1080 pixels. The second video was captured at 30 fps and also had frame dimensions of 1920x1080 pixels.

The videos were imported into Tracker: a free, open source video analysis and modeling tool built on the Open Source Physics (OSP) Java framework. Once imported, the videos were cropped to only include frames of the impacts being studied. Next, the scale was set using a scale bar calibration tool. Using this tool, a known length can be assigned to a portion of the first frame of interest and the image is scaled accordingly. Two different calibration lengths were used to account for the possible error associated with scaling. First, the outer diameter of one of the ram's horn curl was defined as being 380 mm (15 in), which was approximately the outer diameter of the horn curl geometry in the finite element model. An average animal shoulder height was also used to scale the frames, and was given a value of 980 mm (~38 in). Calibration points were another tool used in the analysis and accounted for any pan, zoom or rotation of the camera and also acted as reference points for calculating relative distances traveled. Two calibrations points were chosen for each video, one in front and one behind the animals. Calibration points had to appear in all frames of the impact sequence and had to be easily trackable. Dark colored rocks were typically chosen as calibration points (Figure 25). Relative changes in the distance and angle between calibration points from frame to frame were reflected on the scale bar and coordinate system, respectively, therefore accounting for rotation and zoom

of the camera. Calibration points were tracked using an automated texture recognition tool. Given a template region defined in the first frame, the software automatically searched and found the same region in consecutive frames and marked the point. The tip of the horn was used to represent motion of the ram's skull because it was easily trackable and has close proximity to the impact location. The horn tip of each animal was tracked using the automated technique; however, manual point tracking was required in some instances. The horn tip position relative to the calibration points was used to determine horn tip displacement between frames, therefore the calibration points served as points of reference as well.

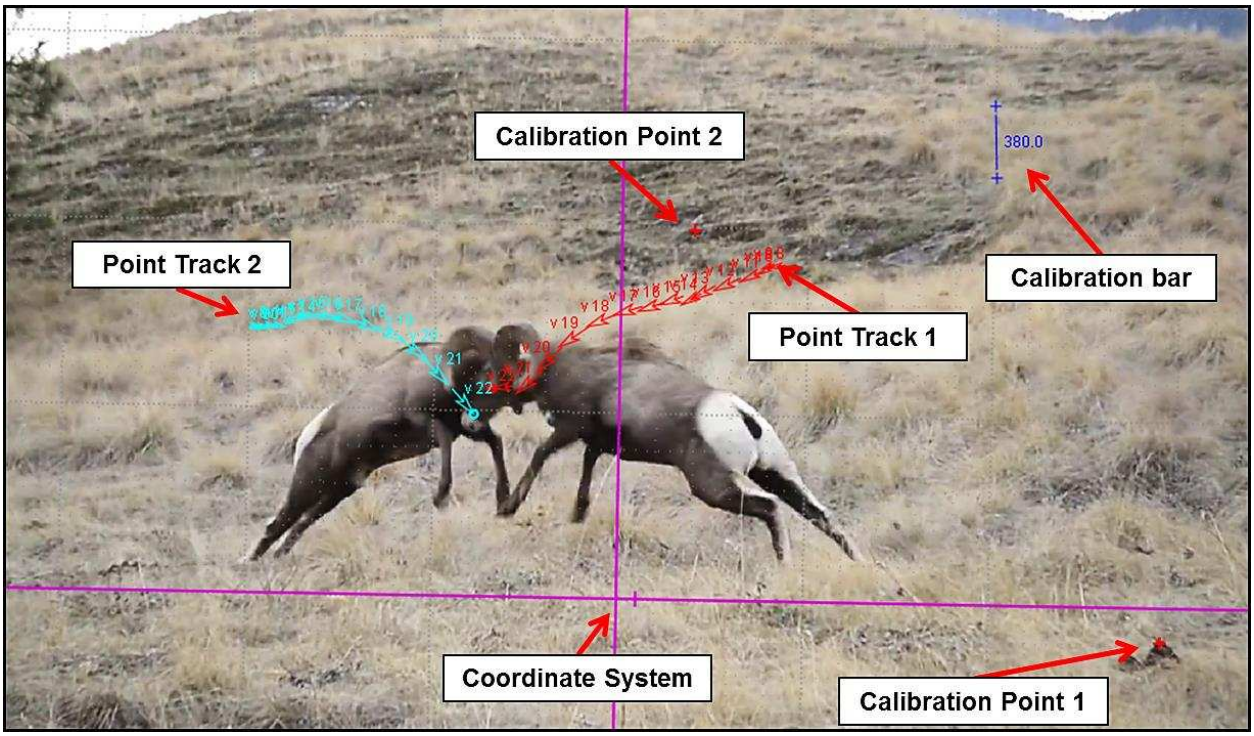

Figure 25: Ramming Video Analysis. Attribution: Tony Bynum Photography: https://www.youtube.com/watch?v=V__T34iqNOA

A perspective filter was applied to all frames of one of the ramming sequence videos to account for the out of plane motion of the rams. This filter can correct the distortion that occurs when an object is not photographed perpendicular to the camera. To apply this filter, a quadrilateral was created outlining the two rams and was then distorted into a rectangle which essentially makes

the two rams appear to be the same size and appear in the same plane, even though the video was captured slightly out of plane. This filter is applied after the calibration is set, so distances traveled are also distorted accordingly. The video of the second ramming sequence occurred nearly perpendicular to the camera, so a perspective filter was not necessary.

Horn tip velocity was calculated in the X-direction, Y-direction and as a magnitude by dividing the respective displacement value by the step time between frames (Δt). Accelerations of the horn tip were calculated in a similar manner, but instead dividing the calculated velocity values by Δt. It should be noted that the step time creates a limitation on the ability to accurately predict velocity values which has an amplified effect on the corresponding accelerations. This limitation has the effect of underestimating peak accelerations. An estimate of total horn-to-horn contact time was generated using the velocity values as well as measured distances between the horns in frames just before and after impact. For this calculation, the time required to travel the measured distance between the animals' horns (assuming constant velocity) before and after impact was subtracted from the total frame time. This resulted in a rough approximate for total horn-to-horn contact time. Again, frame rate was a major limitation to this estimate.

2.5 Results: Video Analysis

The video analysis results that convey the most information about the impact are presented graphically in this section. First, the X and Y coordinates of each animal is reported to get an idea of the general trajectory of each animal's head during a ramming sequence. In the first video, the impact is very direct (primarily X-direction motion) and symmetric. The heads of both animals rebound backward and slightly downward after impact. This is not the case in the second

video. The impact is not as direct and the head of the right animal recoils up (+Y) and backwards and the head of the left ram deflects down (-Y) and backwards.

As the rams approach one another, their velocity increases gradually at first, and then increases dramatically just before impact, as they thrust themselves at one another. This is evidenced by the plots of velocity magnitude and the X-component accelerations. The Video 1 X-component acceleration plot clearly shows the thrust and rapid deceleration due to impact by a hump in the acceleration value in one direction followed by a sharp spike in the opposite X-direction.

There are two different values presented for contact time: the maximum contact time and the estimated contact time. To determine the upper limit of contact time (maximum contact time), the time difference was taken between frames that were distinctly before and distinctly after contact. The estimated contact time was calculated using velocities measured before and after impact and distances measured in the films, as described in the methods section (2.4).

Video 1

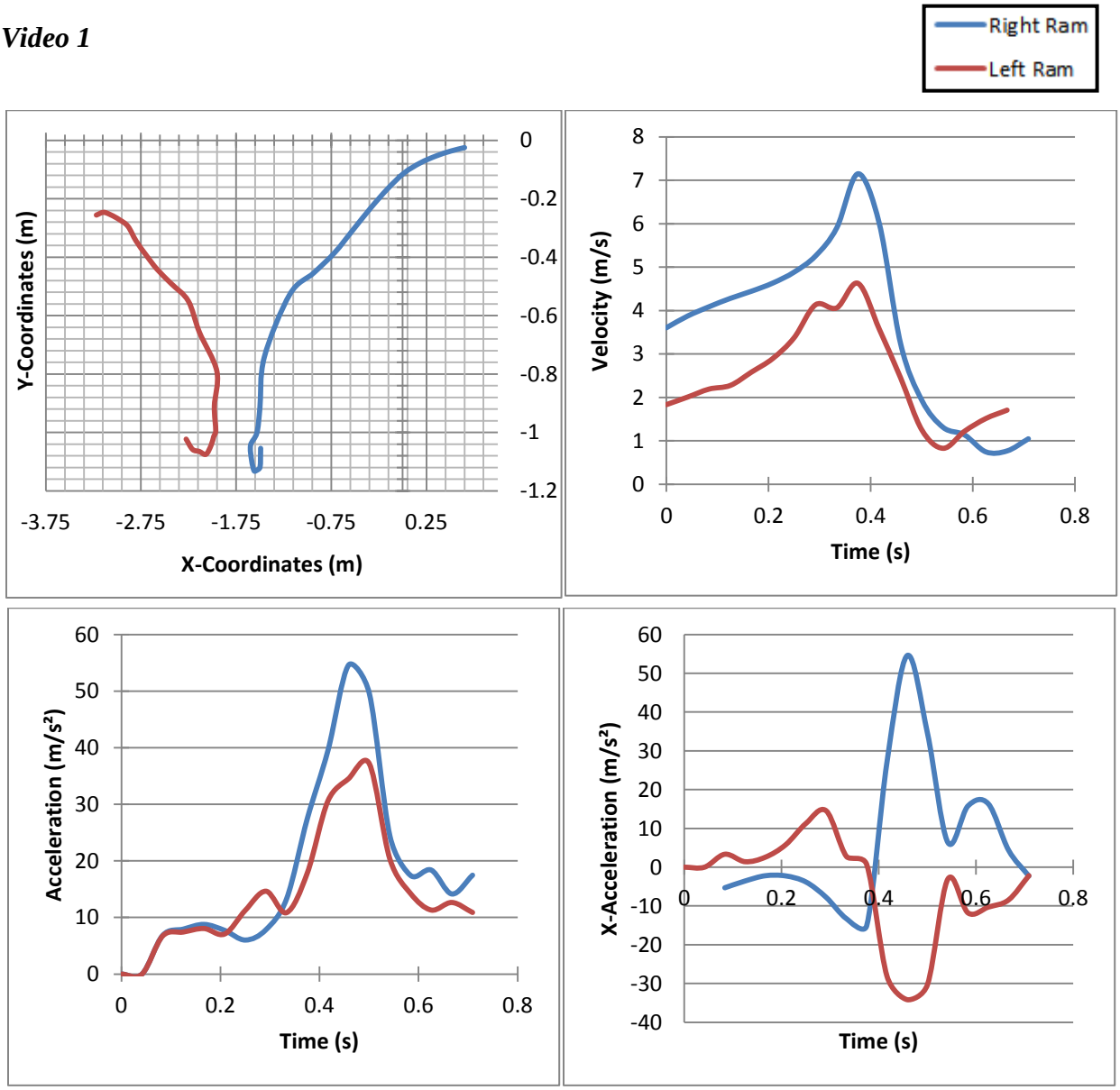

Figure 26: Video 1 Dynamics Plots. The right ram was delivering the blow in this ramming sequence and this is evidenced by the larger accelerations and velocities observed. Impact occurred at around 0.375 seconds. In the X-Acceleration plot you can see a distinct peak in one direction followed by a larger peak in the opposite x-direction. This describes the final lunge prior to impact and the subsequent deceleration due to impact.

Table 2: Video 1 Results

	Contact Time Estimate (s)	Maximum Contact Time (s)	Impact Velocity (m/s)	Peak Acceleration (m/s^2)
Right Ram	0.015	< 0.083	7.1	54.6
Left Ram	0.015	< 0.083	4.6	34.2

Video 2

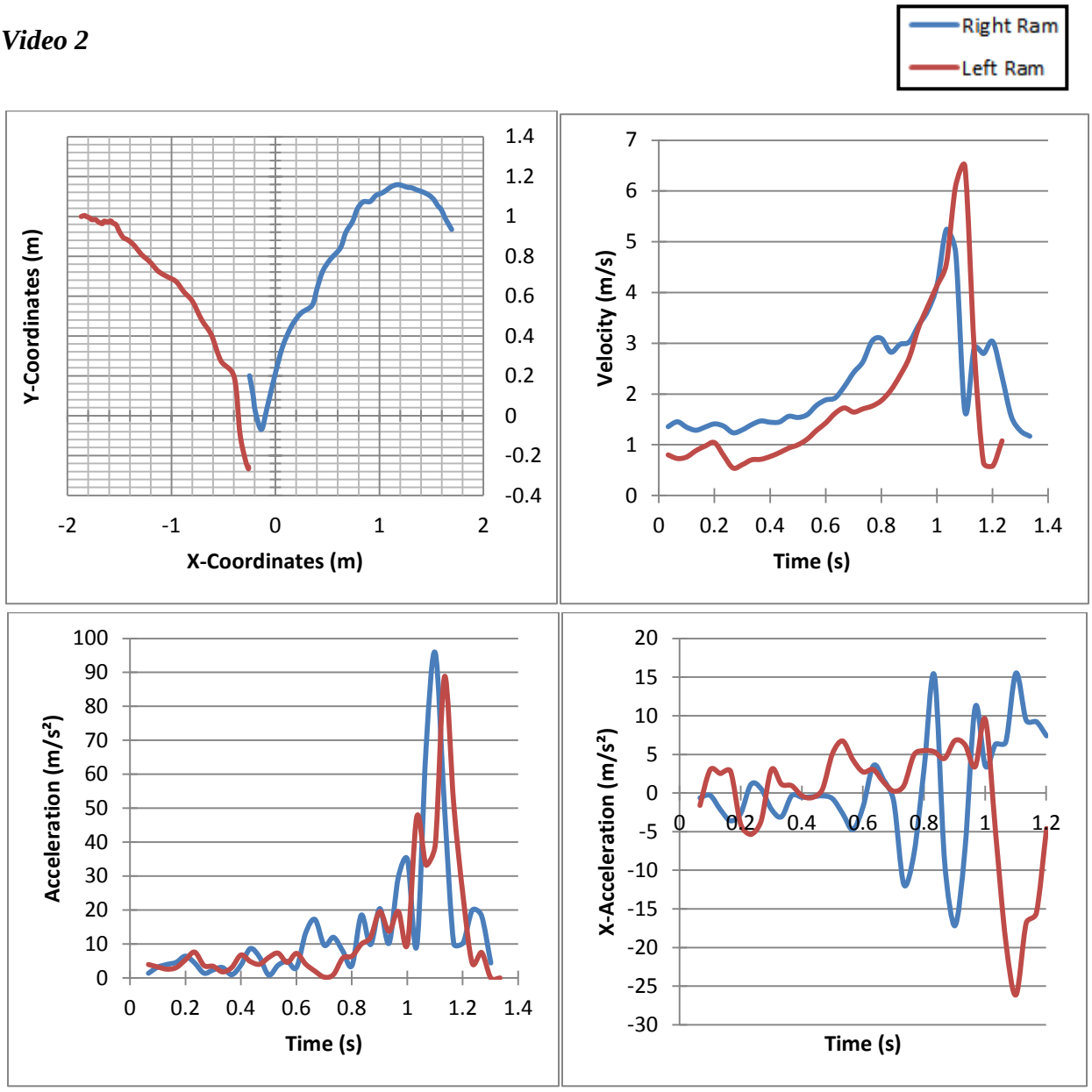

Figure 27: Video 2 Dynamics Plots. In this ramming sequence the head of the right ram jarred upward after impact and the head of the left ram downwards (coordinates plot). Impact occurred at around 1.1 seconds.

Table 3: Video 2 Results

	Contact Time Estimate (s)	Maximum Contact Time (s)	Impact Velocity (m/s)	Peak Acceleration (m/s²)
Right Ram	0.037	< 0.067	5.2	95.7
Left Ram	0.037	< 0.067	6.5	88.8

2.6 Discussion: Impact

Role of Horn Keratin

The finite element impact model results indicate that the horn material distributes the highly localized impact stress over a large surface area in the horncore as cantilever-like bending. There are multiple benefits to this loading scenario. First, horn material displays a large degree of toughness [35], so it is better suited to withstand the localized load at the impact site than the more brittle bone material. Next, by distributing this load over the horncore bone, the relatively high load bearing capability of bone is recognized. In general, it seems that the horn also directs some of the energy of the impact away from the center of the skull, as strain energy as well as kinetic energy in the form of horn tip oscillations. The peak strain energy in the horn during impact is 44 Joules and the maximum kinetic energy is 18 Joules. In contrast, the peak strain energy in the skull and horncore (bone material) during impact is 132 Joules with a maximum kinetic energy of only 3.5 Joules. This indicates that the dynamic response of the horn is an important aspect of the loading regime.

Role of Horncore Bone

The horncore is essentially loaded as a curved cantilever beam with a nearly circular cross-section. The strain energy present in the bone during impact is very large (24% of total impact energy), with significant stresses present at the base of the horncore. These results indicate that the role of the bone is to sustain the bulk of the load at the peak of impact. Therefore, the horncore is a vital structural component and its presence is essential to prevent the horn from failing catastrophically. The bone material in the model (horncore and skull) stored a maximum strain energy of 132 Joules during impact, and impacts with energy inputs between 45 and 113

Joules are likely to cause fracture in human skulls [36]. Therefore, the skull of a ram is better equipped for impact loads than the human skull. The solid, cortical bone of the horcore structure is concentrated at the outer diameter of the nearly circular cross-section, while the interior is filled with the porous bone strut architecture (Figure 28). This configuration is ideal for sustaining the complex combinations of bending and torsional loads sustained during ramming, while allowing the structure to have minimal weight.

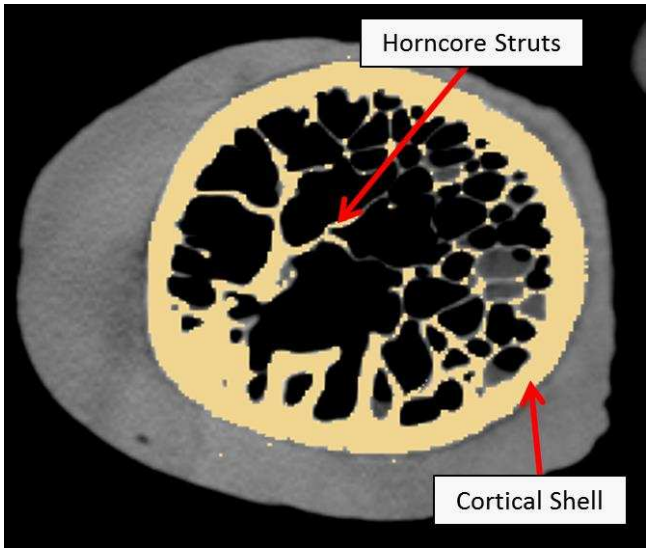

Figure 28: Horncore Cross-Section.

Curvature

The curved nature of the horn and horncore allows for a larger area of high compressive stresses to occur on the inner diameter of the curl than the area of high tensile stresses that occurs on the outer surface, due to differences in surface area. As mentioned, there exists a region of high tensile stress in the front of the horncore and a region of high compressive stress on the back surface. The average stresses during impact in both of these regions is around 200 MPa, however the compressive region occupies approximately 52% more area than the tensile region. Therefore, much more of the bending load is sustained in compression and this could be

advantageous, as bone displays higher strength in compression than tension. The curvature of the horn keratin forms nearly a full circle, and during loading the back portion of the curl decelerates at a slower rate than the impacting, front portion. This produces momentum loading of the horn which creates a stress state similar to that of a loaded torsion spring, with compression on the inner diameter and tension on the outer diameter. This loading mechanism distributes energy away from the brain cavity and likely helps prevent brain trauma.

Horn Dynamic Response

During and after initial impact, the horn undergoes an intriguing dynamic loading and unloading sequence. Initially, the momentum of the lagging back half of the horn causes it to load in a manner similar to a torsion spring. The strain energy stored in this initial phase is next translated into kinetic energy, in the form of side-to-side (lateral-medial) horn tip oscillations. This phenomenon is interesting in that it essentially changes the direction in which the energy is traveling. Converting some of the Z-direction (impact direction) energy created by ramming into X-direction (side-to-side) horn tip oscillations could reduce subsequent forces in the brain cavity. Furthermore, side-to-side horn tip vibrations would likely produce forces that cancel one another, whereas front to back vibrations would not. Much of the kinetic energy associated with lateral-medial horn tip oscillations may be quickly dissipated as heat via hysteretic damping. Energy dissipated in the horn is surmised to be beneficial in preventing brain trauma as it is directed away from the brain cavity. The progression of strain and kinetic energy through the horn towards the tip promotes energy dissipation in the horn, rather than in the skull and brain, which could harm the delicate tissue.

Video Analysis

The peak velocities and accelerations observed in this study are higher than those stated in previous literature, however average velocities were similar (Previous study: 4.7m/s, Current study: 5.85 m/s). Studies carried out with more primitive means in 1985 recorded maximum impact velocities and accelerations of 6 m/s and 34 m/s², respectively [17]. On the other hand, the present study resulted in maximum impact velocities and accelerations of 7.1 m/s and 95.7 m/s². High acceleration values were recorded for the second video (88.8 & 95.7 m/s²) and this could be due, in part, to the higher frame rate that this video was captured at. Recall that the frame rates of the videos in this study were 24 and 30 frames per second, respectively. A smaller time difference between frames would result in higher, more accurate acceleration estimates for the same impact. Also, in the second video, the head of the right animal jolted upward and the left animal downward, creating motion that was relatively unhindered by the mass of the animal's torso. This creates a high Y-direction acceleration that would not be present in an ideal, 1-dimensional impact. Researchers employing video analysis techniques in a previous study stated values of maximum force produced during impact, however these are likely inaccurate due to the low frame rate of videos used (large Δt between video frames). The actual horn deceleration upon impact occurs over a time span much smaller than what typical videos can resolve. After performing video analysis and realizing the variability in results, and large frame rate limitations it is recommended that different means of estimate peak fighting forces be used. At a minimum, videos taken at very high frame rates should be used for future video analysis if peak forces or accelerations are of interest. That being said, it is believed that this technique is useful for estimating velocities prior to impact, and the presented velocity results correlate well with previous literature.

The highest impact velocity observed was 7.1 m/s, which is about 16 miles per hour. The fastest NFL football players can reach top velocities around 20 miles per hour during a 40 yard sprint, and typical hits likely occur at velocities substantially lower than this. Mature male bighorn sheep can weigh between 200 and 300 pounds, which is a weight range that many professional football players fall into. Therefore, impacts produced by bighorn sheep during ramming are likely very similar to relatively hard hits produced in professional football. Brain injuries are a major issue in professional football and often result from head to head contact. The similarities in the scale and the nature of impacts in bighorn sheep ramming and NFL football hits should provide motivation for further research in this area.

Chapter 3 - Geometric Feature Analysis

3.1 Introduction: Geometric Feature Analysis

This section aims to inspect the relative structural and energy dissipative contributions of two geometric features of the bighorn sheep horn and skull. The spiral of the horn and the 3D bone strut architecture within the horncore are the geometric features of interest. It has been hypothesized that the tapered spiral geometry of bighorn sheep horns provides some means of injury prevention during impact. Also, the unique architecture and size scale of horncore spongey bone (when compared to traditional trabecular bone) and its proximity to the impact site imply that this structure has been evolutionarily adapted to sustain ramming. Three separate models were created and subjected to the same impact load to analyze comparatively the contributions of these geometric features. The first model was the full impact model (*Full Model*), which included all geometric features of the horn and skull and was discussed in detail in Chapter 2. The *Full Model* served as the baseline or control model for this study. The second model had approximately one half of the overall horn length removed (*Cut Horn Model*), but was otherwise identical to the first. For the third model, all bone struts and plates within the horncore were manually removed (*No Struts Model*), leaving only void space within the horncore's cortical shell. All other geometric features were left intact, including the full horn curl. Several output parameters were compared between the three models, including brain cavity accelerations and strain values. Concussion input variables were of primary interest in this study and relative comparisons of translational and rotational acceleration values between models were the key results.

3.2 Methods: Geometric Feature Analysis Model Development

The *Full Model* (Figure 29a) in this study is identical to the impact model developed in Chapter 2, and served as the control. Many of the techniques used to develop the three models in this study are the same as discussed in Chapter 2 and will not be reiterated. This section will instead focus on modifications that were made to the *Full Model* to create the *Cut Horn Model* and *No Struts Models* (Figure 29).

The *Cut Horn Model* (Figure 29b) was identical to the *Full Model*, but with one half of the circumferential horn length removed. To remove the posterior portion of the horn, the nodes and elements of this section were simply deleted. The nodes and elements of remaining horn and skull mesh were renumbered to eliminate any potential continuity issues. It also would have been possible to remove the posterior portion of the horn within the segmentation software (3D Slicer) or within the meshing software (ICEM CFD) to create a smooth cut; however, these techniques would have required remeshing the geometry. Simply deleting the elements and nodes of the posterior horn portion left the remaining mesh unaltered from that of the *Full Model*, which eliminates any potential error due to mesh differences. All other aspects of the model (i.e. boundary conditions, material properties, initial velocity, etc.) remained identical in the *Cut Horn Model* as were developed for the *Full Model.*

Creating the *No Struts Model* (Figure 29c) was not as simple as creating the *Cut Horn Model.* Removal of the horncore bone struts was performed manually within the segmentation software (3D Slicer). To do so, a paint style deletion tool was used to remove the material within the horncore that had been previously assigned as bone material.

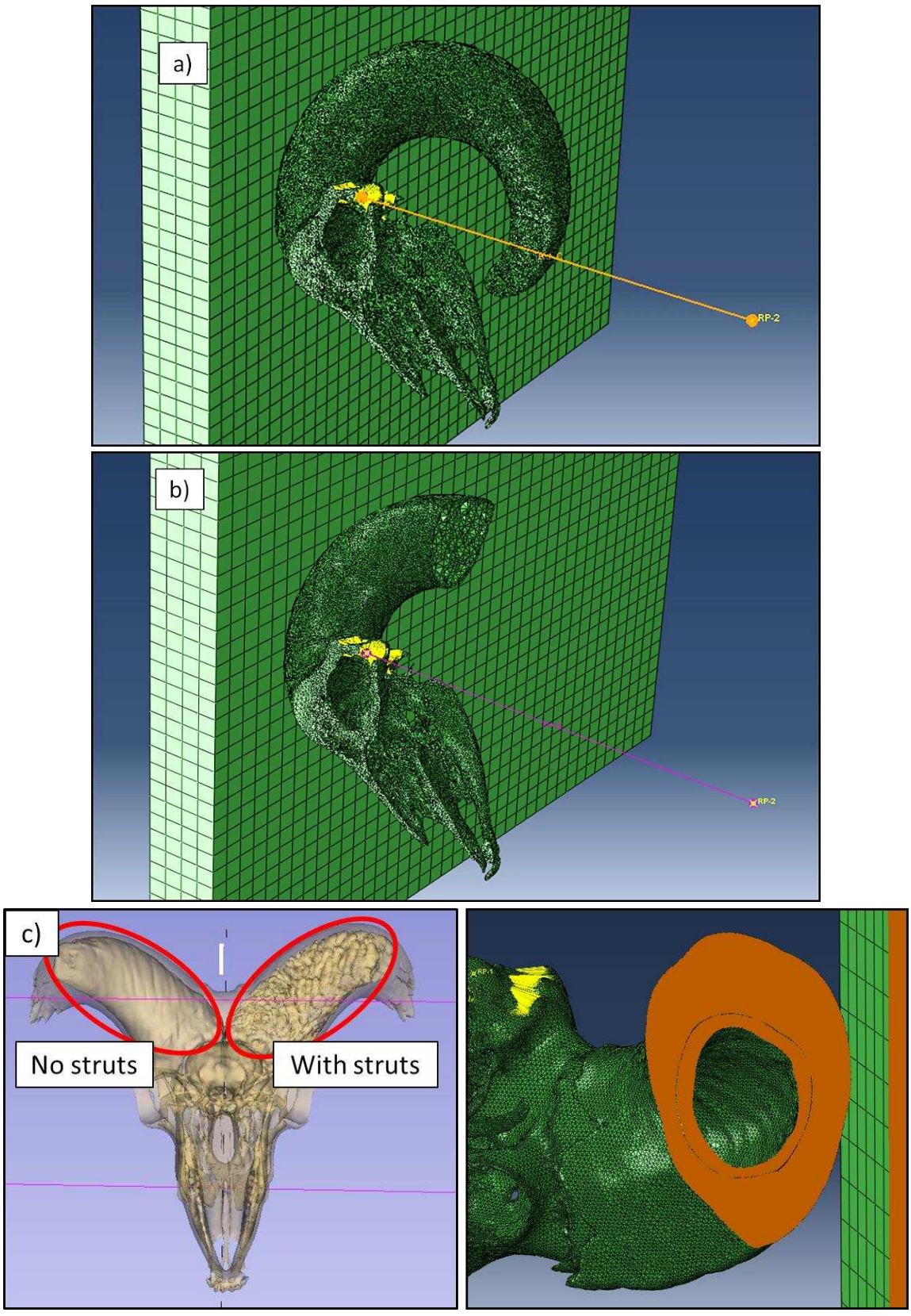

Figure 29: Geometric Feature Analysis. a) *Full Model* b) *Half Horn Model* c) *No Struts Model* (Left: semi-transparent comparison of horncore with and without struts. Right: cross-section of horn and horncore without struts)

Removal of the horncore trabecular like bone was done slice by slice for every DICOM image containing bone struts, with extreme care being taken to not remove any cortical bone thickness. The same smoothing parameters were applied to the segmented bone labels as were used for the *Full Model* geometry in generating the 3D surface model. Also, the same meshing parameters were applied in generating the tetrahedral mesh to reduce potential errors associated with varying the mesh density. Note that the geometry and mesh of the horn remained unaltered in this model and were identical to that of the *Full Model*; only the skull geometry was modified. The mesh of the skull, lacking horncore struts was imported into Abaqus CAE and the conditions applied to the *Full Model* and *Cut Horn Model* were replicated following the guidelines outlined in Chapter 2. To summarize, three separate models were generated with specific geometric features removed from two of the models with all other aspects being identical. The one caveat is that the half skull mesh of the *No Struts Model* was slightly different than the other two due to the process of removing the struts, but had a very similar mesh density.

3.3 Results: Geometric Feature Analysis

Translational Accelerations

This study was primarily aimed at determining the effect of removing geometric features on acceleration magnitudes within the brain cavity. Translational and rotational accelerations of the brain are generally considered to be the primary impact variables influencing brain trauma. Translational accelerations were measured at 5 locations on the inner surface of the brain cavity, as described in section 2.2. These 5 locations consisted of 40 nodes each, and the average of these nodes was considered to be the acceleration value at the location. All of the 5 locations showed the same general trends, so the average plot of all 5 locations is provided (Figure 30).

Both the *Full Model* and *Cut Horn Model* display large peak acceleration upon initial impact, however the value of this peak is about 49% higher in the *Cut Horn Model*. This indicates that the presence of the posterior or back portion of the horn reduces the potential for brain trauma. Smaller acceleration peaks are present throughout the remainder of the simulation and are likely due to vibrations produced by impact. The acceleration responses are quantified as peak value, average value, and the area under the acceleration curves.

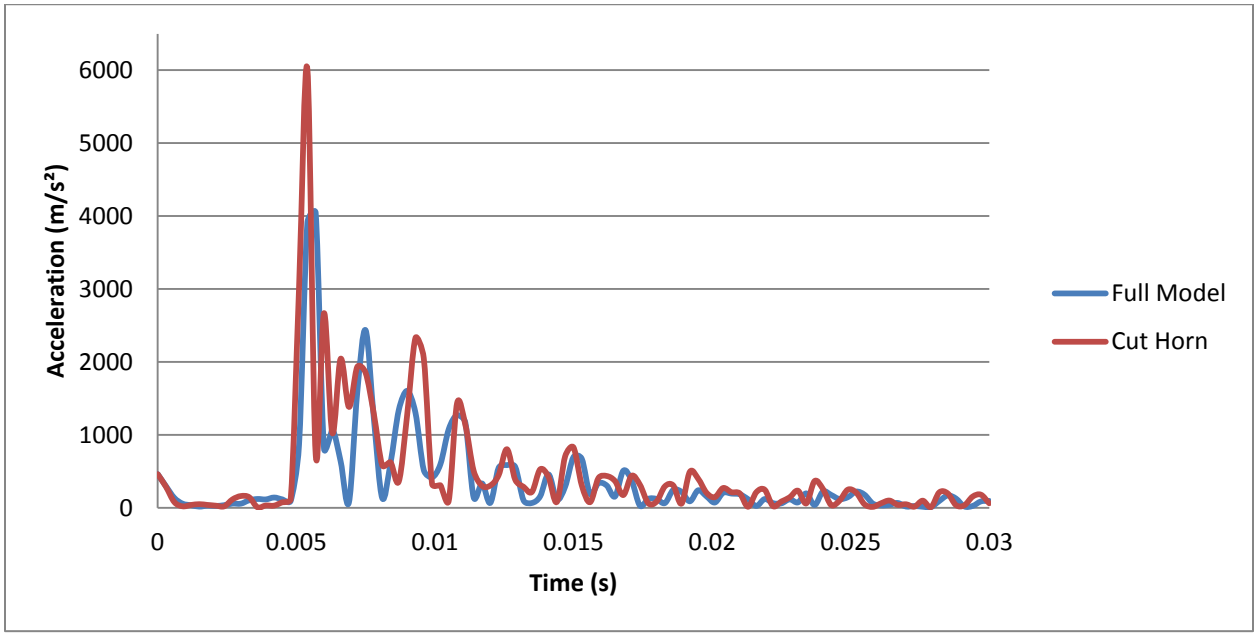

Figure 30: Full Model and Cut Horn Model Translational Brain Cavity Accelerations

The response of the *No Struts Model* (Figure 31) was much different than the *Full Model* and *Cut Horn Model*. There was no large acceleration peak observed upon initial impact in the *No Struts Model*, however; there were several large acceleration peaks throughout the duration of the simulation. This occurred because the structural rigidity of the *No Struts Model* was drastically reduced due to the lack of supportive struts. This is evidenced by the large deformations sustained by the horncore in this simulation, which will be discussed in detail later. Sustained

high accelerations could also be predictive of brain injury, so average accelerations and the area under acceleration curves are particularly telling for the *No Struts Model* (Table 4).

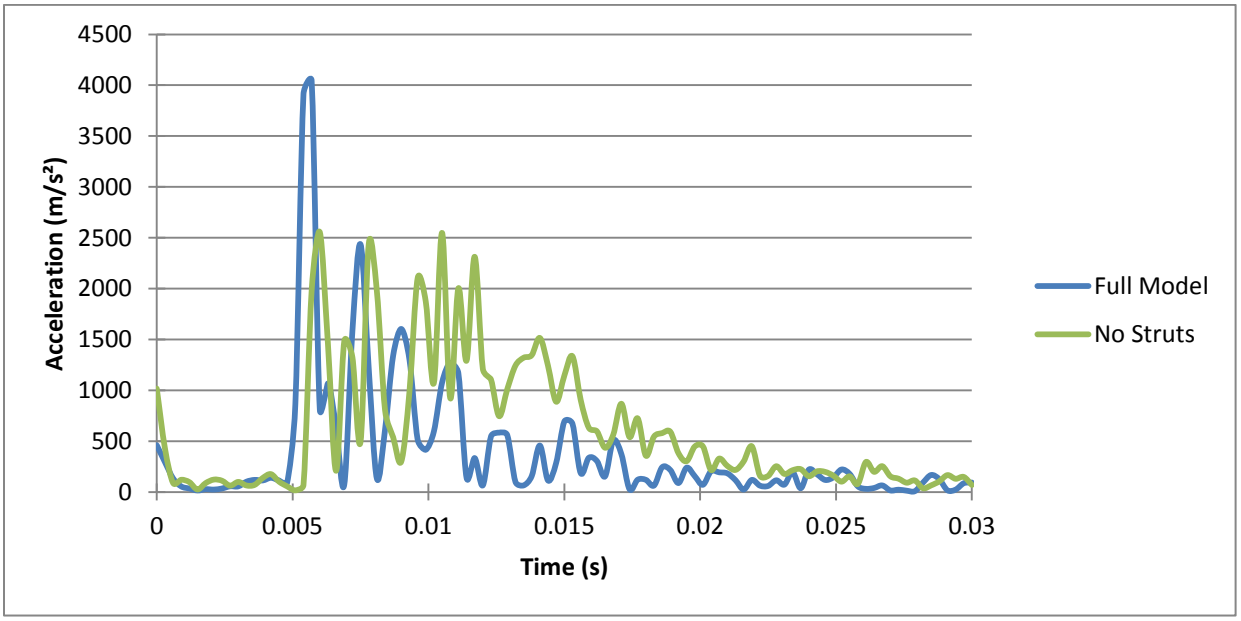

Figure 31: Full Model and No Struts Model Translational Brain Cavity Accelerations

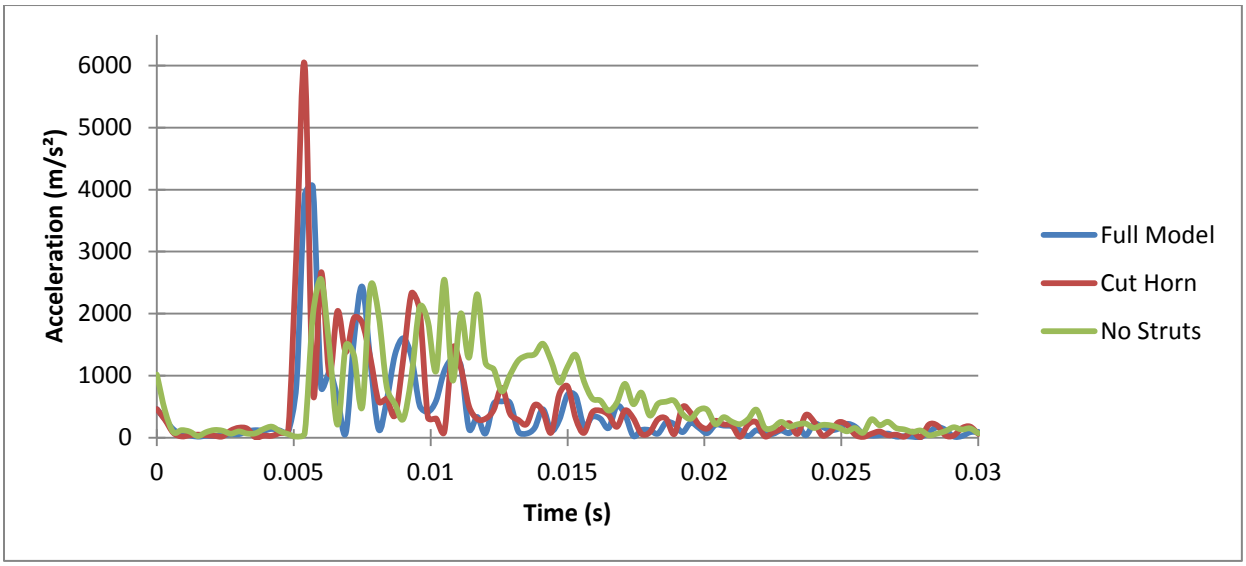

Figure 32: All Models Translational Brain Cavity Accelerations.

Table 4: Translational Acceleration Values

	Translational Accelerations (m/s²)					
	Maximum		Average		Area Under Curve	
	Value	%Δ	Value	%Δ	Value	%Δ
Full Model	4043.24	-	394.8974	-	1.32E+08	-
Cut Horn Model	6014.59	+49%	482.6087	+22%	1.62E+08	+22%
No Struts Model	2555.51	-25%	620.5578	+57%	2.07E+08	+57%

These results show that despite the *No Struts Model* lacking large initial peak acceleration, it still exhibits larger sustained accelerations than the *Full Model*, as evidenced by the large increase in area under the acceleration curve (+57%). Both modified models showed significantly larger average brain cavity translational accelerations throughout the simulation. This indicates that there is a larger potential for damage to the brain in these situations, assuming that translational accelerations cause brain trauma.

Rotational Accelerations

Rotational accelerations were taken at one reference point located in the center of the brain cavity that was linked to all nodes of the brain cavity's inner surface by a kinematic coupling constraint as described in section 2.2. This technique was used because continuum finite elements do not have rotational degrees of freedom, therefore the method used to record translational accelerations could not be used. There was not a dramatic difference in the peak rotational accelerations of the *Full Model* and *Cut Horn Model*, however there were more large peaks observed after impact in the case of the *Cut Horn Model*, which increased the average rotational acceleration value throughout the simulation.

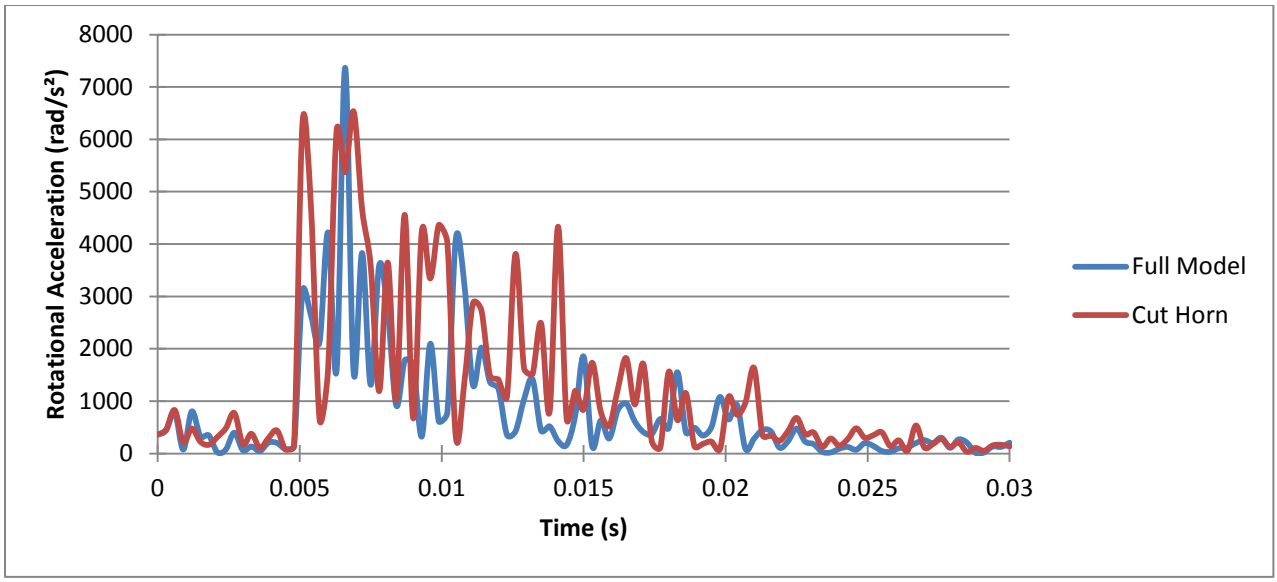

Figure 33: Full Model and Cut Horn Rotational Brain Cavity Accelerations

The rotational accelerations observed in the *No Struts Model* were dramatically higher than the *Full Model* or *Cut Horn Model* throughout the entire simulation (Figure 35, Table 5). This implies that the bone struts in the horncore provide support that resists rotation of the brain cavity. It should be noted that the *No Struts Model* is not identical to the other two, as a new mesh was generated to produce model. Some of the increase in rotational acceleration could be due to the slightly different mesh and different node locations for boundary conditions and constraints. That being said, an effort was made to use approximately the same number of nodes in similar locations for neck and skull boundary conditions and constraints in the *No Struts Model* as in the *Full Model*. Therefore, this drastic change in rotational accelerations in the *No Struts Model* is considered to be primarily due to the lack of horncore internal bone struts.

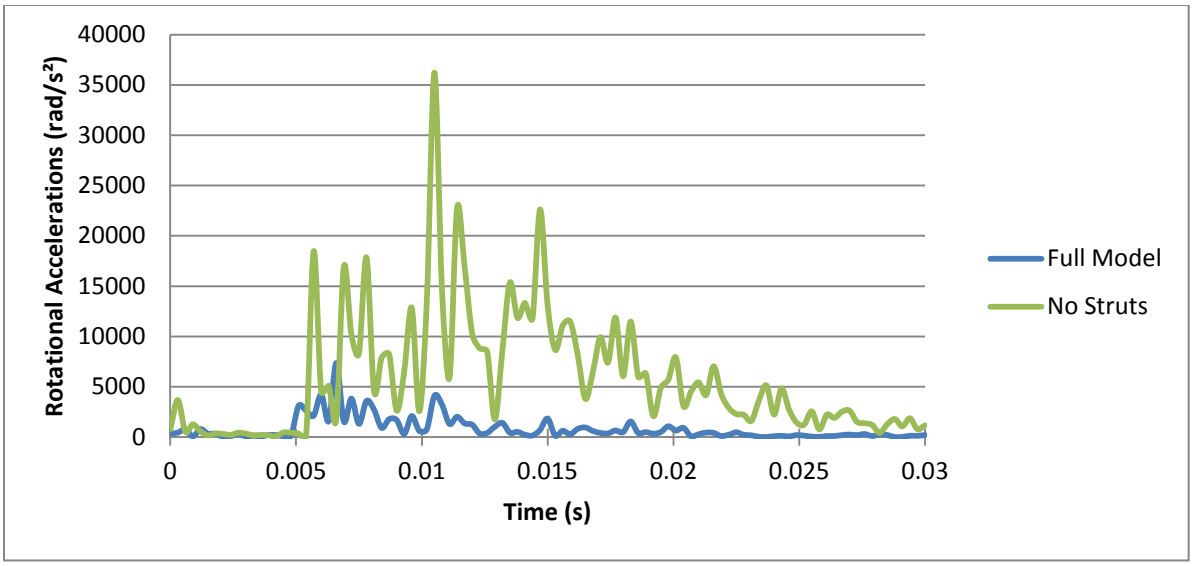

Figure 34: Full Model and No Struts Model Rotational Brain Cavity Accelerations

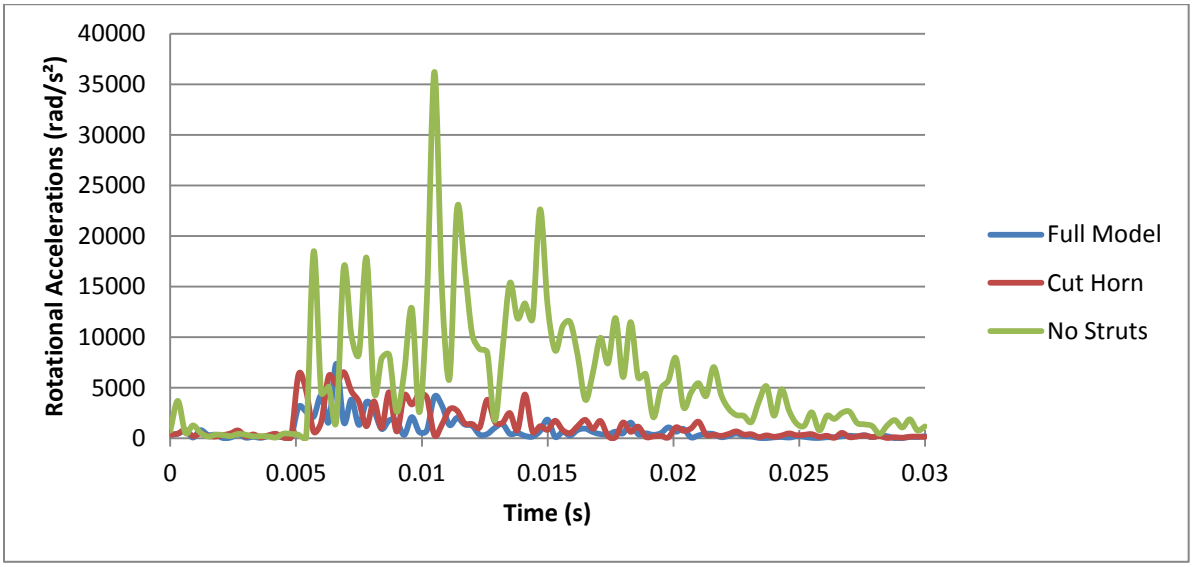

Figure 35: All Models Rotational Brain Cavity Accelerations

Table 5: Rotational Acceleration Values

	Rotational Accelerations (rad/s²)					
	Maximum		Average		Area Under Curve	
	Value	%Δ	Value	%Δ	Value	%Δ
Full Model	7367.37	-	831.7405	-	2.79E+08	-
Cut Horn Model	6530.42	-11%	1251.021	+50%	4.20E+08	+51%
No Struts Model	36215.80	+442%	5827.225	+601%	1.96E+09	+602%

The *Cut Horn Model* displays a lower maximum acceleration value than the *Full Model* which may be due to the decrease in mass and therefore momentum resulting from removing one half of the horn. Otherwise, all values for the modified models show higher rotational acceleration values than were observed in the *Full Model.*

Horncore Strain Comparison

In order to examine the potential for failure in the bone material, strains were compared between the models at a common location of high observed strain. The high tensile and compressive strain locations at the base of the horncore were examined. The trends for both were very similar and the values observed were slightly higher at the back compressive strain locations, so strains at this location will be presented (Figure 36). Approximately 50 nodes were sampled at this location and average strains are reported for the duration of the simulation. High strains were observed elsewhere in the model, such as in individual horncore bone struts, but these were fairly localized and the overall structural trends were of greater interest than focal peak strains.

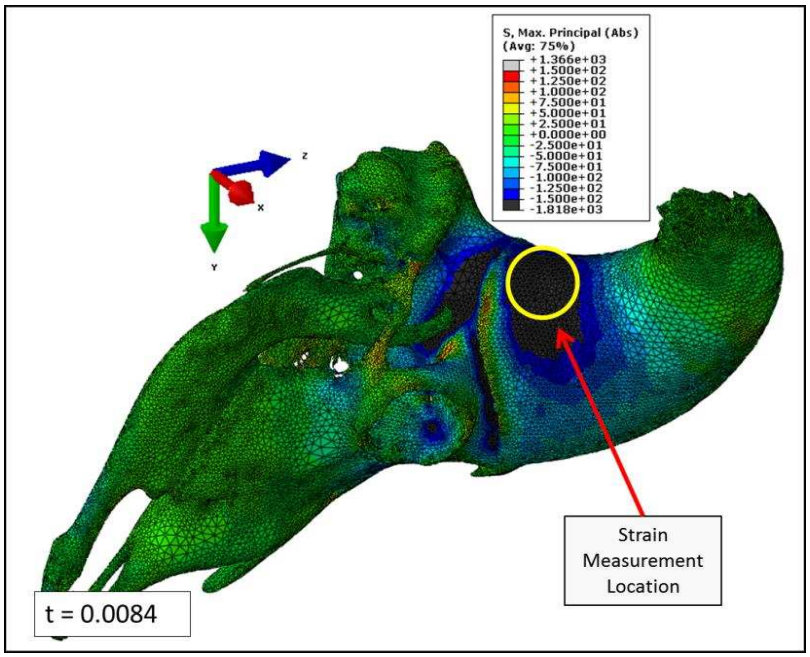

Figure 36: Strain Measurement Location

The strains observed at the base of the horncores were very similar for the *Full Model* and the *Cut Horn Model* with the *Cut Horn Model* having a slightly higher maximum compressive strain peak during impact (Figure 37). The *No Struts Model* endured massive strains (2.8 times higher) at the same location that were sustained for a much longer duration (Figure 38, Table 6). This indicates that the structural rigidity of the horncore was compromised in this geometry due to the absence of the internal bone struts. The large amounts of deformation resulted in a longer impact time, hence the lengthened duration of compressive strain observed.

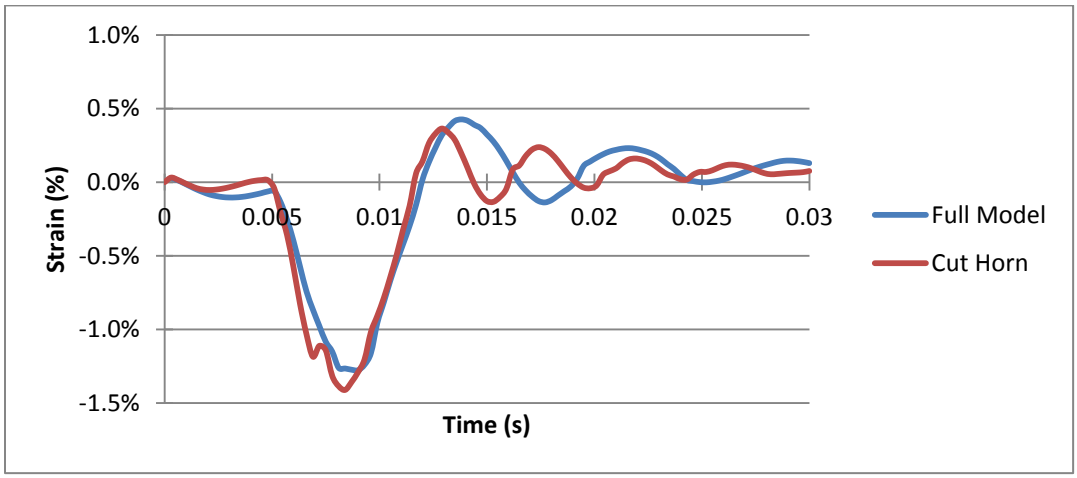

Figure 37: Full Model and Cut Horn Model Strains

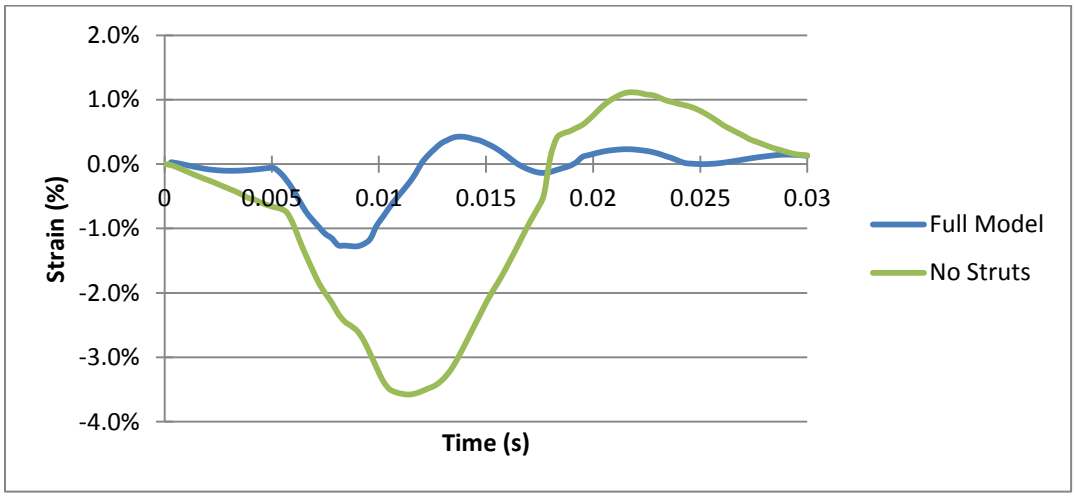

Figure 38: Full Model and No Struts Model Strains

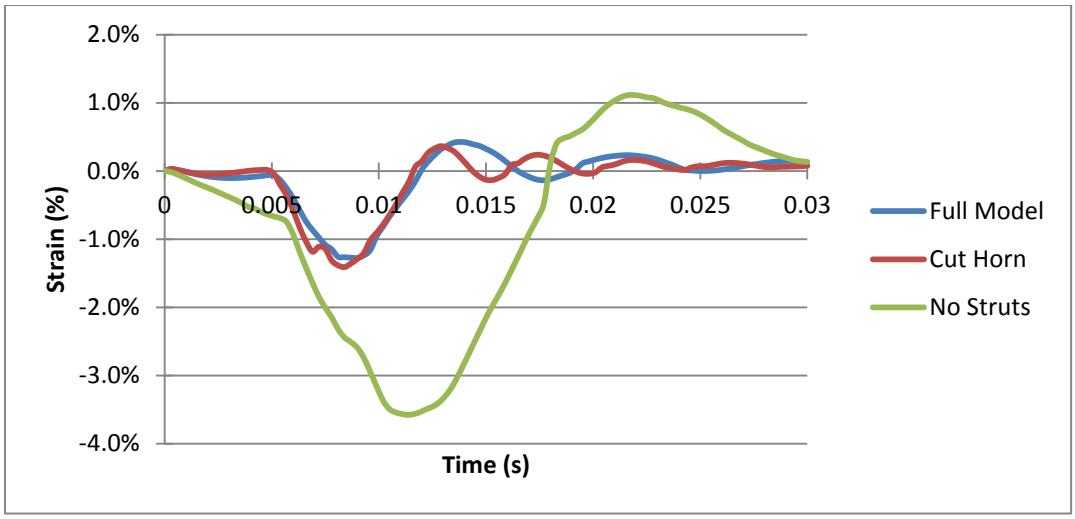

Figure 39: All Model Strains

Table 6: Horncore Compressive Strains and Strain Rates. Values represent maximum principal logarithmic strains and strain rates.

	Compressive Strain Magnitude			
	Strain		Strain Rate (ε/s)	
	Value	%Δ	Value	%Δ
Full Model	1.28%	-	6.17	-
Cut Horn Model	1.41%	+10%	9.21	+49%
No Struts Model	3.58%	+180%	10.8	+75%

The momentum of the point mass applied a force to the neck connection (via the spine spring/dashpot) and therefore a moment is produced in the skull. The *No Struts Model* cannot resist this moment as effectively as the other two models, which resulted in large deformations and strains. The large deformations in the horncore of the *No Struts Model* can be described as bending about both the Y and X axes at the horncore base, as well as some compression of the horcore's cross section. The absence of the horncore struts placed much more of the bending load on the horncore's cortical shell (outer surface), which resulted in higher strains at the horncore base and greater overall deformation (Figure 40).

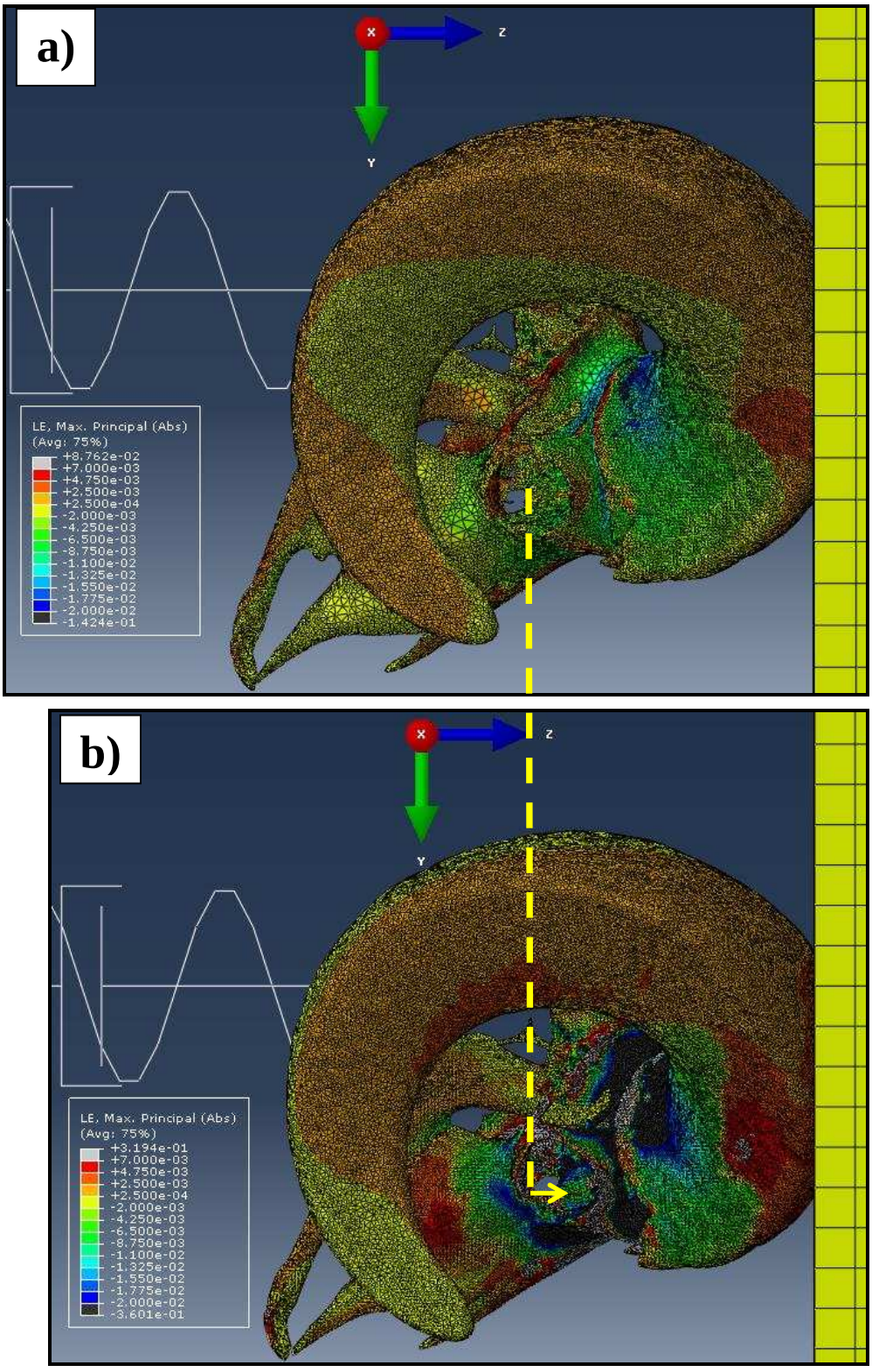

Figure 40: Structural Rigidity Comparison. Log max principal strain at the time of maximum deformation in the a) Full Model and the b) No Struts Model. A deformation scale factor of 2 is applied in both images. Note the much higher strains where the horn meets the skull in the No Struts Model. The yellow line depicts how much farther the No Struts Model deforms (≈2.4 mm without scale factor).

3.4 Discussion

The comparative results of the three models studied indicate that the curl of the horn as well as the horncore bone struts provide a means of brain injury prevention. This is evidenced by the larger brain cavity accelerations that are observed when these geometric features are removed. Also, the drastic reduction in bending stiffness observed when the horncore internal bone struts are removed would likely result in catastrophic failure and injury.

Many researchers have worked diligently to determine an acceleration threshold for predicting concussive injuries in humans. Experiments utilizing football helmets equipped with several accelerometers have been carried out to characterize concussive impacts. There is no universally accepted value that is known to cause concussions, however research suggests that impacts exceeding 82g (translational acceleration) or 5900 rad/s^2 (rotational acceleration) are more likely to cause concussions [33]. Using these values as reference, a comparison can be made between concussive impact in humans and the impacts observed in the present finite element study (Table 7). The *Full Model* translational brain cavity accelerations are slightly higher than what is thought to cause concussion in humans, but the values for the *Cut Horn Model* and *No Struts Model* are much higher than the hypothesized injury threshold for humans. The rotational brain cavity accelerations present in the *Full Model* and *Cut Horn Model* are well below the value thought to cause concussions; however the values observed in the *No Struts Model* are much higher than the proposed injury threshold. These results imply that the horn curvature and the horncore internal strut architecture are important geometric features in preventing brain trauma during bighorn sheep ramming. The results for the *Full Model* display high translational acceleration values and low rotational acceleration values, as compared to the proposed human injury threshold values. This may provide evidence that rotational accelerations are of greater

importance than translational accelerations in predicting and reducing the occurrence of concussion in humans.

Table 7: Average Impact Accelerations. Values presented are the average brain cavity accelerations over the impact time.

	Average Acceleration During Impact	
	Translational (g)	Rotational (rad/s²)
Full Model	111	2165
Cut Horn Model	137	3144
No Struts Model	133	10254

Cut Horn Model

The maximum peak translational acceleration observed in the *Cut Horn Model* is substantially higher than that of the *Full Model* with the only difference between the models being the absence of the back, non-contacting half of the horn. This peak acceleration occurs at 0.0054 seconds of simulation time in the *Cut Horn Model*. At this same time step in the *Full Model,* the onset of momentum loading of the horn occurs, which is evidenced by compressive stresses on the inner curl surface at approximately one half of the horn length. The peak of translational acceleration of the *Full Model* has a smaller magnitude, occurs later, and is more gradual than the peak translational acceleration observed in the *Cut Horn Model* (Figure 41). The momentum change due to impact is translated into the back non-contacting portion of the horn gradually as torsion spring-like loading, which alleviates the peak brain cavity translational acceleration. Horn loading resulted in a dulled translational acceleration peak, despite the horn material only storing about 1/3 as much strain energy as bone material. Also, the reduction in peak acceleration is observed despite the *Cut Horn Model* having a slightly lower mass (and therefore momentum) as a result of removing half of the horn.

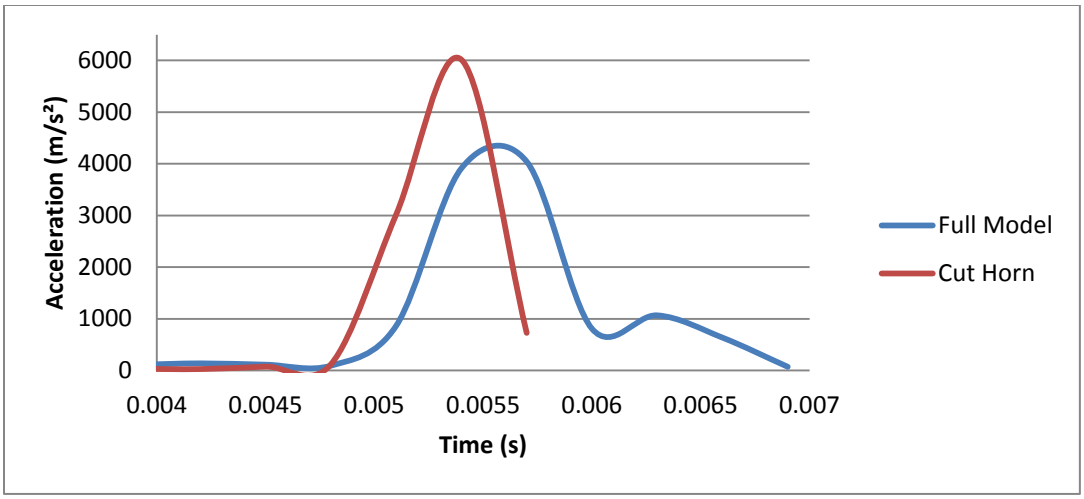

Figure 41: Full Model and Cut Horn Model Peak Translational Acceleration

The rotational accelerations of the *Cut Horn Model* showed a decrease in the single peak maximum value when compared to the *Full Model* (-11%), but due to several rotational acceleration peaks throughout the simulation, the area under the curve was 51% higher. This may be due to the lack of horn tip lateral-medial oscillations that were present in the *Full Model.* The oscillations present in the horn tip contain energy that is translated away from the brain cavity and may help stabilize the observed rotational acceleration peaks.

The strain comparison of the *Cut Horn Model* and the *Full Model* were very similar, with the *Cut Horn Model* exhibiting only a slightly larger peak strain (+10%). This increase in peak strain magnitude can likely be attributed to the lack of strain energy being stored in the horn due to momentum loading. The most notable conclusion from the *Cut Horn Model* is that horn momentum loading reduced the peak translational acceleration magnitude observed in the brain cavity by 49%. This is strong evidence that the horn curl geometry aids in injury prevention in bighorn sheep during ramming.

No Struts Model

The *No Struts Model* did not display the large initial peak in translational acceleration that was seen in the other two models, which is expected considering the impact time was roughly twice as long. Despite not having a large initial peak, the area under the translational acceleration curve was much greater in the *No Struts Model* than the *Full Model* (+57%). The sustained duration of high acceleration peaks could also increase the potential for damage to the brain and bring rise to potential resonance issues.

The drastically higher rotational accelerations observed in the *No Struts Model* create a much higher risk for brain tissue damage occurring in this scenario. For all models there was a significant moment placed on the skull at the neck connection by the point mass and spine spring momentum; however the models with internal bone struts were effective at resisting this moment. As mentioned, the rigidity of the horncore structure was significantly reduced by removing the horncore struts, which reduced its ability to resist the applied moment and therefore rotational accelerations. Also, some of the difference in rotational acceleration could be due to the difference in the mesh and therefore node locations of the *No Struts Model.* The node set that was defined as the "Neck Connection" is likely slightly different for this model than the other two, which would change the moment applied by the point mass slightly. However, the translational accelerations were rather similar in magnitude to the other models; therefore much of the difference in rotational accelerations is attributed to the lack of horncore struts. Comparison of the *Full Model* and the *No Struts Model* provides strong evidence that the horncore struts are a vital structural component for mitigating brain cavity rotational accelerations.

Strain comparisons of the three models revealed that removing the internal bone struts placed a substantially higher load on the bases of the horncores in the *No Struts Model.* Also, the horn and horncore deformed to a much greater extent in the *No Struts Model*. It appears that the horncore's internal bone struts are analogous to shear struts in an otherwise hollow beam (Figure 42). These struts provide force that helps resist bending, and also aid in distributing the load evenly over the horncore's cortical shell. Yield and buckling were not considered in the models discussed, but it is likely that the *No Struts Model* would have failed catastrophically due to buckling. The bone struts would also provide some force to resist horncore buckling. Therefore, the horncore internal bone struts are a not only important for reducing brain cavity accelerations, but are a key structural component in providing the required stiffness during impact.

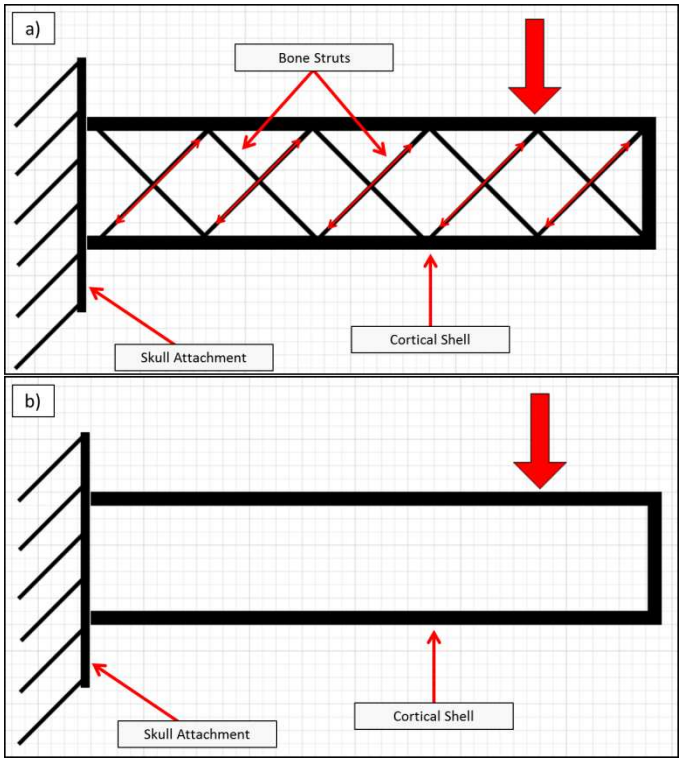

Figure 42: Simplified Horncore Beam Analogy. a) Representative of the horncore with struts intact b) Representative of the *No Struts Model* horncore. This simplified analogy depicts the horncore bone struts resisting a bending load.

This finite element modeling approach illuminated the importance of the horncore and its internal bone struts, which have yet to be characterized experimentally. The material properties and geometric characteristics of this open cell structure warrant further examination. Material characterization should aim to determine the elastic and viscoelastic properties (due to high in *vivo* strain rates) as well as examining anisotropy in horncore and horncore strut bone. Once these materials are characterized, their properties can be reincorporated into finite element models for further analysis. The geometry and spatial arrangement of the bone struts should be also be examined in terms of size, shape, spacing and relative orientation.

Chapter 4 - Vibrations Analysis

4.1 Introduction: Vibration Analysis

Finite element impact simulations of bighorn sheep ramming resulted in oscillatory motion of the horn following impact, with lateral-medial horn tip displacements being the dominant deformation mode. The observation of this phenomenon was the impetus for studying the dynamic vibration response of bighorn sheep horns and skulls. Two approaches were taken to investigate the vibration characteristics of the skull and horn structure: finite element modal analysis and experimental modal analysis. A frequency analysis was performed on the half skull and horn mesh as well as on a symmetric full skull mesh. This type of finite element analysis requires no loads and predicts the vibrational response of a structure based on its geometry and material properties. The dynamic response was also characterized experimentally by employing a technique known as impact hammer modal testing. Using this technique, a hammer equipped with a force sensor provides an impulse to a structure and the dynamic response is captured by accelerometers, and the information is post processed to determine natural frequencies and to estimate damping (i.e. mode shapes). The purpose of this section was to verify the lateral-medial oscillatory response and to create a means of validating the finite element model.

4.2 Methods: Finite Element Modal Analysis

The half skull and right horn meshes that were developed for the impact simulation were also used in this portion of the study. The two meshes were imported into Abaqus CAE, aligned, merged, and assigned material properties following the same protocol outlined in Chapter 2 for

the impact model. The point mass and spine spring however were not included in this simulation, as only the vibrations of the skull and horn structure were of interest. Frequency analysis was performed on two different variations of the model. The first variation included the half skull and right horn instance subjected to the same boundary conditions as the impact model. An X-axis symmetric boundary condition allowed no displacement of symmetry plane nodes in the X-direction and no rotations about the Y-axis or Z-axis. The neck connection boundary conditions restricted the neck attachment region from displacing in the Y-direction and from rotating about the X-axis (simulating neck muscle reaction torques/forces). This model was created in order to have a direct means of comparison between the impact model and the frequency analysis. In the second variation of the simulation, the half skull and right horn instance was copied and replicated but as a mirror image about the symmetry plane, and was then merged to the other half. Doing this effectively produced a full skull model that was perfectly symmetric about the symmetry plane (Figure 43). This variation of the model was not subjected to any boundary conditions and was allowed to vibrate freely, which is the typical protocol for FE modal analysis. This full skull symmetric model was developed to have a direct means of comparison to experimental modal analysis performed using an impact hammer. Experimental modal analysis was carried out on full ram skulls, also allowed to vibrate freely and will be discussed in detail. A linear perturbation frequency analysis was performed in Abaqus CAE on both of the model variations using a Lanczos eigensolver and requesting the first 15 eigenvalues.

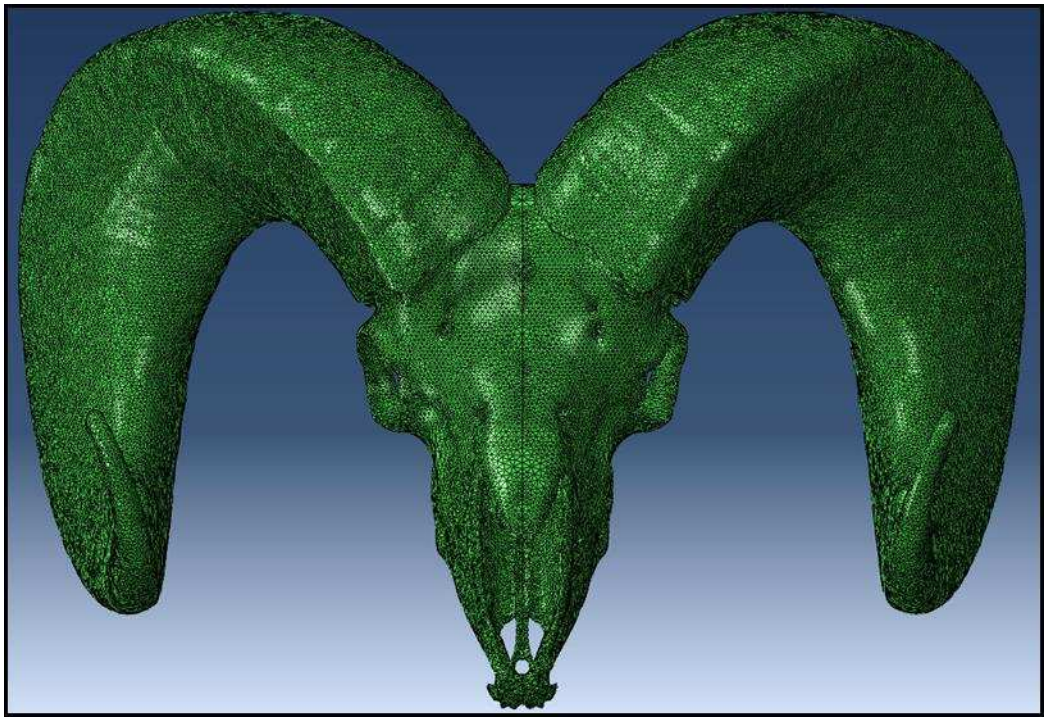

Figure 43: Symmetric Vibration Model. Note the plane of symmetry in the center of the skull.

4.3 Results: Finite Element Modal Analysis

The first five (lowest frequency) natural frequency values were studied for the two model variations, as these are the modes capable of dissipating the most energy via hysteretic damping. For the partially constrained half skull frequency analysis the first five natural frequency values ranged from 118 Hz to 309 Hz (Figure 44). Mode shapes can be described as displacement of the horn either side to side, vertically or a combination of the two. The unconstrained (free vibration) model consisted of the full horn and skull mesh created by mirroring the right skull/horn mesh. The frequency analysis of this symmetric full model resulted in natural frequency values from 142 Hz to 271 Hz (Figure 45) for the first five modes. The mode shapes at each of these five frequencies can generally be described as side to side horn tip displacement. This model was able to detect unbalanced modes (Figure 45: Modes 2 & 4) because the mesh used represented the full horn and skull geometry.

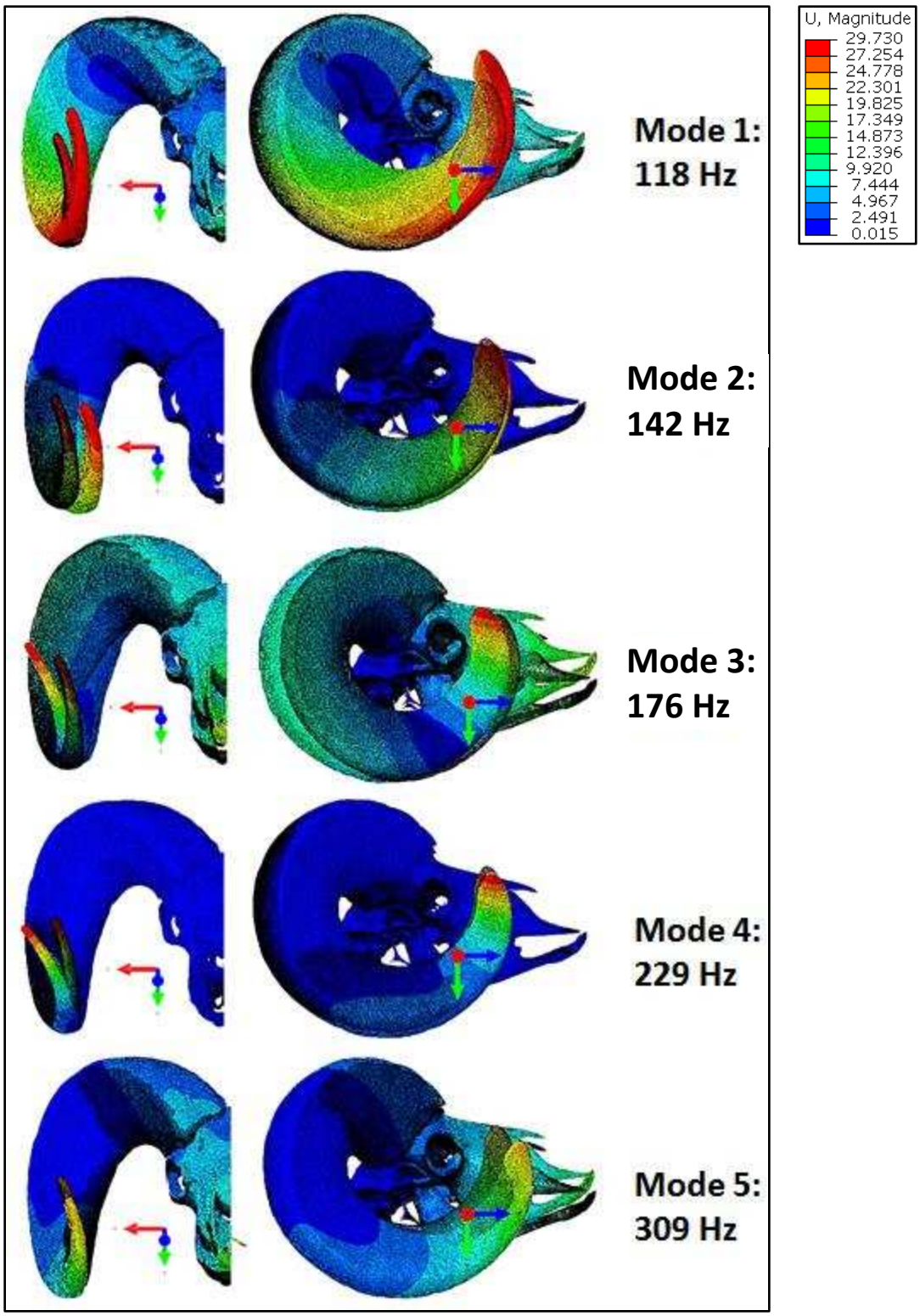

Figure 44: Half Skull FE Modal Analysis. Contour plots on both the original and deformed mesh. The darker of the two is the original shape and the more brightly colored is the deformed mode shape. Colors depict relative displacement in mm. All mode shapes are characterized by horn tip motion, primarily in the x-direction, y-direction, and combinations of the two.

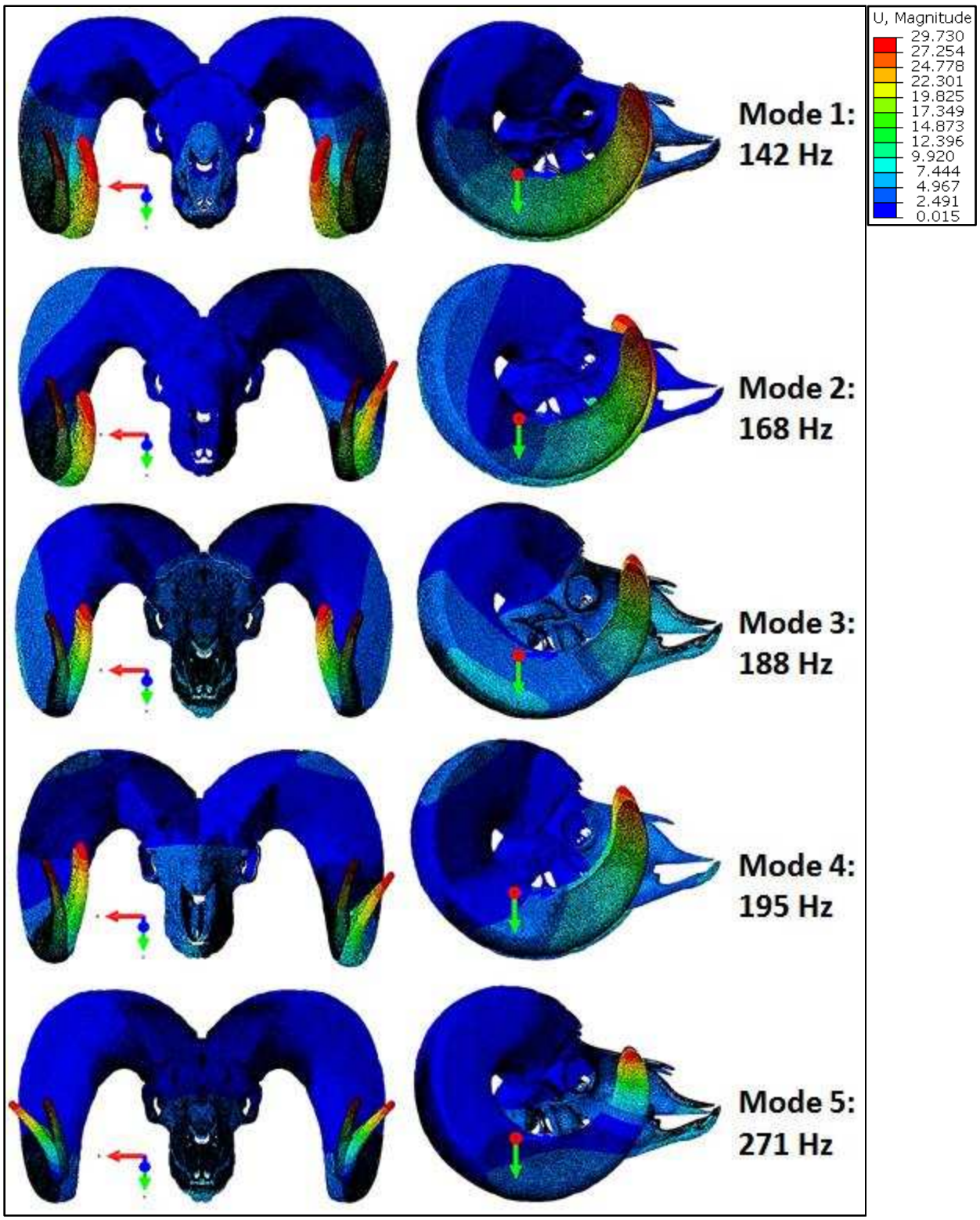

Figure 45: Full Skull FE Modal Analysis. All mode shapes are primarily associated with x-direction (lateral-medial) displacements. Modes 1, 3 and 5 are balanced vibrations, as both horns oscillate as a mirror image of one another. This type of oscillations would produce a relatively small net force, as forces produced by each horn would cancel. The resultant forces in the unbalanced modes (2 and 4) would be much higher as the force vectors would add.

4.4 Methods: Experimental Modal Analysis

The Colorado Parks and Wildlife Department of Natural Resources supplied heads of six male bighorn sheep which were salvaged from animals that had died accidentally in the wild. Heads were stored at -20° Celsius. Two of the six heads were used for experimental modal analysis and were chosen based on size. The two sets of horns nearest in size to the horns in the finite element model were chosen for this experiment. Several criteria were used to quantify horn size including base circumference, outer diameter, inner diameter, tip-to-tip length, and furthest posterior horn separation distance (furthest point length). These dimensional criteria are explained schematically in Figure 46 and are summarized quantitatively in Table 8.

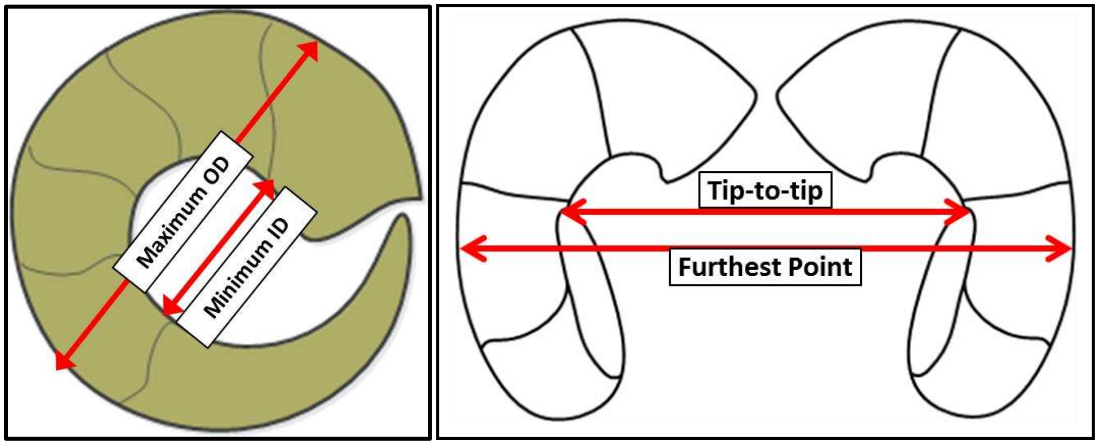

Figure 46: Horn Dimensions

Table 8: Horn Measurements

	Measurements (inches)			
	Tip-to-tip	Furthest Point	Outer Diameter	Inner Diameter
Model Geometry	18.9	21.9	13.5	6.75
Animal Horn #1	18.5	21	13.5	7.5
Animal Horn #2	21	20	13.5	7.5

Table 8 shows the similarities and differences between the measured dimensions of the model geometry and the two sets of horns studied experimentally. The two sets of horns are very

similar in size to one another and to the model horn geometry; however there are subtle differences which could affect the vibrational characteristics slightly. In general, the horns from animal #1 were considered to be slightly smaller than those of the model and the horns from animal #2 were considered to be slightly larger.

The heads were thawed by soaking them in warm water for approximately one hour and holding at room temperature for approximately five hours. Next, the heads were dissected to remove soft tissue such as hair, skin, muscle and connective tissue. This was done to more accurately replicate the structure analyzed in the finite element model, which only included bone and horn keratin. After dissection, the skulls were refrozen and vibration testing was carried out on a later date. Prior to vibration testing, the first skull was thawed for 15 hours in a cold room (4.4° C) and for 6 hours at room temperature. The second skull was thawed for 24 hours in the cold room prior to testing.

A custom vibration testing fixture was manufactured to suspend the skulls during testing, therefore eliminating any outside damping or vibration sources. This fixture was composed of 4x4 inch wooden posts and 2x4 inch wooden boards. Straps and extension springs (2 above, 2 below) were used to suspend the skulls within the fixture. Straps were secured around the base of the horns, as close to the skull as possible, as to leave vibration of the horn unhindered. The large wooden structure had sufficient mass and rigidity to not be affected by movement of the skulls within the suspension straps.

Roving hammer modal analysis was performed on both sets of horns studied. For this type of analysis, accelerometers are placed at regions of interest, and the structure is impacted in multiple locations. It is necessary to impact in multiple locations to ensure excitation of all

natural frequencies of a structure. Three accelerometer locations were chosen for this study: the left horn tip, the right horn tip, and the skull between horn bases. Accelerometers were secured to their respective surfaces with petro mounting wax (Figure 47b). Three axis accelerometers were used at horn tip location and a single axis accelerometer was used at the skull location (Figure 47c). Horn tip locations were first sanded down slightly to create a flat surface for accelerometer placement, and then were patted with tape to remove any powder created from sanding. The skull location was first scraped to remove any remaining soft tissue, then sanded and patted with tape in the same manner as horn tip locations.

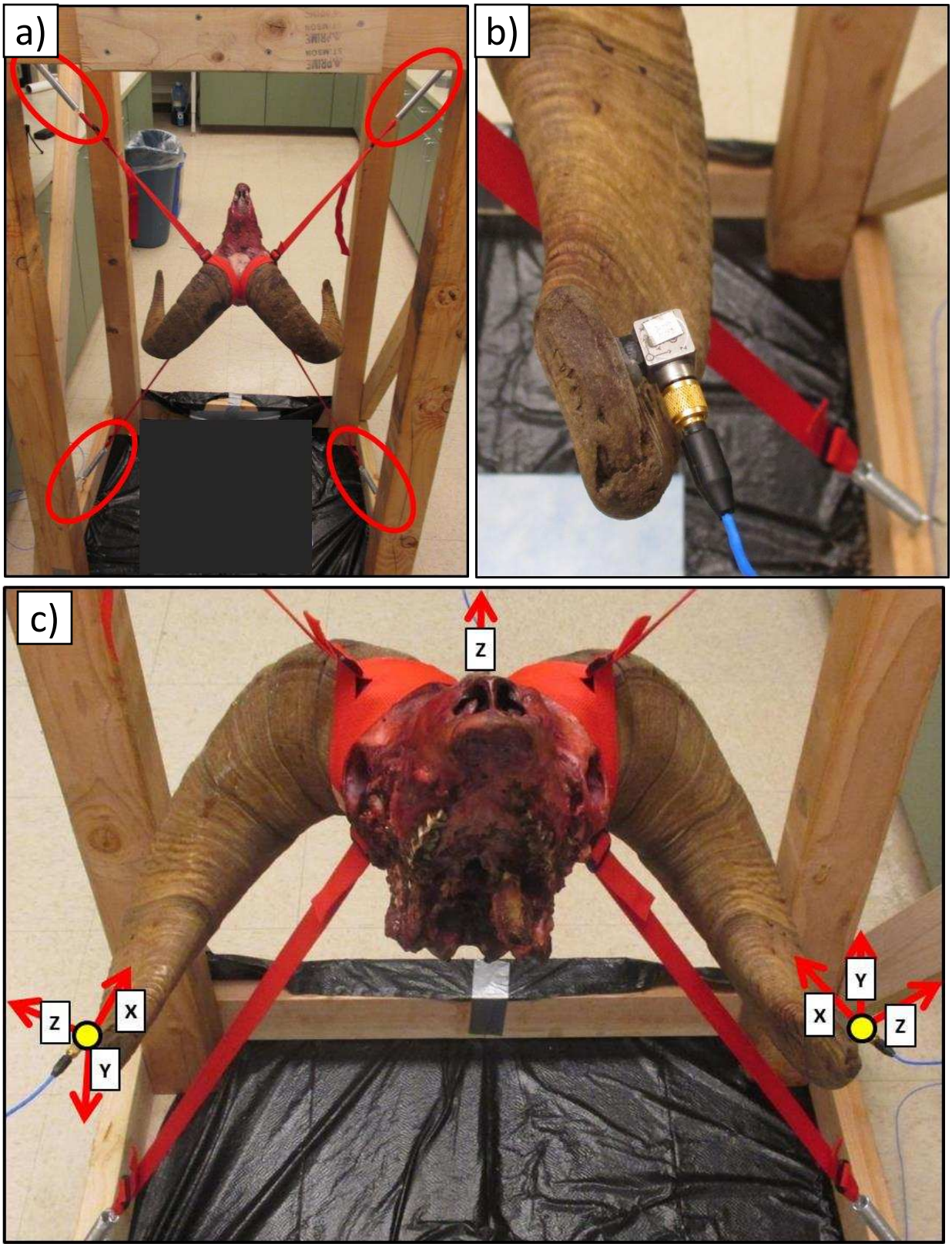

Figure 47: Experimental Modal Analysis Setup. a) Skull suspended by straps and springs (circled in red) in testing fixture b) Accelerometer placement c) Accelerometer locations and orientations (yellow circle represents accelerometer)

A general purpose modal impact hammer equipped with a force sensor was used to excite a vibratory response within the horn and skull structure. Five locations were impacted on each horn and one location on the skull (Figure 48). More hit locations were tested in the front half of the horn because this is where impact occurs in bighorn sheep ramming. Medium-soft (black rubber) to medium (plastic with cover) hammer tips were used for impacts in this experiment and were chosen based on the frequency spectrum excited. Various hit locations showed different frequency spectrum responses, therefore different tips were used to create a similar response at different locations. In general, a harder impact hammer tip excites a larger frequency range, but makes discovering low frequency modes more difficult. Therefore, using a hammer tip that is just hard enough to excite the frequencies of interest is ideal. The typical cutoff frequency for this analysis was around 450 Hz and natural frequencies were expected between 100 and 300 Hz, based on finite element modal analysis. The force response of the impact hammer was examined after each hit to ensure a 'clean' hit. A clean hit is one in which only one distinct peak appears in the force magnitude response. It is possible, and not uncommon, for the impact hammer to contact the structure multiple times upon impact, creating multiple peaks in the force response. If this occurred, the data was not recorded and the hit was resampled. Each hit location was repeated five times ensure consistency.

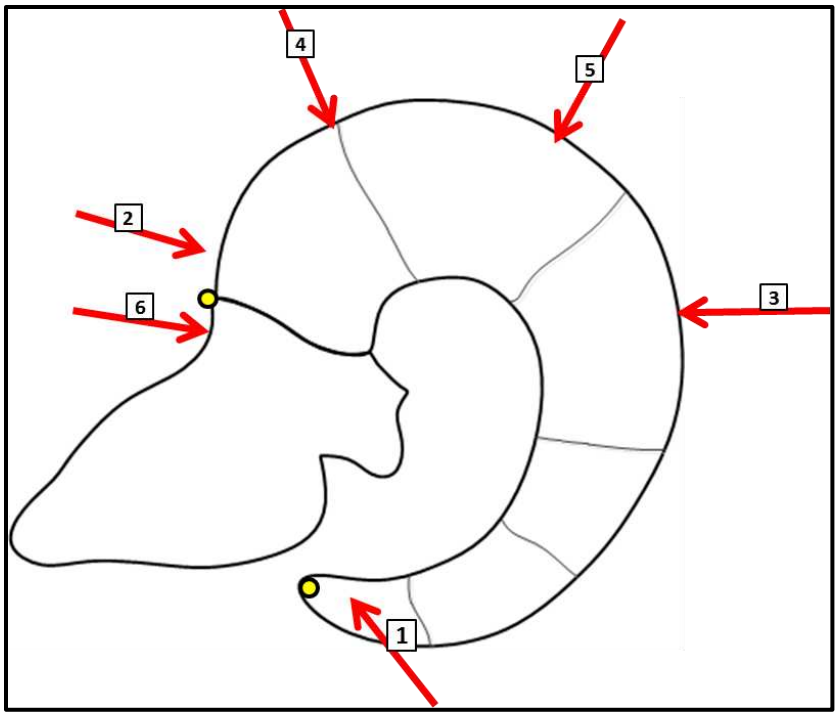

Figure 48: Modal Hammer Hit Locations. Hit locations 1-5 were performed on each horn and hit location 6 was in the middle of the skull 1 inch from the accelerometer (yellow circles represent accelerometers).

The skulls did oscillate within the suspension fixture as rigid bodies and this motion was a concern initially. By displacing the skulls within the structure and measuring the frequency response it was determined that these oscillations occurred at 2-3 Hz. These oscillations were substantially lower than natural frequencies predicted and observed for the horns and skull and were easily omitted from the results.

A total of eight channels of data were recorded for each hit, including three channels for each three axis accelerometer, one channel each for the single axis accelerometer, and one channel for the force hammer. A National Instruments USB module was used for recording all data channels and LabVIEW was used for processing data. Response waveform plots were generated for the impact hammer force and for each direction of each accelerometer. The force response spectrum was calculated using a spectral Fast Fourier Transform based measurement function and plots were generated. Dual channel spectral measurement tools that compared the force response to the

accelerometer response as ordered pairs were used to calculate the Frequency Response Function. These tools produced outputs of magnitude and phase and were also broken up into imaginary and real portions. A custom LabVIEW program recorded and exported all required data (e.g. Figure 49).

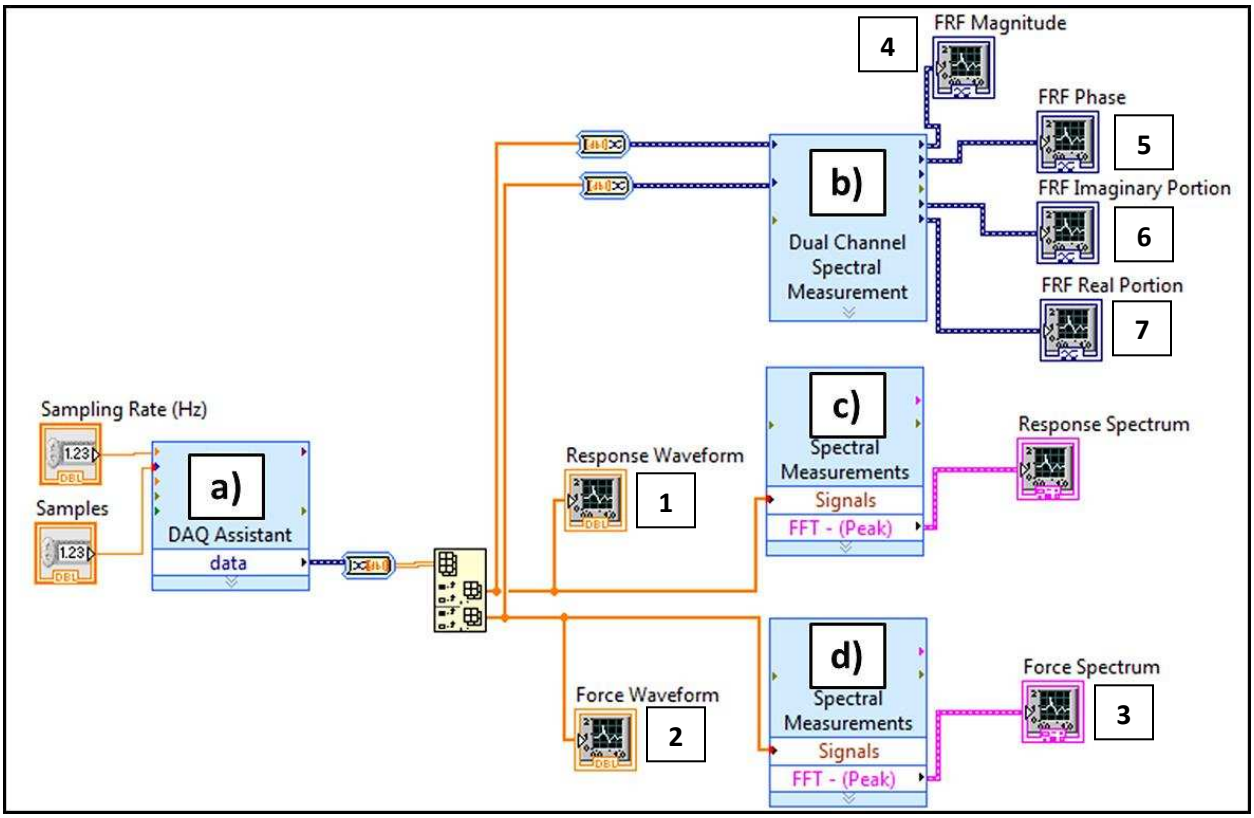

Figure 49: Example LabVIEW Modal Analysis Code. Note: this is an example code for a single accelerometer setup. The real code had several of these modules for multiple accelerometers and accelerometer directions. a) Acquires accelerometer and force hammer data b) Measures the frequency response of the accelerometer signal against force hammer signal as ordered pairs and outputs FRF as Magnitude, Phase, Real and Imaginary c) Measures frequency response of the accelerometer signal. d) Measures frequency response of the force hammer signal

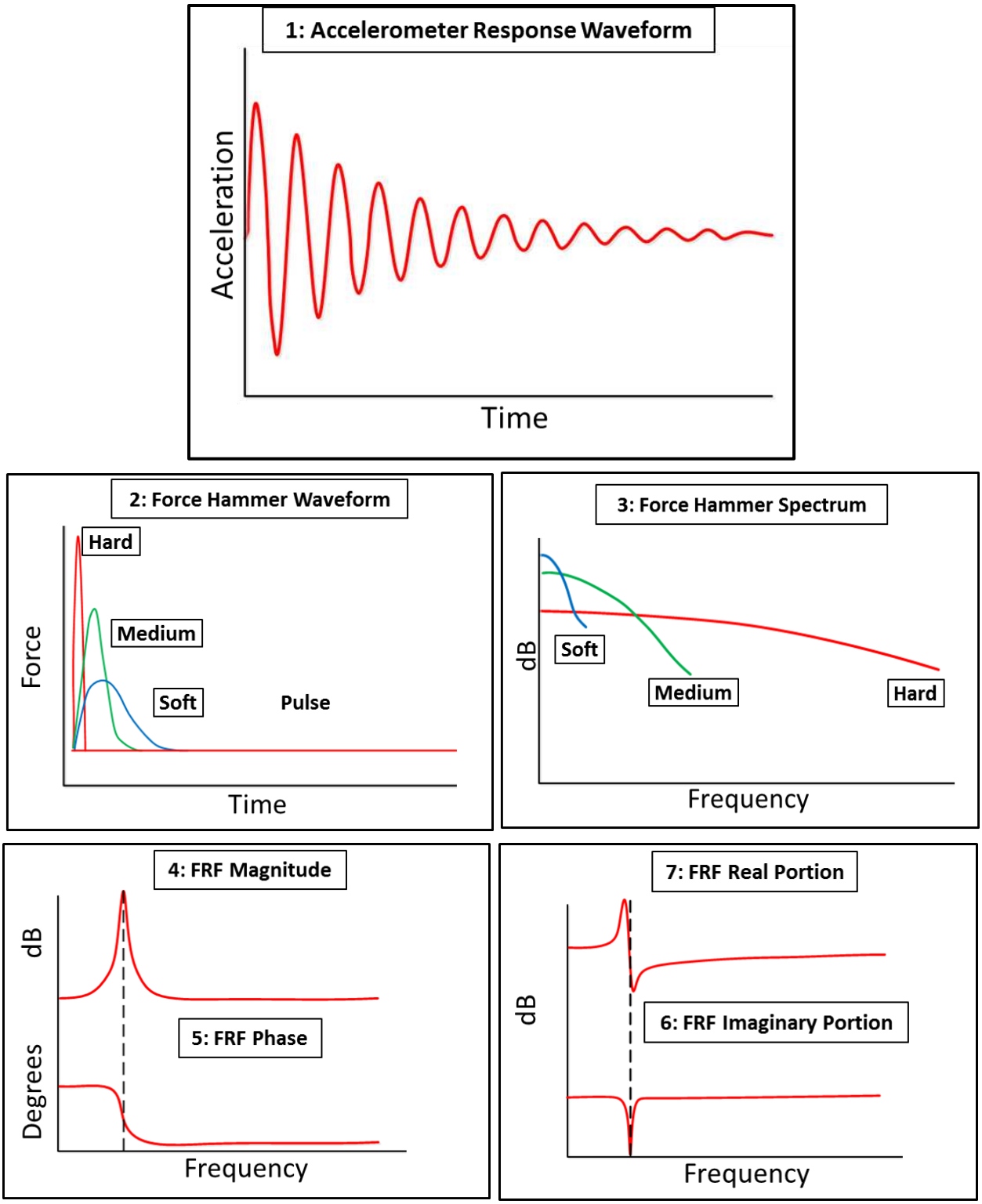

Figure 50: Example Modal Analysis Outputs. Note: these example outputs are for a simple single DOF system with one natural frequency. Plot numbers are associated with numbers in the block diagram shown in Figure 49. 1) Raw accelerometer response (used to calculate damping) 2) Various force hammer waveforms depending on hammer tip hardness 3) Force spectrums for different hammer tip hardnesses (indicates the frequency range excited in the structure) 4) Peak in FRF magnitude indicates natural frequency 5) Shift in FRF Phase indicates natural frequency 6) Peak values of FRF imaginary portion determine mode shapes 7) Zero-crossings in FRF real portion indicate natural frequency

Natural frequency values were determined by manually examining plots of the FRF magnitude, phase, real and imaginary portions in Matlab simultaneously. It should be noted that the system being analyzed was quite complex, so the data was not as clear as the example plots provided. In order for a natural frequency to be recorded, a magnitude peak, phase shift, real portion "zero-crossing" and imaginary portion peak had to all be present. The one exception is that not all FRF real portion zero-crossings actually passed through the x-axis. Some were actually offset in the y-axis, but displayed the shape seen in the real portion plot in Figure 50, and a natural frequency was considered present at this value. Due to slight differences in the size and shape of the horns being analyzed, and to the lack of a definitive material constitutive model, it was not expected for the experimental and theoretical modal analyses results to display identical natural frequency values. Instead, it was surmised that several natural frequencies would fall within the same range and that there would be similar modes shapes. Based on the vibration responses observed in the finite element impact and modal simulations, it was predicted that horn tip lateral-medial oscillation would be a dominant vibration mode during experimental modal analysis.

Critical damping is defined as the minimum value of damping that allows a displaced system to return to its neutral position with no oscillation. The lowest natural frequencies were of primary interest in this study; therefore damping was calculated for the lowest natural frequency observed which occurred at around 150 Hz. A logarithmic decrement method was used to estimate the fraction of critical damping at the horn tip experimentally. The logarithmic decrement is the natural log of the amplitude ratio of two successive peaks. The logarithmic decrement was calculated for several peak pairs (4-5) in the accelerometer response and averaged. Average values for each horn were produced.

4.5 Results: Experimental Modal Analysis

The occurrence of natural frequencies is displayed in histogram form and is separated into three classifications. The first histogram (Figure 51) includes all natural frequencies observed for all accelerometers, orientations and hit locations. The first five dominant modes are estimated by peaks in the occurrence of natural frequencies found in the first histogram. The second histogram (Figure 52) includes natural frequencies for only the horn tip accelerometers in the z-direction, for all hit locations. The third histogram (Figure 53) also only includes natural frequencies from horn tip accelerometers but in the Y-direction and for all hit locations. The Z and Y direction horn tip accelerometer responses were expected to have the largest dynamic response based on theoretical modal analysis results, and were inspected in greater detail. It should be noted that the cutoff frequency for most hits was between 450-500 Hz. The most readily observable trend from this data is the high occurrence of natural frequencies approximately 160 Hz, which falls in the same range of some of the lower natural frequency values obtained from the finite element modal analysis. Many natural frequencies are observed between 200 and 300 Hz and are distributed more heavily in the lower end of that range.

Bighorn Skull 1

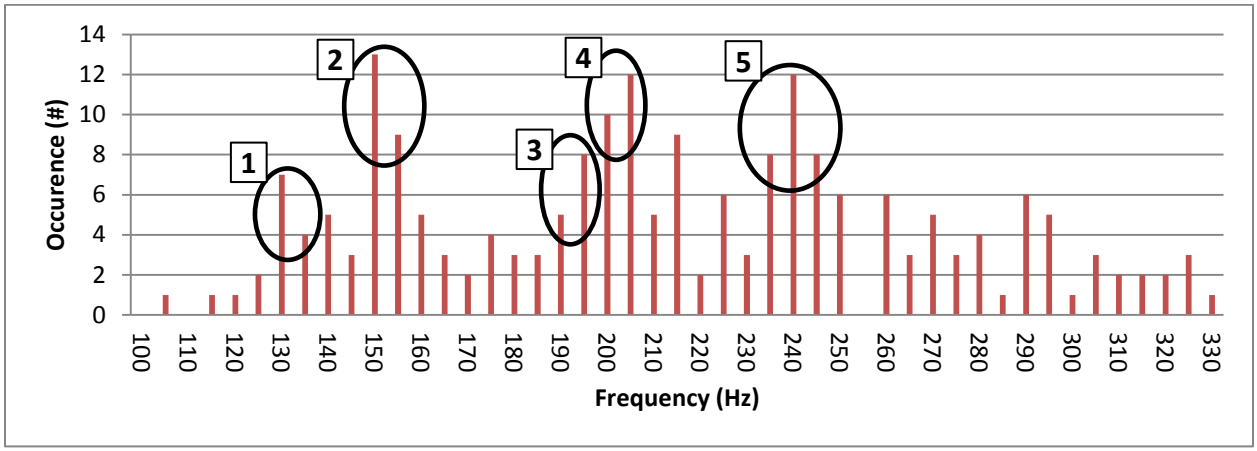

Figure 51: All Natural Frequencies

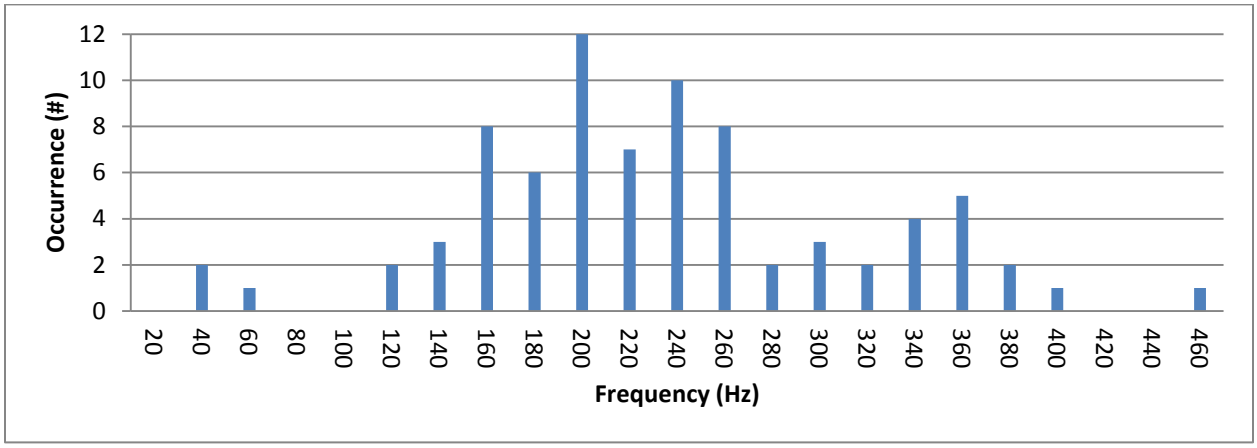

Figure 52: Horn Tip Z-Direction Natural Frequencies

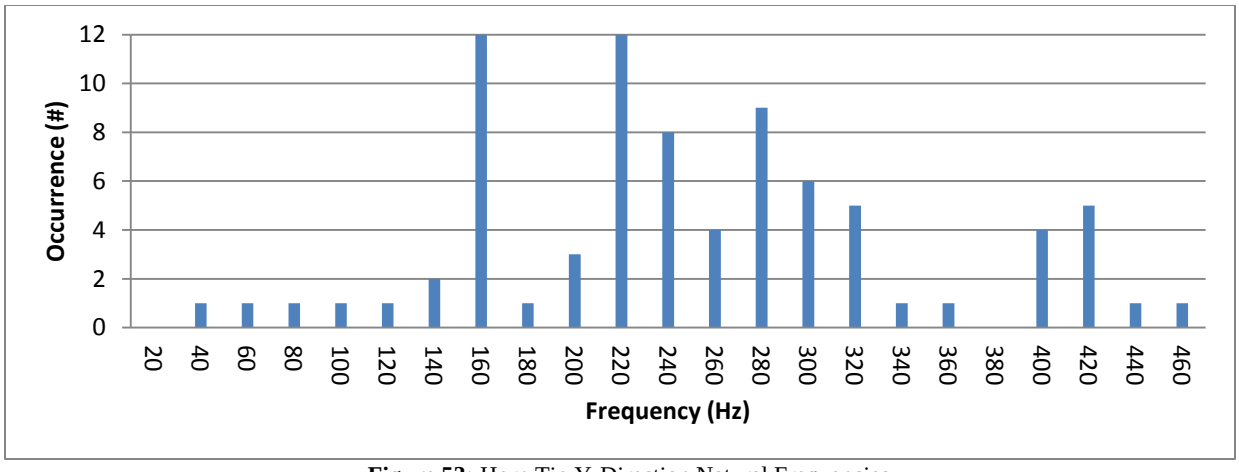

Figure 53: Horn Tip Y-Direction Natural Frequencies

Table 9: Ram Skull 1 Fraction of Critical Damping

	Ram Skull 1	
	Left Horn	Right Horn
Avg. Damping	4.49%	5.51%

Bighorn Skull 2

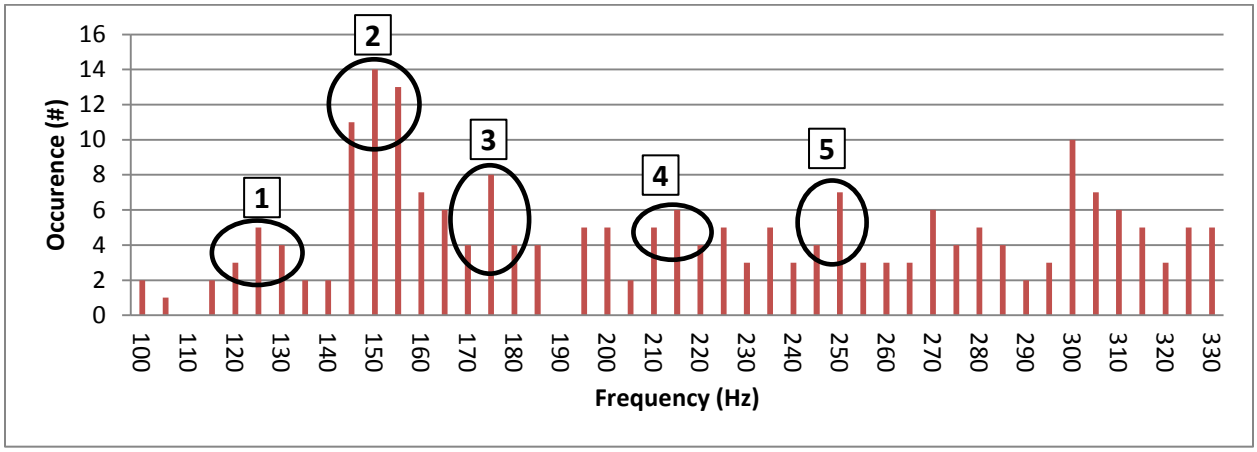

Figure 54: All Natural Frequencies

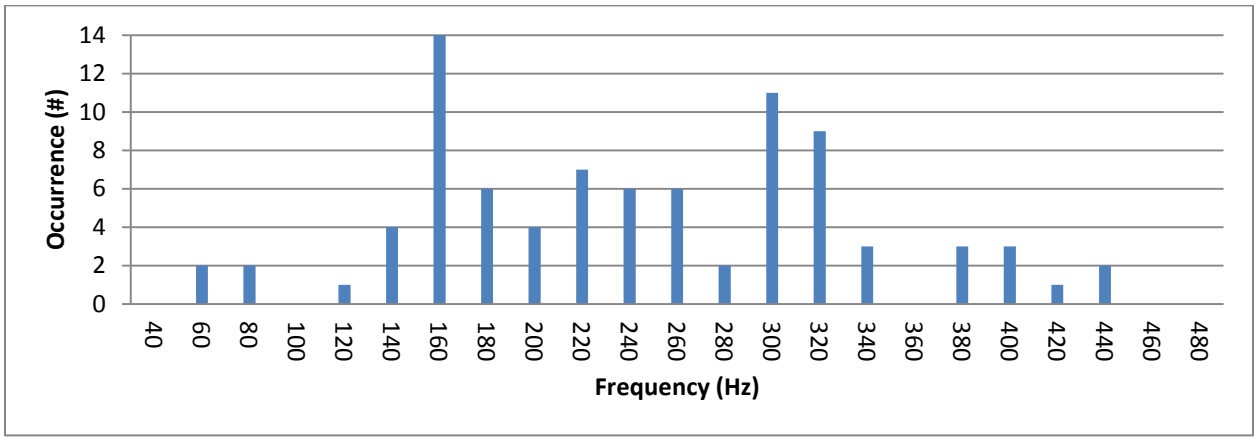

Figure 55: Horn Tip Z-Direction Natural Frequencies

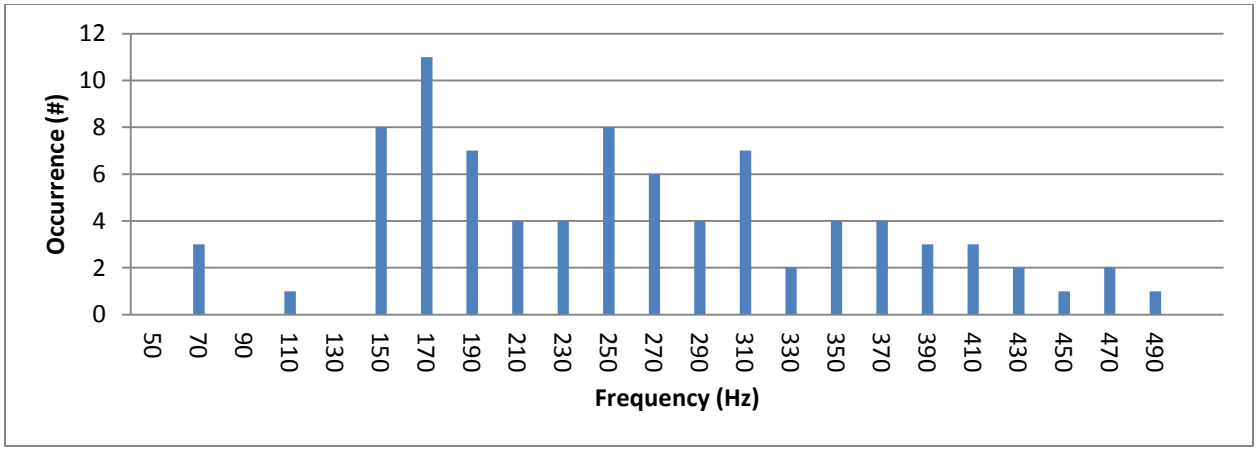

Figure 56: Horn Tip Y-Direction Natural Frequencies

Table 10: Ram Skull 2 Fraction of Critical Damping

	Ram Skull 2	
	Left Horn	Right Horn
Avg. Damping	5.17%	4.76%

Table 11: Dominant Mode Frequencies. This table compares the first five modes found from the finite element modal analysis with estimates of the first five modes found experimentally.

	Dominant Natural Frequencies (Hz)				
	Mode 1	Mode 2	Mode 3	Mode 4	Mode 5
Full Skull FE Modal	142	168	188	195	271
Animal #1 Modal	125-135	145-155	185-195	195-205	230-245
Animal #2 Modal	115-130	140-155	165-180	205-215	240-250

Generally speaking, the majority of the natural frequencies observed experimentally had values between 110 and 320 Hz. This is consistent with the five lowest modes calculated in the finite element modal analysis. The exact values of natural frequencies from the finite element modal analysis are not readily recognized in the experimental modal analysis data; however approximates were made based on the occurrence of frequencies observed in histogram plots (Table 11). The mode estimates found from the horn tip natural frequency values do not match up exactly with frequencies found in the finite element modal analysis, but they are fairly similar, and the frequency gaps between observed modes are quite similar. Natural frequency values depend on material properties, and geometry, neither of which was identical for the experimental and finite element modal analyses. The geometry of the bighorn sheep horns in the finite element model was slightly different than those tested experimentally, and the material properties of bighorn sheep skull bone are not known. Also, due to the high degree of complexity of bighorn sheep horns and skulls, there are several natural frequencies present within a small frequency band, which makes differentiating modes difficult. The only natural frequency that is dominant in all of the results exists at 150-160 Hz, which compares well with the lowest natural frequencies observed in the finite element modal analysis.

The critical damping was calculated for the 150-160 Hz natural frequency, which was the most prevalent natural frequency found and was also one of the lowest natural frequencies. A bandpass filter was applied to the accelerometer response to capture only frequencies between

145 and 175 Hz to calculate the damping response of the 150-160 Hz natural frequency (Table 9 & 10). The average damping for both horns and both animals was 4.98% of critical damping. This is a relatively high value as compared to engineered structures, which are typically comprised of jointed metal struts and trusses. In general, there was no difference in the fraction of critical damping between the horns of the two animals.

4.5 Discussion: Vibration Analysis

The most notable takeaway from the finite element and experimental modal analysis results is that the horns are particularly prone to lateral-medial oscillations. These "side-to-side" oscillations were first observed in the impact model in Chapter 2, and were the primary deformation mechanism observed in the finite element modal analysis. These oscillations were also present in the experimental modal analysis; though differentiating particular modes was difficult. This dynamic response of the horn seems to be the structure's "preferred" vibration mechanism and directs kinetic energy away from the skull and brain cavity. If balanced lateral-medial horn oscillations were present during and following impact they would produce a relatively low force at the centerline of the skull, as the force from one horn would cancel the other. In contrast, if both horns oscillated front to back, during and following impact, the forces would sum and cause gyration of the skull (Figure 57). Therefore lateral, balanced oscillations would likely be less detrimental to the brain than front to back oscillations.

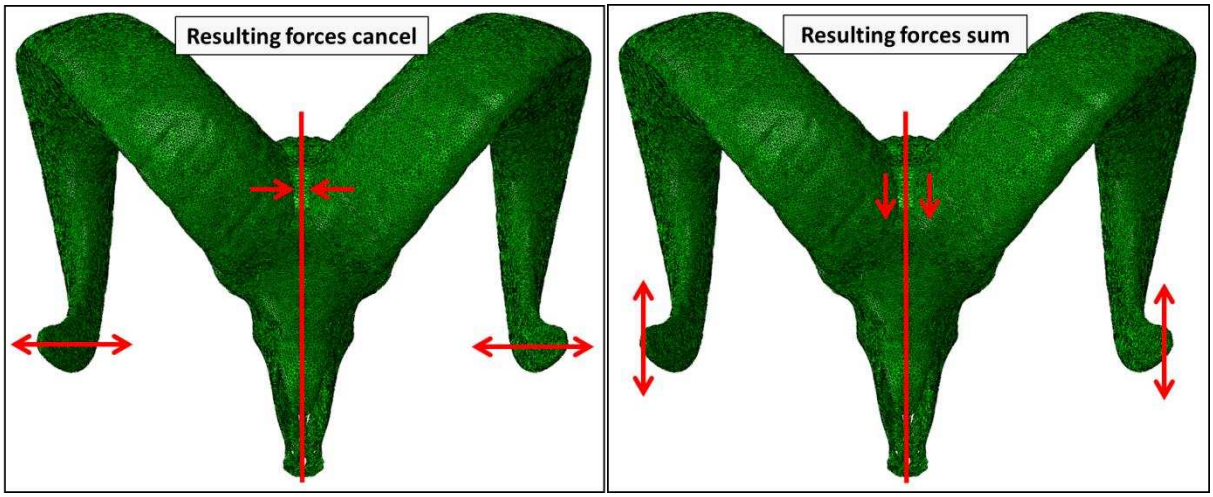

Figure 57: Lateral-Medial vs. Front-to-Back Horn Oscillations. The images depict the advantage of side-to-side oscillations in terms of the force produced at the skull. Balanced side-to-side vibration would produce a relatively small net force as the two horn forces would cancel whereas the front-to-back oscillations would produce a net force in the skull.

One of the major purposes of the experimental modal analysis was to determine if impact to the front of the horn (in the location and direction of real impact), would cause lateral-medial vibration in the horn tip. This phenomenon was present in the finite element impact simulations. The majority of the impacts (hammer hits) performed in this experiment were in the same direction and in similar locations to where impact occurred in the finite element impact model, and the impacts did in fact result in substantial horn tip lateral-medial oscillations.

Horn tip lateral-medial oscillations were quantified in the impact model in Chapter 2, with primary oscillation frequencies of 166 and 266 Hz. These values fall in the range of natural frequencies observed both the finite element and experimental modal analyses. This is evidence that the vibrations observed in the impact model are not an artifact, and that they are likely present in real impacts. Excitation of the finite element impact model produced a vibrational response within the same range as the experimental modal analysis, which provides validation of the impact model. Furthermore, the existence of a natural frequency at 160 Hz in the real horns found from experimental modal analysis compares well with the 166 Hz oscillations present at the horn tip in the impact model. This natural frequency is likely the dominant vibration mode

during impact and would result in some energy being directed away from the brain. The first five natural frequency values estimated for the two sets of horns tested experimentally had very similar values, and compared fairly well with the dominant mode frequencies found in the finite element modal analysis. The values of natural frequencies were similar, and the frequency gaps between observed modes were also very similar, which provides validation of the mesh and material properties used in the finite element models.

The relatively high value determined for the fraction of critical damping (Avg. = 4.98%) implies that the horn material and structure effectively transforms kinetic energy to heat. This supports the assumption that the horns act as vibration dissipaters during, and after impact. Both modal analysis techniques displayed that kinetic energy travels through the horn to the tip as vibrations, and the damping results show that this kinetic energy is quickly be dissipated as heat. Therefore, the horns act as kinetic energy sinks during and after impact, drawing kinetic energy away from the brain cavity and dissipating much of it as heat.

Chapter 5 – Discussion and Conclusions

5.1 Discussion and Conclusions by Section

Finite Element Impact Model

Evidence from the finite element impact model suggests that one role of the horn is to evenly distribute load to the horncore in a cantilever-like loading scenario. During impact, the horncore experiences high tensile stresses at the base on the impact side and high compressive stressed at the base opposite of impact, which is evidence of the cantilever load state. Bone has a crystalline, mineralized component, which provides stiffness in compression, but makes the material more susceptible to fracture than horn material [37]. Horn lacks a mineralized component making it far more compliant (lower modulus) than bone. Horn displays a high degree of fracture toughness [38] which makes it more suitable for sustaining localized, high strain rate loads without catastrophic failure occurring. The curved conical shape of the horncore is an optimal structure for withstanding cantilever loading situations. The curvature allows higher compressive stresses to occur rather than tensile, which is beneficial because bone displays higher strength in compression [39]. The cone shape is favorable for withstanding cantilever bending loads, as it gets wider (higher moment of inertia) at the base, where the highest loads occur. Transferring the load from the horn to the horncore is essential, as bone can withstand higher stresses and the horncore structure is optimized for cantilever-like loading. The higher load bearing capabilities of the horncore were illuminated by strain energy measurements, which were 3 times higher in the bone material than in the horn material.

Horn has a higher impact strength than bone [37], yet the structure of the horncore and horns lends to more strain energy being absorbed by bone than by horn during ramming. An

evolutionary advantage of bone absorbing more energy than horn is the self-repairing ability of bone, which is absent in horn. In ramming instances where the strain energy exceeds the resiliency of the material, the damaged bone can be repaired by bone remodeling. Horn material does not have a self-repairing mechanism and therefore would be permanently compromised mechanically if resiliency was exceeded.

The horn itself undergoes an interesting dynamic loading and unloading sequence, during and after initial impact. Upon initial contact, momentum of the lagging back portion of the horn causes loading of the horn that is analogous to loading of a torsion spring. Stresses produced during this loading event create a torque in the mid body of the horn that causes unloading of the horn to proceed as lateral-medial horn tip oscillations. This loading and unloading phenomenon seems to alleviate the impact by reducing the rate at which deceleration occurs, as well as by dissipating some of the energy produced in the axial direction in the transverse plane as oscillations.

Other general observations about the skull and brain cavity pertain to the relative size and spacing of the brain cavity within the animal's skull. Based on visual observation of CT scans, the brain cavity of a bighorn sheep fills a relatively small fraction of the total skull volume when compared to the human brain cavity, which occupies nearly the entire skull. Therefore, there are large volumes of nearly open space around the brain cavity of a bighorn sheep, which allows longer distances for the brain cavity as a whole to decelerate during impact. Further research should incorporate finite element impact models that compare brain cavity deceleration profiles of bighorn sheep skulls to helmeted and unhelmeted human skulls.

Conclusions:

- The horn distributes localized impact loads to the horncore in a cantilever-like loading scenario, rather than propagating the high strain rate compressive stresses to the bone material.
- The horn undergoes a dynamic loading and unloading sequence that alleviates impact and transfers some kinetic energy of impact into lateral-medial oscillations of the horn tip.
- The horncore provides the majority of the stress bearing capabilities of the structure, with much of the load present as bending of the horncore base.
- The horn/bone composite structure takes advantage of the toughness of horn as well as the high compressive strength of bone.

Video Analysis

Video analysis techniques were useful for estimating impact velocities and the general horn trajectory during ramming sequences. Peak velocities observed compared well with previous literature, however acceleration values observed were much higher. Peak velocities ranged from 4.6 to 7.1 m/s, with an average impact velocity of 5.85 m/s and a previous ramming video analysis study found an average impact velocity of 4.7 m/s. The impacts analyzed in this study were highly variable in terms of impact velocity and contact time as well as the relative horn orientations during ramming. Due to the high degree of variability of impacts it is suggested that further modeling efforts investigate various impact velocities and incidence angles.

It is evident that the impacts observed in these two videos occurred over a time period well under 100 milliseconds, however resolving the exact contact time was difficult due to frame rate

limitations. The lowest estimate of impact time was 15 ms, which is similar to impact durations observed in football helmets during high school practices and games (8.99±3.01) [40]. The impact in the finite element model occurred over approximately 7.2 milliseconds. Impacts were primarily one dimensional (occurred on the X-axis); therefore the entirety of the animals kinetic energy is dissipated over this short time. The impact time of the finite element impact model was lower than estimated from video analysis techniques and this is likely because the model simulated an ideal impact. The boundary conditions in the model restricted neck region rotations and displacements as well as point mass off-axis displacements. These types of movements are likely present to some extent in all real ramming situations and would likely increase the total impact time.

Due to frame rate limitations it was not plausible to obtain peak force values during impact because the actual deceleration occurs over a very small time frame. Previous researchers have estimated peak forces of impact from video footage, but these results are not reliable due to relatively long time between frames (24 frames per second ≈ 42 ms between frames). Videos captured at a very high frame rate, or other force measuring techniques should be employed to estimate peak impact forces.

Conclusions:

- Video analysis is an effective technique for estimating animal velocities just prior to impact.
- Impact velocities were measured between 4.6 to 7.1 m/s (average: 5.85 m/s) which compare well with previous video analysis results.

- Impact accelerations are highly variable and values are dependent on the frame rate at which the video is filmed.
- Very high frame rate video footage must be obtained to resolve the decelerations at impact.
- Techniques other than video analysis should be utilized to estimate forces during bighorn sheep ramming.

Analysis of the Geometric Features of the Horn/Bone Complex

Comparison of three different finite element models (*Full Model, Cut Horn Model, No Struts Model)* yielded interesting results, particularly in terms of potential brain injury prevention. One model included all geometric features, and served as a control for this analysis (*Full Model).* A second model was created with one half of the overall circumferential horn length removed (*Cut Horn Model)*, but was otherwise identical to the *Full Model.* A third model was developed that was completely lacking all of the trabecular-like bone that fills the horncore (*No Struts Model).* In general, both models with geometric features removed displayed higher brain cavity accelerations, which are indicative of greater risk for brain trauma. Simply stated, these geometric features help prevent injury during ramming, but they do so in different ways.

The *Cut Horn Model* displayed a much larger and more abrupt translational acceleration peak than the *Full Model* (+49%). It appears that the horn loading phenomenon discovered in the initial impact simulations reduces the peak translational accelerations in the brain cavity. The tendency of the *Cut Horn Model* was to bounce back immediately upon impact, where in the *Full Model* the back portion of the horn "caught up" gradually, making the recoil of the horn less

abrupt. The horn momentum loading is analogous to loading a torsions spring: compressive stresses are present at the inner diameter and tensile stresses occur on the outer surface. The peak translational acceleration in the *Cut Horn Model* was observed at the same time step that the onset of horn momentum loading occurred in the *Full Model*. This indicates that horn momentum loading was directly responsible for the reduction in peak translational acceleration in the *Full* Model as compared to the *Cut Horn Model.* The strain energy present in the horn is relatively small (7% of total energy); however horn loading has a significant effect on reducing brain cavity translational accelerations.

The effect of removing the horncore struts in the *No Struts Model* was quite dramatic. The ability of the horncore and horn to resist bending was reduced drastically without the horncore struts. This was immediately evident by the large deformations and strains observed in the horn and horncore as compared to the other two models. The strains at the base of the horncore were about 2.8 times higher in the *No Struts Model* than in the other two models. The bone struts within the horncore resist shearing of the outer cortical bone shell and therefore increase the horncore's bending stiffness. Compromising the stiffness of the horncore by removing the internal struts eliminated the structure's ability to resist the moment applied at the neck connection by the point mass and spine spring/dashpot elements. Therefore, massive rotational accelerations were present in the brain cavity, despite the overall impact time being much longer (*No Struts Model:* 13.5 milliseconds, *Full Model*: 7.2 milliseconds). The strain present at the base of the horncore in the *Full Model* was 1.28%, which is near the failure point for human bone. The strains present at the back base of the horncore in the *No Struts Model* were 3.58%, which is much larger than required to cause plastic deformation of bone, and the lack of an internal architecture would likely result in local buckling at the peak compressive strain location (rear horncore base).

Conclusions:

- The horn curl and horncore struts are likely crucial geometric features for preventing damage in brain tissue.
- Loading of the horn makes the impact more gradual, which results in lower brain cavity translational accelerations, reducing the likelihood of brain trauma.
- The horncore's internal struts resist shearing of the outer cortical bone shell, thus increasing the structures rigidity in bending.
- The horncore struts help mitigate rotational accelerations and translational accelerations (to a lesser extent) in the brain cavity by resisting bending of the horncore and rotation of the brain cavity.

Finite Element Modal Analysis

Results from the finite element modal analysis elucidated the dynamic response of the skull and horn structure. The first five modes were examined extensively in this study, as these modes have the lowest frequencies and largest relative displacements. Modes with the largest displacements would dissipate the largest amount of energy as heat, as hysteretic damping is proportional to displacement. All modes shapes were related to displacement of the horn tip, with lateral-medial horn tip oscillations being the most prevalent mode type. This indicates that lateral-medial horn oscillations are the "preferred" vibratory response of the system. The first five natural frequencies observed in the two models existed at values ranging from 118-309 Hz The symmetric, full skull, frequency analysis was subjected to free vibrations, and the half skull

was not, as it had boundary conditions that restricted certain motions. All mode shapes of the free vibration of the full skull were associated with lateral-medial horn tip oscillations.

Conclusions:

- Horn tip movement is a present in all mode shapes, indicating that kinetic energy will travel through the horn to its tip, away from the brain cavity.
- Horn tip lateral-medial oscillation is the preferred vibration mechanism in the horn and skull structure which has implications for energy dissipation and brain trauma prevention.
- Several modes are present within a relatively small frequency band (118-309 Hz).

Experimental Modal Analysis

The experimental modal analysis verified the existence of several natural frequencies within the 100-300 Hz range, and estimates were made predicting frequency ranges for the first 5 modes. The most commonly occurring natural frequency found experimentally existed at 150-160 Hz. The first five modes estimated from natural frequency histograms matched up fairly well with the first five modes of the finite element modal analysis, and the frequency gap between modes was very similar. This provides validation to the material properties and the mesh used in the finite element modal analysis. Also, horn tip lateral displacements observed in the impact finite element model existed at frequencies of 166 and 266 Hz, which fall into the same range as the majority of the natural frequencies observed experimentally. Also, the 166 Hz horn tip oscillation frequency observed in the impact model compares well with the 150-160 Hz natural frequency found experimentally. This fact provides further validation of the impact finite element model.

These experiments proved that frontal horn impacts could result in lateral-medial horn tip oscillations. Finite element modeling efforts show that this kinetic energy is relatively small compared to the energy of the entire system (≈3%), but the loading and vibrational unloading of the horn seems to decrease peak accelerations in the brain cavity. Also, it seems that the horns behave as vibration dissipaters that direct vibrations away from the brain cavity, and then dissipate the kinetic energy. This hypothesis is supported by the larger area under acceleration curves observed in the *Cut Horn Model* than in the *Full Model* (Translational: +22%, Rotational: +58%), which implies that the horn accommodates some vibration that would otherwise be in the skull. Furthermore, the horns have a relatively high fraction of critical damping value (Avg. 4.98%); therefore kinetic energy drawn away from the skull as vibrations will quickly be transformed into heat energy. Vibrations present in the horn have a much lower potential to cause damage to brain tissue than vibrations present in the skull. Vibration of the horn geometry seems to be an important energy dissipation mechanism and warrants further investigation.

Conclusions:

- The natural frequencies observed experimentally fell in the same range as the lowest modes observed in the finite element modal analysis (100-300 Hz).
- Impact to the front of the horns causes side-to-side vibration at the horn tips due to the geometry of the horns. This allows the horns to draw kinetic energy away from the brain cavity and dissipate it as heat.
- Dominant mode natural frequencies compare fairly well with the full skull finite element modal analysis, which provides validation for the mesh and material properties used in the finite element modal analysis.

- Experimentally observed natural frequencies are similar to horn tip oscillation frequencies present in finite element impact model, which provides validation for the impact model.

5.2 General Conclusions

- The horns, horncores and skulls of male bighorn sheep have been evolutionarily adapted to sustain large impact loads while suffering little to no injury or structural damage. Peak stresses and strains in the bone (~ 200 MPa, 1.28%) are near the failure point for human bone at high strain rates, implying that bighorn sheep skull bone has higher material properties.
- The horncore (bone) is loaded in a cantilever-like manner and bears the majority of the stress and strain energy of the structure during impact loading.
- Momentum of the back, non-contacting portion of the horn causes it to load in a manner similar to a torsion spring during impact, which has the effect of reducing peak brain cavity translational accelerations.
- The trabecular-like bone within the horncore resists shearing of its outer cortical shell, increasing the structure's bending rigidity, and in turn drastically reducing brain cavity rotational accelerations.
- Upon excitation, kinetic energy travels through the horn to its tip as lateral-medial vibrations, which direct energy away from the brain cavity and transforms it to heat via damping.

5.3 Future Direction

This project was the first of its kind in many ways, and being such, several gaps in knowledge and areas for potential further research were found. First of all, several changes can be made to the finite element models developed to simulate various conditions. The materials incorporated in the model are not well characterized; especially at physiological strain rates. Varying the modulus values of the materials in the model could provide insight into how stiffness affects horn and skull behavior during impact. Several biological materials display a higher modulus at elevated strain rates, so running the simulation with larger horn and bone modulus values might be more realistic. Also, it is known that bone and horn display anisotropy, and this was not accounted for in the present simulations. Including anisotropic material properties as well as strain rate dependence of the materials would add significant complexity to the model, but could possibly represent the actual physical phenomenon more accurately. It was determined through video analysis that ramming events in bighorn sheep are quite variable in many ways including impact velocity, acceleration, as well as contact angle. These variations could easily be simulated in the impact model by applying various initial velocity fields and by changing the angle of incidence. It would be interesting to see how the loading patterns change with different impact conditions.

The present study analyzed the skull and horns of bighorn sheep from a primarily structural standpoint. Previous literature, and the fascinating function of this structure in nature implies that the material constituents themselves are worthy of investigation. Material testing performed on bighorn sheep horn have been somewhat limited and have not been carried out at the physiological strain rates seen during ramming. Determining the high strain rate properties of horn keratin would be a valuable research effort. To the author's knowledge there is no published

literature on the material properties of the skull bone of bighorn sheep. The maximum strains present in the full impact model were 1.28%, which is approximately the yield point of human bone. Assuming that the bone of bighorn sheep's skulls does not yield during ramming it can be inferred that the modulus of ram skull bone may be higher than that of human bone. It would be valuable to perform material testing on the horncore and horncore bone struts of bighorn sheep, at physiological hydration levels and strain rates. Another interesting prospect for further materials related research is to investigate the interface between the horncore bone and the horn keratin. This interface appears to effectively transfer load from a relatively compliant material to a much stiffer material and likely has an interesting microstructure and/or shear properties.

In general, further work needs to be done to accurately estimate forces produced by bighorn sheep ramming. Knowing these forces would be beneficial for further modeling efforts. Also, future studies should further examine the horn's ability to dissipate energy through vibrations and damping. Furthermore, performing *in vitro* impact studies on ram skulls and horns equipped with strain gauges would be the most straightforward way to further validate the finite element impact model in this study. There are several aspects of the bighorn sheep ramming phenomenon that warrant further investigation and the results could present valuable implications for preventing brain injuries in humans.

References

[1] K. M. Guskiewicz, "Cumulative Effects Associated With Recurrent Concussion in Collegiate Football Players: The NCAA Concussion Study," *JAMA: The Journal of the American Medical Association*, vol. 290, no. 19. pp. 2549–2555, 2003.

[2] M. R. Schulz, S. W. Marshall, F. O. Mueller, J. Yang, N. L. Weaver, W. D. Kalsbeek, and J. M. Bowling, "Incidence and risk factors for concussion in high school athletes, North Carolina, 1996-1999," *Am. J. Epidemiol.*, vol. 160, pp. 937–944, 2004.

[3] M. W. Collins, G. L. Iverson, M. R. Lovell, D. B. McKeag, J. Norwig, and J. Maroon, "On-field predictors of neuropsychological and symptom deficit following sports-related concussion.," *Clin. J. Sport Med.*, vol. 13, no. 4, pp. 222–229, 2003.

[4] J. A. Langlois, W. Rutland-Brown, and M. M. Wald, "The Epidemiology and Impact of Traumatic Brain Injury," *Journal of Head Trauma Rehabilitation*, vol. 21, no. 5. pp. 375–378, 2006.

[5] P. McCrory, W. H. Meeuwisse, M. Aubry, R. C. Cantu, J. Dvořák, R. J. Echemendia, L. Engebretsen, K. Johnston, J. S. Kutcher, M. Raftery, A. Sills, B. W. Benson, G. A. Davis, R. Ellenbogen, K. M. Guskiewicz, S. A. Herring, G. L. Iverson, B. D. Jordan, J. Kissick, M. McCrea, A. S. McIntosh, D. Maddocks, M. Makdissi, L. Purcell, M. Putukian, K. Schneider, C. H. Tator, and M. Turner, "Consensus statement on concussion in sport: The 4th international conference on concussion in sport, Zurich, November 2012," in *Journal of Athletic Training*, 2013, vol. 48, no. 4, pp. 554–575.

[6] P. McCrory, W. H. Meeuwisse, M. Aubry, R. C. Cantu, J. Dvorák, R. J. Echemendia, L. Engebretsen, K. M. Johnston, J. S. Kutcher, M. Raftery, A. Sills, B. W. Benson, G. A. Davis, R. Ellenbogen, K. M. Guskiewicz, S. A. Herring, G. L. Iverson, B. D. Jordan, J. Kissick, M. McCrea, A. S. McIntosh, D. L. Maddocks, M. Makdissi, L. Purcell, M. Putukian, K. Schneider, C. H. Tator, and M. Turner, "Consensus Statement on Concussion in Sport-The 4th International Conference on Concussion in Sport Held in Zurich, November 2012," *PM R*, vol. 5, no. 4, pp. 255–279, 2013.

[7] P. McCrory, W. Meeuwisse, K. Johnston, J. Dvorak, M. Aubry, M. Molloy, and R. Cantu, "Consensus statement on concussion in sport: The 3rd International Conference on Concussion in Sport held in Zurich, November 2008," in *Journal of Athletic Training*, 2009, vol. 44, no. 4, pp. 434–448.

[8] S. A. Herring, J. A. Bergfeld, A. Boland, L. A. Boyajian-O'Neill, R. C. Cantu, E.

Hershman, P. Indelicato, R. Jaffe, W. Ben Kibler, D. B. McKeag, R. Pallay, and M. Putukian, "Concussion (mild traumatic brain injury) and the team physician: A consensus statement," *Medicine and Science in Sports and Exercise*, vol. 38, no. 2. pp. 395–399, 2006.

[9] R. C. Cantu, "SECOND-IMPACT SYNDROME," *Clin. Sports Med.*, vol. 17, no. 1, pp. 37–44, Jan. 1998.

[10] W. P. Meehan and R. G. Bachur, "Sport-related concussion.," *Pediatrics*, vol. 123, no. 1, pp. 114–123, 2009.

[11] K. M. Guskiewicz, S. W. Marshall, J. Bailes, M. Mccrea, H. P. Harding, A. Matthews, J. R. Mihalik, and R. C. Cantu, "Recurrent concussion and risk of depression in retired professional football players," *Med. Sci. Sports Exerc.*, vol. 39, no. 6, pp. 903–909, 2007.

[12] J. W. Powell, "Cerebral Concussion: Causes, Effects, and Risks in Sports," *J. Athl. Train.*, vol. 36, no. 3, pp. 307–311, 2001.

[13] M. Aare, S. Kleiven, and P. Halldin, "Injury tolerances for oblique impact helmet testing," *International Journal of Crashworthiness*, vol. 9, no. 1. pp. 15–23, 2004.

[14] C. T. McCarthy, A. N. Annaidh, and M. D. Gilchrist, "On the sharpness of straight edge blades in cutting soft solids: Part II - Analysis of blade geometry," *Eng. Fract. Mech.*, vol. 77, pp. 437–451, 2010.

[15] V. Geist, *Mountain Sheep: A Study in Behavior and Evolution*. University of Chicago Press, 1974.

[16] W. M. Schaffer, "Intraspecific Combat and the Evolution of the Caprini," *Evolution (N. Y).*, vol. 22, pp. 817–825, 1968.

[17] A. Kitchener, "An analysis of the forces of fighting of the blackbuck (*Antilope cervicapra*) and the bighorn sheep (*Ovis canadensis*) and the mechanical design of the horn of bovids," *J. Zool.*, vol. 214, no. 1, pp. 1–20, 1988.

[18] C. R. Jaslow and A. A. Biewner, "Strain patterns in the horncores, cranial bones and sutures of goats (Capra hircus) during impact loading.," *J. Zool.*, no. 235, pp. 193–210, 1995.

[19] A. A. Farke, “Frontal sinuses and head-butting in goats: a finite element analysis.,” *J. Exp. Biol.*, vol. 211, no. Pt 19, pp. 3085–3094, 2008.

[20] P.-Y. Chen, J. McKittrick, and M. A. Meyers, “Biological materials: Functional adaptations and bioinspired designs,” *Prog. Mater. Sci.*, vol. 57, no. 8, pp. 1492–1704, Nov. 2012.

[21] R. D. Fraser, T. P. MacRae, D. A. Parry, and E. Suzuki, “Intermediate filaments in alpha-keratins.,” *Proc. Natl. Acad. Sci. U. S. A.*, vol. 83, no. 5, pp. 1179–1183, 1986.

[22] R. M. Kenedi, “Strength of Biological Materials,” *J. Anat.*, vol. 108, no. Pt 3, p. 582, 1971.

[23] L. Tombolato, E. E. Novitskaya, P.-Y. Chen, F. A. Sheppard, and J. McKittrick, “Microstructure, elastic properties and deformation mechanisms of horn keratin.,” *Acta Biomater.*, vol. 6, no. 2, pp. 319–30, Feb. 2010.

[24] M. W. Trim, M. F. Horstemeyer, H. Rhee, H. El Kadiri, L. N. Williams, J. Liao, K. B. Walters, J. McKittrick, and S.-J. Park, “The effects of water and microstructure on the mechanical properties of bighorn sheep (Ovis canadensis) horn keratin.,” *Acta Biomater.*, vol. 7, no. 3, pp. 1228–40, Mar. 2011.

[25] R. D. Fraser and T. P. Macrae, “Molecular structure and mechanical properties of keratins,” *Symp Soc Exp Biol*, vol. 34, pp. 211–246, 1980.

[26] A. Kitchener, “Composite theory and the effect of w a t e r on the stiffness of horn keratin,” vol. 22, pp. 1385–1389, 1987.

[27] a. Kitchener, “Effect of water on the linear viscoelasticity of horn sheath keratin,” *J. Mater. Sci. Lett.*, vol. 6, no. 3, pp. 321–322, 1987.

[28] K. Johnson, M. W. Trim, M. F. Horstemeyer, and R. Prabhu, “Examination of Geometric Effects on Stress Wave Propagation and Applications in football Helmet Design,” pp. 2013–2014, 2014.

[29] P. Maity and S. A. Tekalur, “Finite element analysis of ramming in Ovis canadensis.,” *J. Biomech. Eng.*, vol. 133, p. 021009, 2011.

[30] L. J. Gibson, “Woodpecker pecking: How woodpeckers avoid brain injury,” *J. Zool.*, vol.

270, no. 3, pp. 462–465, 2006.

[31] L. Wang, J. T.-M. Cheung, F. Pu, D. Li, M. Zhang, and Y. Fan, "Why do woodpeckers resist head impact injury: a biomechanical investigation.," *PLoS One*, vol. 6, no. 10, p. e26490, Jan. 2011.

[32] C. R. Jaslow, "Mechanical properties of cranial sutures," *J. Biomech.*, vol. 23, no. 4, pp. 313–321, 1990.

[33] K. M. Guskiewicz and J. P. Mihalik, "Biomechanics of sport concussion: quest for the elusive injury threshold.," *Exerc. Sport Sci. Rev.*, vol. 39, no. 1, pp. 4–11, 2011.

[34] M. G. Gardner-Morse and I. A. Stokes, "Physiological axial compressive preloads increase motion segment stiffness, linearity and hysteresis in all six degrees of freedom for small displacements about the neutral posture," *J. Orthop. Res.*, vol. 21, no. 3, pp. 547–552, 2003.

[35] J. McKittrick, P. Y. Chen, L. Tombolato, E. E. Novitskaya, M. W. Trim, G. A. Hirata, E. A. Olevsky, M. F. Horstemeyer, and M. A. Meyers, "Energy absorbent natural materials and bioinspired design strategies: A review," *Materials Science and Engineering C*, vol. 30. pp. 331–342, 2010.

[36] E. S. Gurdjian, J. E. Webster, and H. R. Lissner, "Studies on skull fracture with particular reference to engineering factors," *Am. J. Surg.*, vol. 78, no. 5, pp. 736–742, Nov. 1949.

[37] S. Lee, E. E. Novitskaya, B. Reynante, J. Vasquez, R. Urbaniak, T. Takahashi, E. Woolley, L. Tombolato, P.-Y. Chen, and J. McKittrick, "Impact testing of structural biological materials," *Mater. Sci. Eng. C*, vol. 31, no. 4, pp. 730–739, 2011.

[38] A. Kitchener, "Fracture toughness of horns and a reinterpretation of the horning behaviour of bovids," *J. Zool.*, vol. 213, no. 4, pp. 621–639, 1987.

[39] D. T. Reilly and a H. Burstein, "The elastic and ultimate properties of compact bone tissue.," *J. Biomech.*, vol. 8, no. 6, pp. 393–405, 1975.

[40] S. P. Broglio, J. J. Sosnoff, S. Shin, X. He, C. Alcaraz, and J. Zimmerman, "Head impacts during high school football: A biomechanical assessment," *J. Athl. Train.*, vol. 44, pp. 342–349, 2009.

Appendix A

Transformation Matrix

- Applied to skull geometry to align in Cartesian coordinate system

0.999657	0	0.026177	1.99715
-0.00069	0.999657	0.026168	-0.00354
-0.02617	-0.02618	0.999315	-0.13515
0	0	0	1

Video Analysis Links

1) https://www.youtube.com/watch?v=E6Fx3CaJhgk
2) https://www.youtube.com/watch?v=V__T34iqNOA